Reliability of Neural Coding on Different Stages of Visual Information Processing in an Insect Brain.

Doctoral Dissertation
by
Jan Grewe

Fakultät für Biologie
Universität Bielefeld

December 2006

Reliability of Neural Coding on Different Stages of Visual Information Processing in an Insect Brain.

Ausdruck[1] der genehmigten Dissertation
zur Erlangung des akademischen Grades
Doktor der Naturwissenschaften (Dr. rer. nat.)

der Fakultät für Biologie der Universität Bielefeld
vorgelegt von

Jan Grewe

Bielefeld, Dezember 2006

betreut von
PD Dr. Anne-Kathrin Warzecha

[1]Gedruckt auf alterungsbeständigem Papier nach ISO 9706

Erklärung

Ich versichere, dass ich diese Arbeit selbständig und ohne unzulässige Hilfe verfasst habe, keine anderen als die angegebenen Quellen und Hilfsmittel benutzt und Zitate kenntlich gemacht habe.

Jan Grewe

Contents

1 Summary

Humans as well as animals react to environmental changes by adjusting their behaviour. Thereby the nervous system which processes sensory information about environmental changes and controls behavioural responses has to rely on its sensory cells and neurons that respond with limited reliability. Even if exactly the same stimulus is presented repeatedly, considerable response variability can be found in various cell types in different animals. Neurons in the visual cortex of monkeys, for examples, show an extremely high variability with spike count variances in the range of the mean response amplitude. Somewhat smaller, nevertheless formidable, variability is found in the visual system of insects. These observations lead to the questions where all this variability originates and how the animal deals with it. In my thesis I address these questions investigating peripheral as well as central processing stages of the blowfly visual system which served for long as a model system for studies on the reliability of neural coding.

Visual information processing starts with the sensing of light by the photoreceptors in the retina. Classically their coding performance is characterised using information theoretical approaches, e.g. the widely used Shannon information capacity. I additionally applied a discrimination measure to assess the photoreceptor response reliability. This measure, in contrast to the information capacity, takes the time course of the responses into account. Quite different conclusions about photoreceptor coding performance are drawn on the basis of these two measures. The discrimination measure shows a safe discriminability of responses to stimuli which, on the basis of information theoretical approaches, would have been classified ineffective in evoking responses having any significant information capacity. These results once more illustrate the dependence of drawn interpretations on applied measures.

From the photoreceptors to the next higher level of visual information processing, the large monopolar cells in the first optic lobe, the photoreceptor responses pass a specialised synapse. Depending on the adaptational state, determined by the mean light level, the synaptic transfer properties change from lowpass to bandpass behaviour at low respectively high light levels. From information theoretical considerations it has been concluded to be advantageous to bandpass filter the signals in order to optimize channel capacity. Can this interpretation be supported by the response discriminability? Therefore, I assessed the reliability of photoreceptor responses to random brightness fluctuations in a discrimination task and investigated the impact of synaptic filtering on the discriminability of response time-courses. I found that the filter characteristics of the first synapse can increase response discriminability if the random brightness fluctuations that are to be distinguished are superimposed on a large low frequency modulation of the background illumination. The advantage of filtering results from an increased noise induced by the slowly varying background illumination. I further compared these findings with the effects

of filtering on the discrimination performance of photoreceptor models that can reproduce the time course of photoreceptor responses accurately. These simulations included photon noise as the only noise source leading to response variability in the range observed experimentally. Filtering did not affect the disciminability of the model responses. Comparing the cellular and model noise led to the conclusion that the increased low frequency noise is attributable to a light or activity dependent intrinsic noise source not included in the simulations. Thus, the synaptic transfer characteristic does not only reduce redundancy but also removes noise emerging within the photoreceptor itself.

Photon noise, i.e the randomness in photon emission from a light source, is one of the main noise sources in photoreceptors. This unavoidable noise source inherent in the visual input sets the ultimate limit to the reliability of neural coding especially at low light levels when photons are rare and the gain of photoreceptors is large. Along the pathways evaluating the visual signals other noise sources add to the overall variability that can be observed at higher order processing stages. H1 like the other large motion sensitive tangential cells in the third optic lobe of the fly visual system integrates over many local motion sensitive elements. Despite this extensive spatial integration that reduces uncorrelated noise from the individual input channels, it has been claimed that response reliability of H1 is limited by photon noise even under daylight conditions. Using the discriminability measure I was able to show that, at least at the light level used in the experiments and brighter, though far below daylight conditions, H1 is not limited by photon noise, but more likely by noise arising from neuronal noise sources such as synaptic or ion channel noise.

At this central processing stage also higher level noise may play a role for the encoding and representation of visual motion stimuli. The tangential cells obtain their selectivity for particular visual motion patterns by spatially integrating excitatory and inhibitory outputs of thousands of local motion sensitive elements. During the animal's normal behaviour they are exposed to a large diversity of motion patterns to which they are not invariably tuned. From the tangential cell perspective such motion can be considered as a higher level sort of noise that makes it more difficult to evaluate the overall motion pattern. This motion noise, even if it does not drive the neuron, i.e. it induces no distinct excitation or inhibition, modulates the responsiveness of the tangential cell. I investigated the tangential cell performance in the presence of motion noise on the basis of the time courses of their membrane potential as well as of spike sequences. I could show that (i) the very pronounced changes in the input-output characteristic induced by the motion noise can be attributed to a shunting effect, i.e. a reduction of neuronal gain resulting from a stimulus-induced increase in membrane conductance of the neuron, (ii) despite these changes the direction tuning is very robust, and (iii) the representation of pattern velocity in the response amplitude is almost as good as without any motion noise.

Using the fly visual motion pathway as a model system I have investigated how the nervous system deals with inevitable noise sources at peripheral as well as central processing stages. Using a novel measure for the reliability of the responses I was able to show that peripheral synaptic filtering is not only advantageous to optimise the neural code in an information theoretical sense but also is a prerequisite to enhance reliable over un-

reliable response components. The filtering and the convergence on different processing levels contribute to the performance of a central neuron not being limited by photon noise. The tangential cells could also be shown to be robust against motion noise which is unavoidable as it results from the complex visual motion patterns experienced during behaviour.

2 Introduction

Any organism has to adapt its behaviour to environmental changes dynamically. These changes can be slow and the behavioural adjustment may take place on timescales of minutes, hours, or even days. On the other hand, changes may be extremely rapid in the range of a few tens of milliseconds. On these timescales the precision of the animal's reaction to changing sensory input is of great importance, for example, in the case of a predator wanting to catch its fleeing prey or the prey trying to avoid the predator. Not only during these critical moments but also during everyday life precise reactions are, most likely, of an evolutionary advantage increasing an animal's fitness. Surprisingly, the neuronal signals which control behaviour exhibit a great deal of variability. That is, when the same stimulus is presented to a sensory neuron, say, ten times, the ten corresponding neuronal responses may have a common coarse structure induced by the stimulus but are different in detail at each presentation. Response variances ranging up to the level of the mean activity, suggesting a random process generating the responses, have been observed in vertebrate cortical neurons (Tolhurst et al., 1983; Vogels et al., 1989; Britten et al., 1993). Somewhat smaller variability is described for peripheral stages of visual processing in vertebrates (Levine et al., 1988; Levine and Cleland, 1992; Berry et al., 1997; Reinagel and Reid, 2000; Kara et al., 2000) and also in motion sensitive neurons of the fly, the experimental model system used in the present account (e.g. de Ruyter van Steveninck et al., 1997; Warzecha and Egelhaaf, 1999; Warzecha et al., 2000). Irrespective of its actual degree neuronal variability sets the upper bound for any behavioural performance of any nervous system.

In my thesis I will address different general aspects of neuronal variability using the blowfly's visual system. The fly's visual system is well suited for studies on neuronal response variability and the underlying causes. Several stages of visual information processing are easily accessible with electrophysiological approaches using *in vivo* preparations while stimulating the system with its natural (visual) input instead of electrical stimulation as is often applied in *in vitro* preparations. The blowfly *in vivo* preparation offers the opportunity of long-term electrophysiological recordings as is needed for reliability analyses and allows interpreting the results in behaviourally contexts. Over the last decades much knowledge has been collected ranging from the anatomy (e.g. Strausfeld, 1979) to the electrical and biophysical properties of single neurons on peripheral (e.g. Lillywhite, 1977; Laughlin, 1994; Uusitalo et al., 1995; Vähäsöyrinki et al., 2006) and more central processing stages (e.g. Hausen, 1976, 1982; Hengstenberg, 1982; Borst and Haag, 1996; Haag et al., 1997). The fly visual system is organised in optic lobes (figure 2.1) representing different aspects of information processing.
Starting in the retina (R in figure 2.1) the photoreceptors transduce light intensities into graded changes of the photoreceptor membrane potential (e.g. Juusola et al., 1994). These signals are transmitted to the lamina (L), the first optic lobe, where temporal

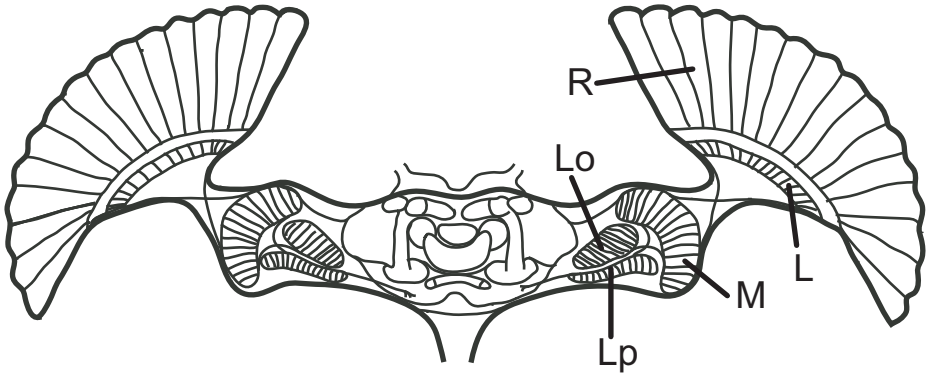

Figure 2.1: Fly visual system. Sketch of a horizontal section through the fly visual system [adapted from Hausen (1976)]. **R** Retina: lines indicate the ommatidial structure of the compound eye. **L** Lamina: the first optic lobe; information processing in cartridges corresponding to the ommatidial organisation. **M** Medulla: second optic lobe. The retinopic structure is preserved. Here, motion compuation is expected to take place. **Lo** and **Lp** Lobula and lobula-plate constitute the lobula complex, third optic lobe. In the lobula-plate large interneurons, the tangential cells, spatially integrate the retinotopic information received from the medulla.

signal processing takes place (e.g. Uusitalo et al., 1995). In the second optic lobe, the medulla (M), visual motion is detected (e.g. Douglass and Strausfeld, 1995). So far all information is processed in separate columns with each column representing one "pixel" of the fly's retinal image. The third optic lobe is the lobula complex which is subdivided into the lobula (Lo) and the lobula plate (Lp). In the lobula plate an ensemble of about 60 so called tangential cells is very well investigated (e.g. Hausen, 1976, 1982; Hengstenberg, 1982; Egelhaaf, 1985; Borst and Haag, 2002; Egelhaaf et al., 2002). These tangential cells are direction-selective motion sensitive elements that spatially integrate the columnar outputs of the medulla and project mostly via interneurons onto motoneurons indicating their central role for controlling behaviour. The fly visual system is a well established system to study principles of visual motion processing and the evaluation of optic flow (e.g. Krapp et al., 1998; Egelhaaf et al., 2002) and offers the opportunity to interpret electrophysiological data in a behavioural context (e.g. Kern et al., 2005). Furthermore, the blowfly has been proven to be a valuable model system for the analysis of neuronal response reliability on different stages of visual information processing (e.g. Laughlin, 1994; de Ruyter van Steveninck and Laughlin, 1996; Juusola and French, 1997; Egelhaaf and Warzecha, 1999; Warzecha and Egelhaaf, 2001; de Ruyter van Steveninck et al., 2001; Egelhaaf et al., 2002).

In my thesis I address aspects of neuronal response variability in the periphery and in more central parts of the visual system, i.e. photoreceptors in the retina (chapters 3 and 4) and tangential cells in the lobula plate (chapters 5 and 6). With a novel measure to discriminate time-dependent neuronal responses (see below, chapter 3) I asked for the origin of neuronal variability and investigated the ways the nervous system may deal with noise, for instance, by synaptic filtering and convergence (chapters 4 and 5). Chapter 6 addresses the robustness of neuronal coding in the presence of visual motion noise, again on level of the tangential cell in the lobula plate.

In the following I will briefly and quite generally introduce into the topic of how neuronal variability manifests itself in neuronal responses and describe methods I applied to analyse it. Subsequently, I will introduce into the scientific background of the four subprojects presented in later chapters in more detail. Finally I will briefly discuss some important aspects.

Variability of Neuronal Responses Basically, two response modes are employed by nervous systems to transmit information: (i) action potentials (spikes) and (ii) graded membrane potential shifts. These modes may also be used by individual neurons in combination. Both response modes have their advantages and disadvantages. Spikes are binary which limits the amount of information that can be transmitted per unit time but they are robustly transmitted over long distances. Thus, spikes are often employed to transmit information over long distances, for instance, by human motoneurons where spikes are generated at the soma located in the spinal cord and conducted to muscles in more than half a meter distance. Graded membrane potential shifts, on the other hand, can code for many more stimulus quantities at any instance of time but they are transmitted in an electrotonic way entailing signal attenuation with increasing distance. Thus, graded membrane potential shifts are employed on short distances, for example in many sensory systems like the retina (for review: Roberts and Bush, 1981).

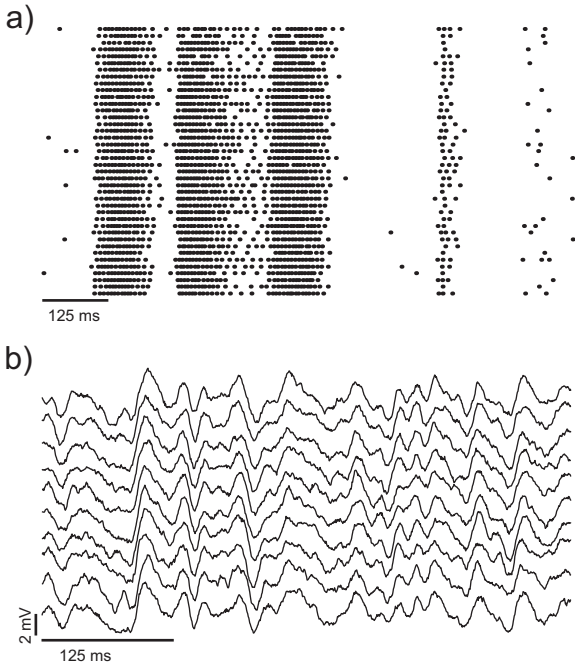

Figure 2.2: Variability in neuronal responses. (a) Rasterplots of the fly's H1 spike responses to 40 repeated presentations of the identical stimulus. Every Line respresents a single response and each dot marks the occurence of an H1 spike. Both manifestations, i.e. *spike time jitter* and *spike count variance*, of neuronal response variability can be observed. **(b)** The neuronal response variability as also observed in graded responses of fly photoreceptors causes every single response to have an individual time-course.

Irrespective of the type of response every neuron shows response variability. In spiking neurons response variability expresses itself in a variable number of spikes generated in response to repetitions of the same stimulus (*spike count variability*) or in variable timing of individual action potentials (*spike time jitter*). Often, variability in spike count and jitter in the timing of spikes can be observed in parallel as shown in figure 2.2a for the H1 neuron in the fly's brain. Neurons that transmit information not by spikes but by graded changes of the membrane potential show membrane potential noise. For instance, the membrane potential time-course varies between responses to repeated presentations as is illustrated for a fly photoreceptor in figure 2.2b.

2.1 Approaches to Analyse Neuronal Response Variability

The reliability of neuronal responses is often quantified in the frequency domain by the *signal-to-noise-ratio* (SNR) (Bendat and Piersol, 2000; Dayan and Abbott, 2001) or with information theoretical approaches like the Shannon information capacity (Shannon, 1948). The fly photoreceptors, for example, have been extensively studied using these methods (e.g. Juusola et al., 1994; de Ruyter van Steveninck and Laughlin, 1996; Juusola and Hardie, 2001; Vähäsöyrinki et al., 2006). Since I applied spectral analyses quite extensively throughout my studies, I will introduce the used methods briefly in the following paragraphs.

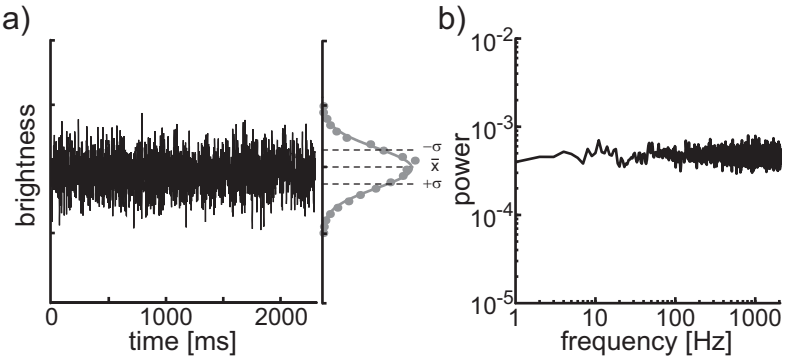

Figure 2.3: White noise stimulation. **(a)** White noise is basically a random sequence of stimulus intensities, for example a series of light intensities. The contrast is defined by the mean intensity $\overline{x}$ and the standard deviation σ (equation 2.1). **(b)** Characterisitc of white noise is the flat power spectrum. Indicating that the white noise stimulus containes all frequencies in equal shares.

White Noise Stimulation White noise stimulation is very common when analysing systems in the frequency domain (Bendat and Piersol, 2000). A white noise stimulus is basically a random sequence of stimulus intensities (figure 2.3a) that, theoretically, contains all frequencies in equal shares (figure 2.3b). I applied white noise stimuli to characterise the response reliability of fly photoreceptors. For this, random sequences of

light intensities with a band-limited spectrum (figure 2.5a) were presented repeatedly to the fly. The amplitude of the light intensity modulation is defined as the contrast c:

$$c = \frac{\sigma}{\overline{x}}, \tag{2.1}$$

with σ the standard deviation of the stimulus' light intensity and $\overline{x}$ the mean light intensity.
Typical photoreceptor responses to the same sequence of white noise contrast modulations (c = 0.31) are shown in figure 2.4 top. Different response traces have a common temporal structure, but are different in detail although evoked by the same stimulus.

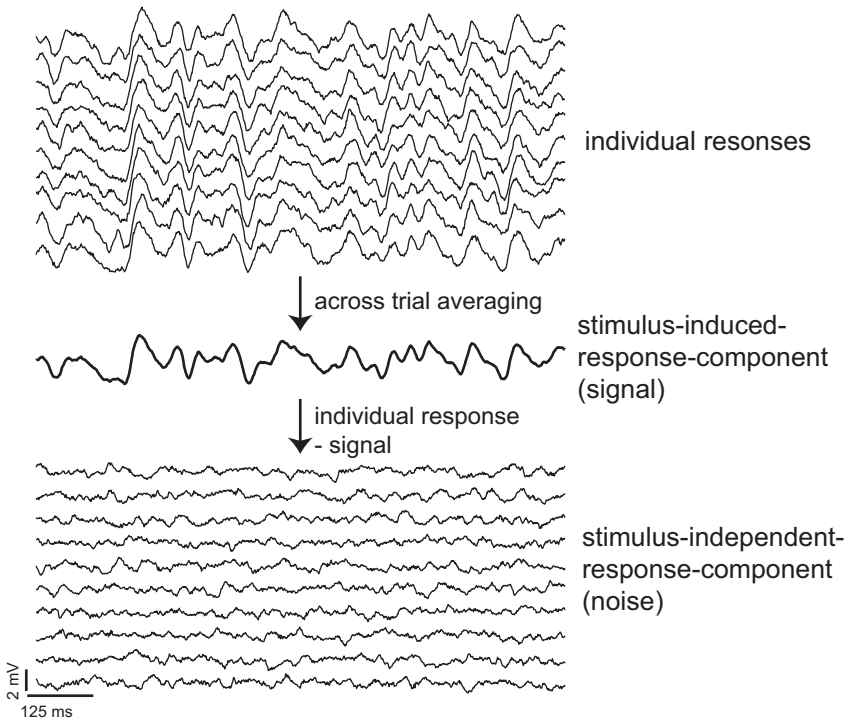

Figure 2.4: Stimulus-induced and stimulus independent response component. The individual responses shown on top are responses of *Calliphora* photoreceptors repeatedly stimulated with the same stimulus. Across trial averaging leads to the *stimulus-induced-response-component* (*signal*) common to all individual responses (center). The difference between the induvidual responses and the signal is the *stimulus-independent-response-component* (*noise*) assumed to be a consequence of unreliable processes (bottom traces).

Separating Signal and Noise Generally, the response component common to all individual responses is considered to be stimulus-evoked, whereas deviations from this are stimulus-independent and, thus, can be regarded as noise. The first step of analysing the reliability of the cellular responses is to separate these two response components from each other. To do this, responses to a number of repeated presentations of the same stimulus (trials) are recorded. The average response estimated across trials is assumed to be the 'real' response, meaning the response that would have been generated, if the system

were deterministic and free of noise. This average response is often called the *stimulus-induced-response-component* (SIRC) or, simply, *signal* (figure 2.4, center). Consequently, the difference between each individual response trace and the estimated noise-free signal is the *stimulus-independent-response-component* (*noise*) assumed to be evoked by unreliable processes in the nervous system (figure 2.4 bottom).

SNR in the frequency domain *Signal* and *noise* response components are further analysed in the frequency domain by calculating their power spectra (figure 2.5b). The spectral view on the *signal* and *noise* response components allows analysing which frequencies are most faithfully represented by the responses and which are not. The SNR is defined as the ratio of the *signal* and *noise* power spectra (Bendat and Piersol, 2000):

$$SNR(f) = \frac{|\langle S(f)\rangle|^2}{|\langle N(f)\rangle|^2} \tag{2.2}$$

where S(f) and N(f) are the Fourier-spectra of *signal* and *noise* response component, respectively. || denotes the absolute value of the Fourier spectra and $\langle\rangle$ averaging over several data segments. The SNR is given as a function of the frequency (figure 2.5c) and provides an intuition of the quality with which different stimulus frequencies are represented by the responses. Large SNRs, as in the middle frequency range in figure 2.5c, indicate a high quality signal while SNRs below one show that the respective frequencies have a stronger *noise* than *signal* component.

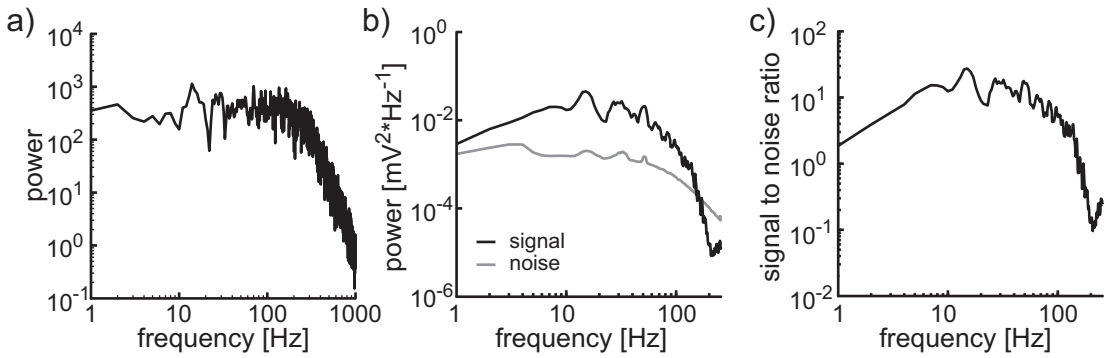

Figure 2.5: Spectral response analysis. (a) Stimulus power spectrum of a white noise light stimulus as used to stimulate photoreceptors. The white noise stimulus was low-pass filtered with a 2nd-order Butterworth low-pass filter giving the band limitation. **(b)** Power spectra of the *signal* (black) and *noise* (grey) response components as estimated from repeated presentations of a white noise stimulus (see figure 2.4). **(c)** *signal-to-noise-ratio* calculated from the *signal* and *noise* power spectra (equation 2.2).

Shannon Information Capacity According to Shannon (1998), the amount of information that a photoreceptor can transmit to subsequent processing stages can be estimated from the SNR (figure 2.6). The so called information capacity R is calculated as

$$R = \int_0^\infty df log_2 \left[1 + \frac{|\langle S(f)\rangle|^2}{|\langle N(f)\rangle|^2}\right], \tag{2.3}$$

with R the information capacity, S(f) and N(f) the Fourier-spectra of the signal and noise response components, respectively. || denotes the absolute value of the Fourier spectra and ⟨⟩ averaging over several data segments.
Shortly after Shannon formulated the theoretical framework to calculate the amount of information that can be transmitted in an electrical communication channel (Shannon, 1948), information theoretical approaches, e.g. the information capacity, have been widely applied to quantify information processing in nervous systems (for review e.g. Borst and Theunissen, 1999). The application of the Shannon information capacity is bound to assumptions: (i) The system has to be linear, (ii) signal and noise must be normally distributed, and (iii) signal and noise must be additive. These assumptions are largely met by fly photoreceptors when stimulated with white noise stimuli (see e.g. de Ruyter van Steveninck and Laughlin, 1996).
SNR and Shannon information capacity are based on spectral analysis of the responses by calculating *signal* and *noise* power spectra. However, power spectra ignore the phase information which, together with the amplitude spectrum, represents the temporal structure of the responses.

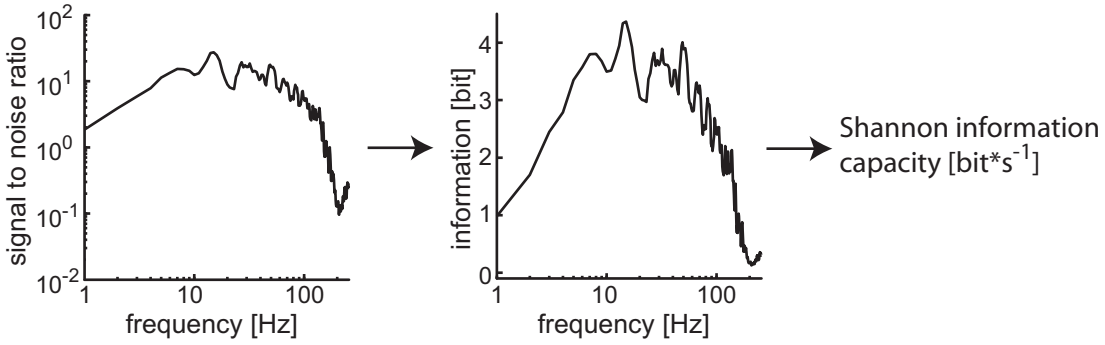

Figure 2.6: Estimation of the Shannon information capacity. (left) The response *signal-to-noise-ratio* as in figure 2.5c). **centre** Transmitted information as a function of the frequency. Integrating this information spectrum (applying equation 2.3 to the SNR) gives the Shannon information capacity given in bit/s.

2.2 Comparison of Shannon Information Capacity and Response Discriminability

For a nervous system the time-dependent activity of its neurons may be important for controlling behavioural responses successfully. Furthermore, a differentiated behaviour can only be evoked if different stimuli lead to distinguishable responses of the involved neurons. Assessing whether responses have a different time course is impossible on the basis of the Shannon information capacity, since the temporal information is lost by omitting phase information. Therefore, as an alternative way to assess photoreceptor coding performance, I analysed photoreceptor responses in a discrimination task in which responses to different stimuli are to be distinguished. The question arises whether or not equivalent conclusions about photoreceptor coding performance would be drawn on basis of

the Shannon information capacity and the discriminability of time-dependent responses. Discrimination tasks have been applied in different formats and in different systems ranging from insects to monkey cortex (e.g. Britten et al., 1992; Machens et al., 2001). The discrimination task I developed estimates response discriminability by assessing response similarity combined with a two-alternative-forced-choice method. Because of its prominent role in the projects of my doctoral thesis I will explain this method as applied to fly photoreceptor responses in some more detail.

Estimating Response Discriminability The photoreceptors are stimulated with random light intensity fluctuations of a certain contrast (equation 2.1, see above). The basic idea is to estimate the system's reliability by asking for the contrast of the stimulus that is needed to affect the responses detectably. For this, the contrast is increased until an effect on the responses can be detected with an appropriate measure (see below). In detail:

1. At each contrast level two stimulus groups are presented. The stimuli of one group are called the *reference stimuli* and the others are the *test stimuli* (figure 2.7 top). *Reference* and *test stimuli* have the same statistical properties, i.e. the same contrast and (approximately) the same spectral characteristics. While the *reference stimuli* are exact repetitions of a single stimulus trace, the *test stimuli* are different from each other, i.e. have different time courses. By using stimuli with the same statistical properties cellular nonlinearities and (possibly existent) activity dependent noise sources affect the responses to *reference* and *test stimuli* equally. Thus, this measure does not make assumptions about the system's linearity or the additive nature of inherent noise. The photoreceptor responses are named *reference* and *test responses*, accordingly (figure 2.7 centre).

2. The *test* and *references responses* are compared by estimating their mutual similarity. As illustrated in the central part of figure 2.7, each *reference response* is compared to all other *reference responses*, giving an average similarity *within* the reference group, and to the *test responses*, giving an average similarity *between* the reference and test group. It is assumed that a *reference response* can then be distinguished from the *test responses*, if it is more similar to the other *reference responses* than to the *test responses*. The actual measure of response similarity depends on the type of response analysed. In the case of the graded photoreceptor responses the root-mean-square distance is applied (see below, equation 2.4).

3. In analogy to a two-alternative-forced-choice procedure as frequently applied in psychophsics (Green and Swets, 1974), each *reference response* is regarded as distinguishable from the *test responses*, if it is more similar to the other *reference responses* than to the *test responses*. This judgement is based on the similarities *within* and *between* response groups (see above).

4. The percentage of distinguishable *reference responses* is then plotted as a function of the stimulus contrast (figure 2.7 bottom). The discrimination performance ranges from 50% correct (chance level), if the responses are indistinguishable, to 100% correct, if all *reference responses* are more similar to their companions than to the *test responses*.

5. The resulting physiometric curve is fitted with a logistic curve ranging from 50 to 100% from which the contrast that leads to a safe discriminability (75% correct assignments) can be directly read out. This *threshold contrast* is interpreted as a representative of the photoreceptor response reliability.

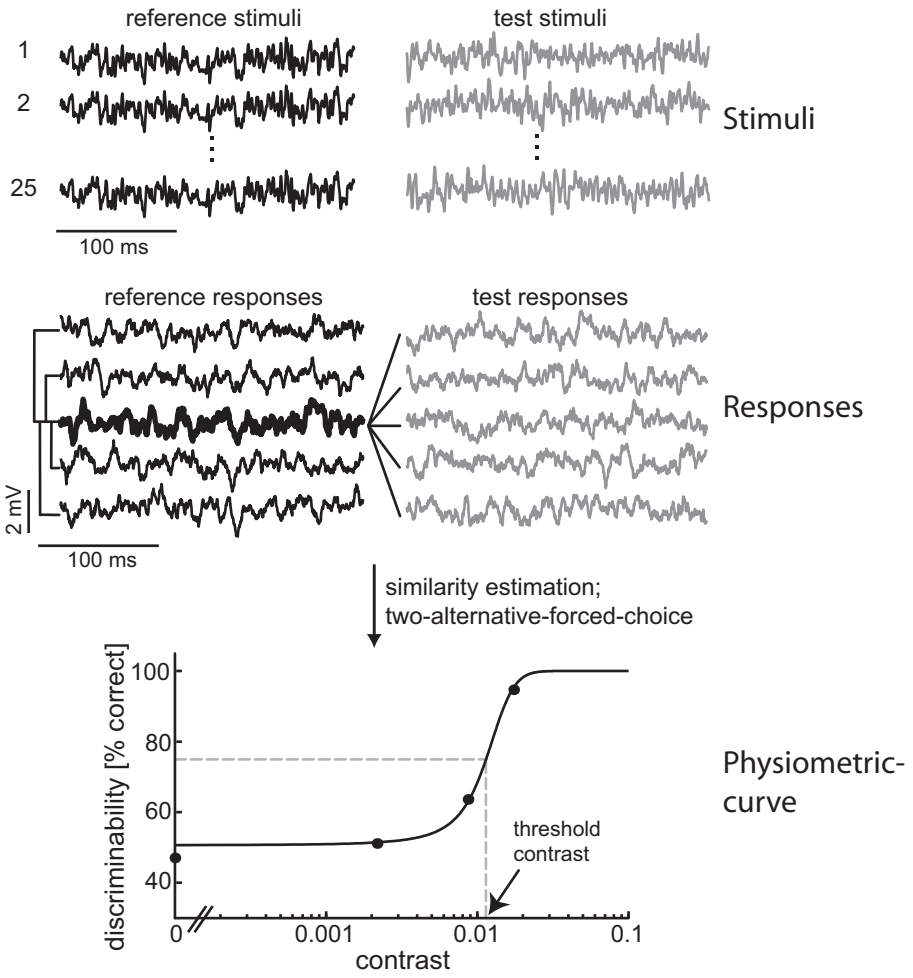

Figure 2.7: Estimating response discriminability. (top) Two types of stimuli, namely the *reference* (left) and *test stimuli* (right) are presented at each contrast level. The *reference stimuli* are exact repetitions while the *test stimuli* all have the same statistical properties as the *reference stimuli* but are different in detail. **(centre)** The similarity of the responses is estimated by comparing each *reference response* (for example the highlighted one) to all other *reference responses* and to all *test responses* giving the average similarity of this resopnse *within* the reference group and *between* the reference and test responses. **(bottom)** In a two-alternative-forced-choice way the individual reference responses are assigned belonging to the reference group (correct assignement) or to the test group (false) on basis of their similarity *within* and *between*. The whole procedure is done at different contrasts and the percentage of correct assignments is plotted as a function of the contrast. The resulting physiometric curve is fitted with a logistic function from which the *threshold contrast* can be estimated. The *threshold contrast* is defined as the contrast leading to a safe (75% correct) discriminability of the responses.

Using this measure, the system's noise can be measured in units of the input signal. This procedure is attractive since it allows interpreting the observed response noise in terms of the natural input and drawing conclusions about its behavioural relevance.

How are the measures based on spectral response analysis (section 2.2) and the response discriminability related? Do both measures lead to the same estimate of the photoreceptor coding performance? This question will be answered in chapter 3 where responses of fly photoreceptors to white noise modulated brightness stimuli are analysed with this discrimination measure. The similarity of reference and test responses is assessed using the root-mean-square distance.

$$D_{x,y} = \sqrt{\frac{1}{N}\sum_{i=1}^{N}(x_i - y_i)^2}, \tag{2.4}$$

with x_i and y_i the two responses and N the number of data points. Two identical responses would have a distance D = 0. The discrimination performances are estimated for different contrasts, and the results are compared to the Shannon information capacity of the responses at the same contrasts.
With the discrimination measure, responses can be safely discriminated already for extremely small contrasts which, on the basis of the information capacity, are concluded not to be coded at all. Furthermore, the analysis shows that even those response components that have a SNR below one are valuable, if the temporal structure of the responses is taken into account.

The results of this analysis are described in chapter 3 and have been submitted for publication as: Jan Grewe, Matti Weckström, Martin Egelhaaf, and Anne-Kathrin Warzecha. *Two Measures Two Interpretations - Shannon Information Capacity and Response Discrimination as Measures of Photoreceptor Coding Performance.*

2.3 Synaptic Filtering of Photoreceptor Responses

As illustrated above, the photoreceptor responses exhibit considerable variability (figure 2.4). At the same time, photoreception is the first step of visual information processing and information lost on this early stage will not be available to subsequent processing steps. In the retinae of vertebrates and invertebrates several mechanisms have been identified enhancing signal quality.
One of these mechanisms is the convergence, i.e. the combination of the sensory information received by many units. In the fly retina, for example, six photoreceptors sampling the same point in the visual space are electrically coupled (e.g. Meinertzhagen and O'Neil, 1991) and the information combined in this way is transmitted to the same 1st-order neurons and to subsequent processing stages. Similar convergence is also found in the rod pathway in the mammalian retina to improve signal quality before synaptic transmission to the bipolar cells (e.g. DeVries et al., 2002; Hornstein et al., 2005). By this convergence uncorrelated noise in the individual photoreceptor responses is reduced. Thereby the signal quality is improved, but spatial resolution is sacrificed.
The subsequent transmission of the retinal signals to higher-order processing stages offers

the opportunity for further signal processing. The synapses connecting the different cells are important sites of neuronal signal processing. By synaptic filtering information can be extracted and the signal quality can be improved. Synaptic transfer characteristics that increase signal quality have been characterised in the retinae of vertebrates and invertebrates (e.g. Armstrong-Gold and Rieke, 2003; Field and Rieke, 2002; Laughlin, 1994; Juusola and French, 1997).
In the fly retina the multiple parallel synapses between photoreceptors and first order neurons (the large monopolar cells, LMCs) are specialised to conserve the signal quality while it simultaneously processes the photoreceptor responses. Due to its architecture, with many active zones at which histamine is released into the synaptic cleft, it has been shown to transmit the photoreceptor signals very faithfully (e.g. de Ruyter van Steveninck and Laughlin, 1996). The synapse processes the signals by its bandpass-like transfer properties (e.g. James, 1992) which were concluded to be optimal when viewing natural scenes. In natural scenes neighbouring points are likely to have similar light intensities. Thus, a photoreceptor is likely to receive similar light intensities at subsequent instances of time that originate from the same object when the animal moves around. The visual input is therefore dominated by relatively slow changes of the light intensity. From an information theoretical point of view, the transmitted information at the photoreceptor output is thus redundant. This redundancy is reflected in the spectral properties of natural input signals. Natural scenes have, on average, a power spectrum with the power decreasing following the 1/f rule (e.g. van Hateren, 1997) meaning that the power decreases with the frequency (f). Assuming that a neuronal "communication channel" has a limited capacity it would be most efficient to transmit only those stimulus/response components that are not redundant. These are the higher frequencies since they are evoked by environmental brightness changes, thus, the contrast in the texture of the different objects. In this context the bandpass-like transmission of the synapse between photoreceptors and 1st-order neurons would attenuate the redundant information and emphasise the more informative middle frequencies (for review see Laughlin, 1994).

Can this conclusion, drawn on the basis of information theoretical considerations, be supported by the response discriminability? In chapter 4 I analyse the effects of filtering mimicking different aspects of the synaptic transfer properties found in the fly (e.g. James, 1992), on the discriminability of the time-dependent photoreceptor responses. For this I apply the discrimination measure as described above. The experimentally determined results are compared to the discriminability of the responses of photoreceptor models. The models mimic the responses of photoreceptors phenomenologically either exclusively by a linear filter or by a combination of a linear filter and a non-linear characteristic curve. These models have already been used in similar form (van Hateren and Snippe, 2001). In my study, however, the models are not driven by the light as a continuous function of time but by barrages of simulated individual photons as would be the case for the real photoreceptors. Thus, the model simulations contain photon noise as the only noise source.
I show that the bandpass-like transfer behaviour of the photoreceptor-LMC synapse can be advantageous for discriminating between the responses. However, the discrimination performance of the bandpassed responses is only better than the discriminability of the unfiltered responses, if the stimulus contains large low frequency modulations. These

large and slow modulations lead to an increased low frequency noise. The impact of this noise is reduced when the responses are passed through a bandpass filter. The models, although reproducing the average photoreceptor responses successfully, do not show any advantage of bandpass filtering. This is, most likely, due to the lack of any intrinsic noise sources that constitute the additional low frequency noise observed in real photoreceptors. Furthermore, the models allow concluding that the intrinsic noise source is light or activity dependent suggesting that an activity related process, like voltage-gated potassium channels, are responsible for the increased low frequency noise. The membrane potential noise induced by the random absorption of photons (photon noise), however, can be concluded to be a major noise source in photoreceptors.

The results of this project are presented in chapter 4 and will be submitted as: Jan Grewe, Martin Egelhaaf, and Anne-Kathrin Warzecha. *Intrinsic Photoreceptor Noise Reduced by Synaptic Filtering.*

2.4 Sources of Noise Responsible for Response Variability

The response reliability of nervous systems is affected by several noise sources intrinsic to the systems. One noise source is the so-called ion channel noise. The functioning of ion channels controls the ion-specific conductance changes that are essential for e.g. action potential generation. Ion channels are stochastic elements and transition from closed to their open conformation is a stochastic process with the transition probability depending on the actual membrane potential or the binding of transmitter molecules in the case of voltage or ligand gated channels, respectively. Therefore, even at resting potential a portion of channels is switching between states inducing conductance changes and thereby small membrane potential fluctuations (for review White et al., 2000).
Furthermore, the transmission of responses of sensory cells or neurons to the next neuron through chemical synapses often includes the introduction of noise. Variability induced by chemical synapses has been concluded in many systems to be a major noise source (e.g. Laughlin et al., 1987; Simmons, 1999; Zador, 1998). Variability introduced by synapses has been attributed to three sources: (i) the quantal nature of transmitter release by exocytosis of a limited number of synaptic vesicles, (ii) the site of transmitter release, which influences the efficacy of the transmitter, and (iii) the stochasticity of the postynaptic receptors (Franks et al., 2003).
For visual systems also the sensing of light as the very first step of seeing introduces noise. Unreliability of the transduction process as well as the spontaneous isomerization of rhodopsin corrupts the signals of visual neurons. The spontaneous activation of rhodopsin molecules leads to the same quantum events as a real photon's absorption does (e.g. Lillywhite, 1977). Although the spontaneous bump rate in insect photoreceptors is very low (Lillywhite, 1977), the spontaneous rhodopsin isomerizations form the prominent "dark noise" in vertebrate rods (e.g. Schneeweis, 2000). However, also bump waveforms are quite variable with respect to their latency as well as the amplitude, indicating even more unreliable processes involved in phototransduction (figure 2.8).

Closely related to the spontaneous activation of rhodopsin is the extrinsic noise source

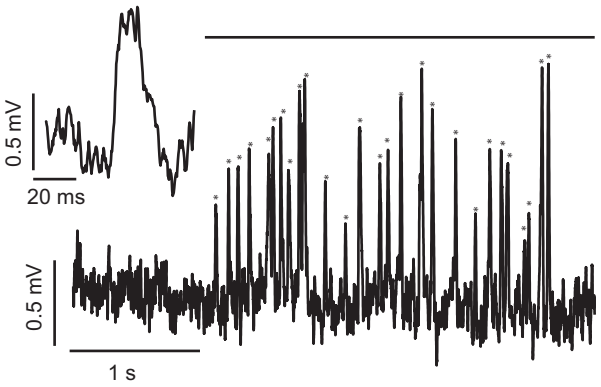

Figure 2.8: Single photon events in fly photoreceptors. Single photon absorptions are leading to discrete membrane potential deflections, so-called quantum bumps (e.g. Lillywhite, 1977). The photoreceptors were adapted to absoulte darkness for more than 20 minutes and then stimulated with very weak constant light. The black line on top of the response indicates the light-on period. Stars mark single bumps as identified by eye inspection. The bump amplitudes are very variable which is typical for fly photoreceptors (e.g. Dubs et al., 1981). Inset shows a single bump.

of visual systems, photon noise. Photon noise results from the probabilistic manner with which any light source emits photons. The appearance of photons follows a Poisson process in which each single photon emission is stochastic and independent of preceding emissions. Increasing the light intensity of a light source increases the average probability of photon emission. Resulting from the random emission also the absorption is characterised as a Poisson process. In the dark-adapted photoreceptors of vertebrates and invertebrates single photon absorptions lead to distinct membrane potential deflections, called quantum bumps (figure 2.9 e.g. Baylor et al., 1979; Lillywhite, 1977; Dubs et al., 1981). This underlines the importance of the exact timing of the absorption for the neuronal response waveform. At higher light levels, when more photons are absorbed the size of the quantum bumps decreases and the single events merge to a continuous membrane potential deflection.

For the peripheral processing stages photon noise is a major source of noise as described in the preceding sections. At any step of neuronal processing synapses and ion channels underlying neuronal excitability contribute to the overall noise. For the response reliability of the fly's so-called H1 cell all internal sources of variability were claimed to be of minor relevance and photon noise to limit the response reliability up to daylight conditions (de Ruyter van Steveninck and Bialek, 1995; Lewen et al., 2001; Borst and Haag, 2001). The H1 cell is a direction-selectively motion sensitive neuron (Hausen, 1976) and a well-established system for analysing the processing reliability of visual motion information (for review see e.g. Egelhaaf and Warzecha, 1999; Warzecha and Egelhaaf, 2001; de Ruyter van Steveninck et al., 2001; Haag and Borst, 2002; Egelhaaf et al., 2002). It belongs to the tangential cells located in the fly's third optic lobe, the lobula plate (figure 2.1), several synapses away from the retina. In contrast to the claim that the reliability of the H1 cell is limited by photon noise, the noise introduced by the first synapse of the visual system, between photoreceptors and first-order neurons (the large monopolar cells in the lamina) has been shown to affect significantly the reliability with which

visual information is signalled to higher-order processing stages (Laughlin et al., 1987; de Ruyter van Steveninck and Laughlin, 1996).

In order to resolve these contradicting conclusions I use the discrimination measure to analyse whether H1 response variability can be attributed to photon noise (chapter 5). Therefore, the neuron is stimulated by a motion stimulus (random dot pattern) moving at a constant velocity in H1's preferred direction. A random luminance modulation, mimicking photon noise, is superimposed on this pattern. The amplitude (contrast) of the luminance modulation is gradually increased and the discriminability of different time-dependent H1 responses estimated. Again, I ask for the minimal contrast of the luminance modulation that allows a safe discrimination of *reference* and *test responses*. The similarity of the spiking responses is estimated by the use of a measure that calculates the minimal "costs" of transforming one response into another (Victor and Purpura, 1997). In this context "costs" refer to the number of elementary formal operations (e.g. deleting or inserting a spike or shifting a spike by a certain time interval) that are required for the transformation of the responses (figure 2.9b).

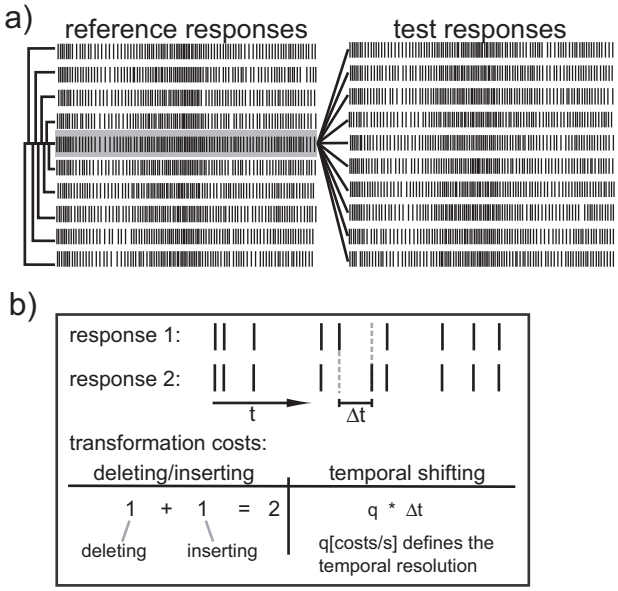

Figure 2.9: Estimating the similarity of spike responses. (a) *Reference* and *test responses* of the H1 neuron. Every line indicates a single trial. The vertical lines indicate the occurance of a spike. The similarity of each *reference response* (for example the highlighted one) is estimated *within* the *reference responses* and *between* this *reference response* and the *test responses* by estimating the transformation costs according to the metric developed by Victor and Purpura (1997). **(b)** Illustration of similarity estimation. The costs are estimated from the minimal number of elementary operations (deleting/inserting a spike or shifting a spike by a certain time interval) that have to be performed to transform one response into the other. Deleting and inserting of a spike have a cost of 1 while shifting a spike depends on the time interval and the costs per second 'q'. Varying 'q' defines the temporal resolution of the measure.

In a first set of experiments the luminance modulation is independent for each stimulus element (dot) as it would be as a consequence of photon noise. The amplitude that affects the responses significantly is found to be much larger than the luminance modulation in-

duced by photon noise under the experimental conditions. This difference suggests that noise sources intrinsic to the nervous system override the impact of photon noise. With its large dendrites H1 spatially integrates the motion information conveyed by a larger number of retinotopic inputs. This convergence reduces uncorrelated noise as used in the experiments. The real photon noise is also uncorrelated for any input channel. In a second set of experiments the luminance modulation is the same for different fractions of the dots thereby introducing noise correlation into the stimulus. With 100% correlation the modulation amplitude necessary for affecting the responses detectably is smaller than with uncorrelated noise but still larger than the photon noise estimate. This further supports the conclusion that photon noise does not limit the reliability with which wide-field motion is encoded by the fly visual system. Rather, intrinsic noise sources dominate over photon noise. The comparison of correlated vs. uncorrelated noise demonstrates that convergence reduces the impact of uncorrelated noise.

These results are presented in chapter 5 and have already been published as:
Jan Grewe, Jutta Kretzberg, Anne-Kathrin Warzecha, and Martin Egelhaaf: *Impact of Photon Noise on the Reliability of a Motion Sensitive Neuron in the Fly's Visual System.*, Journal of Neuroscience 23(34): 10776 - 10783, 2003

2.5 Robustness of global motion computation in the presence of noise

Noise is always present in any kind of neuron. The extent of this noise may vary but, obviously, nervous systems are able to work efficiently even in the presence of noise. So far, I have analysed individual neurons or pairs of neurons. In the last project of my doctoral thesis the view will be shifted to neuronal networks.
The synaptic inputs received by cortical neurons have been described as driving and modulating inputs (Sherman and Guillery, 1998). The driving input excites or inhibits the receiving neuron and is thought to contain the relevant information that is to be processed. The modulating synaptic inputs, however, do not necessarily carry relevant information from sensory inputs but may be a consequence of stimulus-independent activity in presynaptic elements. This modulating input can thus be considered as an additional noise source affecting neurons working in networks and is often called synaptic background input. The background input was shown to lead to a higher membrane conductance and increased membrane potential fluctuations (e.g. Destexhe et al., 2003). However, besides decreasing the response reliability the effects of synaptic background input are discussed to be a mechanism controlling the neuronal gain (e.g. Chance et al., 2002; Fellous et al., 2003; Prescott and De Koninck, 2003). These studies are mainly based on data obtained from *in vitro* experiments in brain slices with the background input mimicked by the so-called dynamic clamp technique (e.g. Prinz et al., 2004). The functional interpretations based on these experiments about the implications of synaptic background input are thus limited.

In chapter 6 I use the fly tangential cells (TCs) as a model system to analyse the consequences of such background input for the neuronal gain and for the computationally

important characteristics like the tuning to the direction of motion or the representation of pattern velocity. As already mentioned above, the TCs can be recorded *in vivo*, while the animal is stimulated directly by visual input, thus ensuring to drive the neurons in a physiologic range. In the lobula plate (figure 2.1) an ensemble of about 60 TCs evaluate optic flow and are thought to be involved in controlling behaviour (e.g. Egelhaaf and Borst, 1993; Egelhaaf, 2006). TCs are direction-selective motion-sensitive cells with large receptive fields. The H1 cell, for example, is excited by back-to-front motion and inhibited by motion in the opposite direction (e.g. Hausen, 1976). This preference is conveyed by the presynaptic elements which on their own are assumed to be direction selective. The TCs pool the excitatory and inhibitory outputs of thousands of these retinotopically arranged presynaptic elements (e.g. Brotz et al., 1996). During preferred direction motion, the excitatory inputs are activated to a larger extent than the inhibitory input elements. The situation reverses during null direction and both inputs are equally active during visual flicker or movement orthogonal to the preferred direction (Egelhaaf et al., 1989; Borst et al., 1995; Single et al., 1997). During natural behaviour the TCs are exposed to optic flow patterns containing motion vectors in a wide range of directions. These drive the neuron, if pointing in preferred or null direction, or do not polarise the membrane, if the motion vectors are orthogonal to the preferred direction. In the latter case the input signal would be similar to the modulating input as described for cortical neurons which does not drive the neuron but activates excitatory and inhibitory inputs to an equal extent. To analyse the implications of modulating input on the TC properties I present visual motion stimuli that contain both, a driving preferred- or null-direction component and a modulating motion noise component. The strength of each input component can be controlled individually.

I find the modulating input to have a strong impact on the neuronal gain. The observed gain reduction can be shown to be a result of a reduced input resistance evoked by the modulating input, although the cell's membrane potential remains almost unaffected by the background input alone. I further analyse the direction tuning and the representation of pattern velocity in the response amplitude of the H1 neuron. Both response features are very robust against the background input. The direction tuning only degrades when a relatively weak driving input is combined with a strong modulating input. The coding of pattern velocity in the H1 response in the presence of the background input is found to be almost as good as without any background input. This is true even though the gain reduction induced by the modulating input reduces the average rate of generated action potentials about 50%.

In the TC ensemble the different TCs are tuned to different kinds of optic flow (e.g. Krapp et al., 1998; Karmeier et al., 2003). The optic flow a freely behaving animal induces on its eyes by its own movements is wildly varying over time and in most situations not matched to the optic flow a TC is tuned to. Thus, in natural situations modulating input such as evoked by flicker stimulation or by optic flow orthogonal to the preferred direction can hardly be avoided. Irrespective of the driving or modulating impact the continuous input signals to all TCs reduces the TC gain by its shunting impact. Therefore, I propose that the specific way of the TC wiring immanently leads to an equalised gain in the TC ensemble irrespective of the specific behavioural situation of the animal.

The results of this project will be presented in chapter 6 and have already been published as: Jan Grewe, Nélia Matos, Martin Egelhaaf, and Anne-Kathrin Warzecha: *Implications of Functionally Different Synaptic Inputs for Neuronal Gain and Computational Properties of Fly Visual Interneurons.*, Journal of Neurophysiology 96: 1838 - 1847, 2006

2.6 Discussion

Noise in neuronal signals eventually limits the precision with which an animal can react to environmental changes detected with its sensory equipment. Noise is a feature observed in any neuron and is a result of several unreliable processes involved in neuronal information processing. The questions about the origin of neuronal noise and the way nervous systems cope with it is investigated in many systems. I analysed different aspects of these questions in the fly's visual system using electrophysiological and modelling approaches. In particular, I asked for (i) the origin of noise, (ii) the effects of synaptic filtering and of convergence on the discriminability of time-dependent responses, and (iii) the robustness of the coding of motion stimuli in the presence of noise.
In the following I will discuss several important aspects that go beyond the project specific discussions given in the respective chapters: (i) advantages and disadvantages of the discrimination measure that has been employed for assessing response discriminability, (ii) the impact of photon-noise on different stages of visual information processing, (iii) mechanisms to cope with noise in different visual systems, and (iv) functional implications of modulating background input on the tangential cell ensemble.

Advantages and disadvantages of the discrimination measure In contrast to the usually used response analyses in the frequency domain, the discrimination measure I used in my studies takes the temporal structure of the responses into account. However, both ways to analyse response reliability are artificial and neither can fully describe the performance of a system.
The Shannon information capacity and the discrimination measure each have certain advantages and disadvantages. While the Shannon information capacity (Shannon, 1998) may only be calculated if *signal* and *noise* are normally distributed, additive, and independent of each other, the discriminability may be estimated in any case. This advantage, on the other hand, is traded in for the requirement of more data, since responses to both *reference* as well as *test stimuli* at the same contrast level have to be obtained.
Common to both measures is that the reliability of the results increases with the amount of available data. Additionally, as shown in chapter 3, the threshold contrast estimated from the physiometric curves (figure 2.7) depends on the amount of data: decreasing response length entails a decreasing discrimination performance. As soon as sufficiently long responses are analysed, however, the discrimination performance appears to saturate. Control simulations showed that further increasing the duration of the response traces up to 80 seconds does not shift the threshold to smaller and smaller values (usually I evaluate response segments of one second and less). Thus, discrimination performance becomes almost independent of the length of the responses once sufficiently long responses can be analysed.
The major advantage of the discrimination measure is that the resulting threshold con-

trast (figure 2.7) is given in units of the input signal. In chapter 5, for example, this allows relating the estimated threshold (the luminance modulation leading to a safe response discriminability) to the luminance modulation induced as a consequence of photon noise under the actual experimental conditions.
In chapter 3 I compare the discrimination measure to the Shannon information capacity (Shannon, 1998) which results in different interpretations about the photoreceptor coding performance. Which interpretation is the genuine one? This question cannot be fully clarified at this stage. Whether the application of a certain measure is appropriate depends on the behavioural context. One aspect that needs to be taken into account is the behaviourally relevant timescale. For a flying fly the interval between subsequent saccadic turns that characterises the animal's spontaneous orientation behaviour (Schilstra and van Hateren, 1998) represents the time available for evaluating the optic flow (Kern et al., 2005). On this timescale contrast modualtions are already discriminable that lead to responses with an almost neglible information capacity. Hence, even on this short timescale the discriminability measure is more sensitive than the information capacity (chapter 3) indicating that the discrimination measure is the better choice to investigate the limits of photoreceptor coding performance. On the other hand, using the information capacity allows evalutating the coding performance when signals of large contrasts are encoded at which the discriminability is already saturated.

Impact of photon noise on different stages of visual processing The responses of photoreceptors and of tangential cells in the third optic lobe, for example the H1 neuron, are corrupted by noise. For the photoreceptors my results show that photon noise plays a prominent role in determining the reliability of encoding light stimuli (chapter 4). The relevance of photon noise at the first stage of visual information processing is obvious at very low light levels, when the absorption of single photons leads to distinct single photon responses, so-called quantum bumps (figure 2.8; e.g. Lillywhite, 1977). Photon noise still affects the photoreceptor responses at higher light levels (at about 30000 absorbed photons per photoreceptor and second) as used in chapter 4. However, it is not the only noise source shaping the performance of photoreceptors. I identified an activity-dependent noise source that affects the response discriminability (chapter 4).
Photon noise was claimed to be the limiting noise source even of the tangential cells (de Ruyter van Steveninck and Bialek, 1995; Lewen et al., 2001; Borst and Haag, 2001), although the tangential cells are several synapses away from the photoreceptor level, and chemical synapses are generally concluded to be a significant source of response variability (e.g. Franks et al., 2003; Laughlin et al., 1987; Simmons, 1999; Zador, 1998). Analysing H1 responses with the discrimination measure revealed that photon noise is of only minor importance at this rather central part of the visual system (chapter 5) and that it is overridden by noise originating within the nervous system such as ion channel and synaptic noise.
The question of whether processing of visual information is limited by noise sources intrinsic to the nervous system or by photon noise has been discussed also for vertebrate visual systems (review: Field et al., 2005). Vertebrate rods, as well as insect photoreceptors, can signal the absorption of single photons (e.g. Baylor et al., 1979), and behavioural responses have been found even at light levels when only few photons were absorbed (e.g. Hecht et al., 1942; Bouman et al., 1985). This implies that further signal processing is

rather perfect and noise-free. Field et al. (2005) argue that this interpretation might not be entirely correct, which is supported by recent findings that the reliability of retinal ganglion cells is limited by intrinsic noise introduced during retinal information processing rather than by rod noise (Dunn et al., 2006).
Intrinsic noise was concluded to dominate over photon noise in higher-order neurons of both flies and vertebrates (chapter 5; Dunn et al., 2006). How does this finding relate to the observed single (or few) photon events measured electrophysiologically in the H1 neuron (Lillywhite and Dvorak, 1981) or even in behavioural and perceptual responses (e.g. Hecht et al., 1942; Reichardt, 1965; Bouman et al., 1985)? All the experiments that report the effects of single photon absorptions were done with the investigated system adapted to total darkness. Under these conditions the system operates with an extremely high gain when quantum bumps may have amplitudes of several millivolts (figure 8; e.g. Lillywhite, 1977; Dubs et al., 1981). Even at the moderate light conditions as used in my experiments which were still much dimmer than daylight each individual photon already contributes much less to the photoreceptor potential than in total darkness. A detailed discussion of the contradicting conclusions that photon noise limits up to daylight conditions as put forward in other studies (Lewen et al., 2001; Borst and Haag, 2001) is included in chapter 6.

Mechanisms to cope with noise If every synapse and the biophysical machinery of each interneuron involved in the information processing add to the overall noise, it would be astonishing to some extent that animals are able to perform differentiated behavioural responses. To ensure functioning of the nervous system in presence of noise it uses several mechanisms that reduce the influence of noise on the processing of information. One such mechanism is filtering of the signals as occurs at synapses. I simulate the effects of synaptic filtering similar to the transfer properties of the synapse between photoreceptors and 1st order neurons (chapter 4) and find that the transfer characteristics reduce noise originating in the photoreceptors themselves thereby enhancing response discriminability. Similarly, the synaptic transfer properties of rod - rod bipolar synapses in the mouse retina have been found to improve the rod bipolar response reliability at visual threshold by rejecting unreliable signal components (van Rossum and Smith, 1998; Field and Rieke, 2002; Armstrong-Gold and Rieke, 2003).
Together with synaptic filtering both invertebrates and vertebrates use convergence of signals conveyed by parallel elements to reduce uncorrelated noise. Convergence is accomplished by the direct electrical coupling or by dendritic integration. In the fly retina coupling of photoreceptors (e.g Meinertzhagen and O'Neil, 1991) has been shown to increase the sensitivity of 1st-oder neurons at visual threshold (Dubs et al., 1981). Similarly, electrical coupling can be found between rods as well as cones in the vertebrate retina (Hornstein et al., 2005). Convergence of many input signals takes place at subsequent processing stages in the visual system, i.e. on the dendrites of bipolar cells and ganglion cells in the vertebrate retina (e.g. Tsukamoto et al., 2001) as well as on the tangential cell dendrites in the fly visual system (e.g. Brotz et al., 1996).
Mimicking correlated noise (chapter 5) revealed a much stronger impact of the noise on the H1 responses than in the uncorrelated situation which corresponds more closely to the natural situation where photon noise in different photoreceptors is uncorrelated. This finding underlines the importance of convergence to remove uncorrelated noise. The

impact of photoreceptor coupling in the fly retina, however, on the response discriminability in 1st oder interneurons needs to be investigated. This would further allow to test whether the predictions about effect of synaptic filtering on response discriminability, made in chapter 4, are correct.

Functional implications of modulating background input A different kind of noise was investigated in chapter 6. Neurons embedded in networks receive two types of inputs which have been considered as drivers and modulators (Sherman and Guillery, 1998). While driving input is thought to carry relevant information, modulating input is assumed to be induced by noise in presynaptic elements. The specific input organisation of fly tangential cells entails that optic flow not matching the preferred direction, like motion orthogonal to the preferred direction, activates excitatory and inhibitory inputs in equal shares simultaneously. This kind of input can be considered as modulating input since it does not drive the neuron, but affects the computation of preferred direction motion. In Chapter 6 I analysed the consequences of such background input, which on its own did not excite or inhibit the tangential cell, for response gain and for computationally important features like direction tuning and the representation of stimulus velocity. I found that the gain is significantly reduced while direction tuning and representation of pattern velocity are very robust.
The results of this study lead to the hypothesis that the gain of all cells of the tangential cell ensemble, irrespective of their actual preferred optic flow pattern, is constantly equalised by the modulating component of the visual input. In situations in which perceived optic flow matches the preferred optic flow of a particular tangential cell, the cell is strongly excited. However, concomitantly, its gain is reduced due to increased membrane conductance induced by the excitatory synaptic input. This optic flow pattern does not excite all tangential cells. It does not match the preferred optic flow patterns of many other tangential cells. Thus, for the latter cells the modulating input component may prevail, and the gain is reduced by combined excitatory and inhibitory input to a similar extent as in the driven tangential cell. Therefore, the specific input organisation of tangential cells might be a key feature to match the gain of the whole tangential cell ensemble to the actual stimulus conditions. This hypothesis needs to be tested in future experiments where, instead of the artificial stimuli used here for systems analysis, optic flow stimuli and modifications of them are used that resemble input in behavioural situations.

References

Armstrong-Gold C, Rieke F (2003) Bandpass Filtering at the Rod to Second-Order Cell Synapse in Salamander (Ambystoma tigrinum) Retina. J Neurosci 23: 3796–3806.

Baylor D, Lamb T, Yau K (1979) Responses of Retinal Rods to Single Photons. J Physiol 288: 613–634.

Bendat J, Piersol A (2000) Random Data: Measurements and Procedures. 3rd ed., John Wiley and Sons.

Berry M, Warland D, Meister M (1997) The Structure and Precision of Retinal Spike Trains. PNAS 94: 5411–5416.

Borst A, Egelhaaf M, Haag J (1995) Mechanisms of Dendritic Integration Underlying Gain Control in Fly Motion-Sensitive Interneurons. J Comput Neurosci 2: 5–18.

Borst A, Haag J (1996) The Intrinsic Electrophysiological Characteristics of Fly Lobula Plate Tangential Cells: I. Passive Membrane Properties. J Comput Neurosci 3: 313–336.

Borst A, Haag J (2001) Effects of Mean Firing on Neural Information Rate. J Comput Neurosci 10: 213–221.

Borst A, Haag J (2002) Neural Networks in the Cockpit of the Fly. J Comp Physiol [A] 188: 419–437.

Borst A, Theunissen F (1999) Information Theory and Neural Coding. Nat Neurosci 2: 947–957.

Bouman M, van de Grind M, Zuidema P (1985) Quantum Fluctuations in Vision. In: Wolf E, editor, Progress in optics., pp. 79–144, Amsterdam, New York, Oxford, Tokyo: North Holland.

Britten K, Shadlen M, Newsome W, Movshon J (1992) The Analysis of Visual Motion: A Comparison of Neuronal and Psychophysical Performance. J Neurosci 12: 4745–4765.

Britten K, Shadlen M, Newsome W, Movshon J (1993) Responses of Neurons in Macaque MT to Stochastic Motion Signals. Vis Neurosci 10: 1157–1169.

Brotz T, Gundelfinger E, Borst A (1996) Cholinergic and GABAergic Receptors on Fly Tangential Cells and their Role in Visual Motion Detection. J Neurophysiol 76: 1786–1799.

Chance F, Abbott L, Reyes A (2002) Gain Modulation from Background Synaptic Input. Neuron 35: 773–782.

Dayan P, Abbott L (2001) Theoretical Neuroscience: Computational and Mathematical Modeling of Neural Systems. MIT Press.

de Ruyter van Steveninck R, Bialek W (1995) Reliability and Statistical Efficiency of a Blowfly Movement-Sensitive Neuron. Phil Trans R Soc Lond B 348: 321–340.

de Ruyter van Steveninck R, Borst A, Bialek W (2001) Real-Time Encoding of Motion: Answerable Questions and Questionable Answers from the Fly's Visual System. In: Zanker J, Zeil J, editors, Motion Vision, pp. 279–306, Berlin, Heidelberg, New York: Springer.

de Ruyter van Steveninck R, Laughlin S (1996) The Rate of Information Transfer at Graded-Potential Synapses. Nature 379: 642–645.

de Ruyter van Steveninck R, Lewen G, Strong S, Koberle R, Bialek W (1997) Reproducibility and Variability in Neural Spike Trains. Science 275: 1805–1808.

Destexhe A, Rudolph M, Pare D (2003) The High-Conductance State Of Neocortical Neurons *in vivo*. Nat Rev Neurosci 4: 739–751.

DeVries S, Qi X, Smith R, Makous W, Sterling P (2002) Electrical Coupling between Mammalian Cones. Current Biology 12: 1900–1907.

Douglass J, Strausfeld N (1995) Visual Motion Detection Circuits in Flies: Peripheral Motion Computation by Identified Small-Field Retinotopic Neurons. J Neurosci 15: 5596–5611.

Dubs A, Laughlin S, Srinivasan M (1981) Single Photon Signals in Fly Photoreceptors and First Order Interneurones at Behavioral Threshold. J Physiol 317: 317–334.

Dunn F, Doan T, Sampath A, Rieke F (2006) Controlling the Gain of Rod-Mediated Signals in the Mammalian Retina. J Neurosci 26: 3959–3970.

Egelhaaf M (1985) On the Neuronal Basis of Figure-Ground Discrimination by Relative Motion in the Visual System of the Fly: II. Figure Detection Cells, A New Class of Interneurones. Biol Cybern 52: 195–209.

Egelhaaf M (2006) The Neuronal Computation of Visual Motion Information. In: Warrent E, Nilsson DE, editors, Invertebrate Vision, pp. 399–461, Cambridge University Press.

Egelhaaf M, Borst A (1993) Motion Computation and Visual Orientation in Flies. Comp Biochem Physiol 104A: 659–673.

Egelhaaf M, Borst A, Reichardt W (1989) Computational Structure of a Biological Motion-Detection System as Revealed by Local Detector Analysis in the Fly's Nervous System. J Opt Soc Am A 6: 1070–1087.

Egelhaaf M, Kern R, Krapp H, Kretzberg J, Kurtz R, et al. (2002) Neural Encoding of Behaviourally Relevant Visual-Motion Information in the Fly. TINS 25: 96–102.

Egelhaaf M, Warzecha A (1999) Encoding of Motion in Real Time by the Fly Visual System. Curr Opin Neurobiol 9: 454–460.

Fellous J, Rudolph M, Destexhe A, Sejnowski T (2003) Synaptic Background Noise Controls the Input/Output Characteristics of Single Cells in an *in vitro* Model of *in vivo* Activity. Neuroscience 122: 811–829.

Field G, Rieke F (2002) Nonlinear Signal Transfer from Mouse Rods to Bipolar Cells and Implications for Visual Sensitivity. Neuron 34: 773–785.

Field G, Sampath A, Rieke F (2005) Retinal Processing Near Absolute Threshold: From Behavior to Mechanism. Annu Rev Physiol 67: 491–514.

Franks K, Stevens C, Sejnowski T (2003) Independent Sources of Quantal Variability at Single Glutamatergic Synapses. J Neurosci 23: 3186–3195.

Green D, Swets J (1974) Signal Detection Theory and Psychophysics. Robert Krieger Publ. Comp., Huntington, New York.

Haag J, Borst A (2002) Dendro-Dendritic Interactions between Motion-Sensitive Large-Field Neurons in the Fly. J Neurosci 22: 3227–3233.

Haag J, Theunissen F, Borst A (1997) The Intrinsic Electrophysiological Characteristics of Fly Lobula Plate Tangential Cells: II. Active Membrane Properties. J Comput Neurosci 4: 349–369.

Hausen K (1976) Functional charaterization and anatomical identification of motion sensitive neurons in the lobula plate of the blowfly *Calliphora erythrocephala*. Z Naturforsch 31: 629–633.

Hausen K (1982) Motion Sensitive Interneurons in the Optomotor System of the Fly. I. The Horizontal Cells: Structure and Signals. Biol Cybern 45: 143–156.

Hecht S, Shlaer S, Pirenne M (1942) Energy, Quanta, and Vision. J Gen Physiol 25: 819–840.

Hengstenberg R (1982) Common Visual Response Properties of Giant Vertical Cells in the Lobula Plate of the Blowfly Calliphora. J Comp Physiol [A] 149: 179–193.

Hornstein E, Verweij J, Li P, Schnapf J (2005) Gap-junctional coupling and absolute sensitivity of photoreceptors in macaque retina. J Neurosci 25: 11201–11209.

James A (1992) Nonlinear Operator Network Models of Processing in the Fly Lamina. In: Pinter R, Nabet B, editors, Nonlinear Vision: Determination of Neural Receptive Fields, Function, and Networks, chap. 2, CRC Press.

Juusola M, French A (1997) Visual Acuity for Moving Objects in First- and Second-order Neurons of the Fly Compound Eye. J Neurophysiol 77: 1487–1495.

Juusola M, Hardie R (2001) Light Adaptation in *Drosophila* Photoreceptors: I. Response Dynamics and Signaling Efficiency at 25 Degrees C. J Gen Physiol 117: 3–25.

Juusola M, Kouvalainen E, Jarvilehto M, Weckström M (1994) Contrast Gain, Signal-to-Noise Ratio, and Linearity in Light-Adapted Blowfly Photoreceptors. J Gen Physiol 104: 593–621.

Kara P, Reinagel P, Reid R (2000) Low Response Variability in Simultaneously Recorded Retinal, Thalamic, and Cortical Neurons. Neuron 27: 635–646.

Karmeier K, Krapp H, Egelhaaf M (2003) Robustness of the Tuning of Fly Visual Interneurons to Rotatory Optic Flow. J Neurophysiol 90: 1626–1634.

Kern R, van Hateren J, Michaelis C, Lindemann J, Egelhaaf M (2005) Function of a Fly Motion-Sensitive Neuron Matches Eye Movements During Free Flight. PLoS Biol 3: e171.

Krapp H, Hengstenberg B, Hengstenberg R (1998) Dendritic Structure and Receptive-Field Organization of Optic Flow Processing Interneurons in the Fly. J Neurophysiol 79: 1902–1917.

Laughlin S (1994) Matching Coding, Circuits, Cells, and Moleculees to Signals: General Principals of Retinal Design in the Fly's Eye. Progress in Retinal and Eye Research 13: 165–196.

Laughlin S, Howard J, Blakeslee B (1987) Synaptic Limitations to Contrast Coding in the Retina of the Blowfly *Calliphora*. Proc R Soc Lond B Biol Sci 231: 437–467.

Levine M, Cleland R BGand Zimmerman (1992) Variability of Responses of Cat Retinal Ganglion Cells. Vis Neurosci 8: 277–279.

Levine M, Zimmerman R, Carrion-Carire V (1988) Variability in Responses of Retinal Ganglion Cells. Journal of the Optical Society of America A 5: 593–597.

Lewen G, Bialek W, de Ruyter van Steveninck R (2001) Neural Coding of Naturalistic Motion Stimuli. Network 12: 317–329.

Lillywhite P (1977) Single Photon Signals and Transduction in an Insect Eye. J Comp Physiol [A] 122: 189–200.

Lillywhite P, Dvorak D (1981) Responses to Single Photons in a Fly Optomotor Neurone. Vis Res 21: 279–290.

Machens C, Stemmler M, Prinz P, Krahe R, Ronacher B, et al. (2001) Representation of Acoustic Communication Signals by Insect Auditory Receptor Neurons. J Neurosci 21: 3215–3227.

Meinertzhagen I, O'Neil S (1991) Synaptic Organization of Columnar Elements in the Lamina of the Wild Type in *Drosophila melanogaster*. J Comp Neurol 305: 232–263.

Prescott S, De Koninck Y (2003) Gain Control of Firing Rate by Shunting Inhibition: Roles of Synaptic Noise and Dendritic Saturation. PNAS 100: 2076–2081.

Prinz A, Abbott L, Marder E (2004) The Dynamic Clamp Comes of Age. Trends Neurosci 27: 218–224.

Reichardt W (1965) Quantum Sensitivity of Light Receptors in the Compound Eye of the Fly *Musca*. Cold Spring Harbor Symp Quant Biol 30: 505–515.

Reinagel P, Reid R (2000) Precise Firing Events are Conserved Across Neurons. J Neurosci 22: 6437–6841.

Roberts A, Bush B (1981) Neurones Without Impulses. Cambridge University Press: London, New York.

Schilstra C, van Hateren J (1998) Stabilizing Gaze in Flying Blowflies. Nature 395: 654.

Schneeweis J DM; Schnapf (2000) Noise and Light Adaptation in Rods of the Macaque Monkey. Vis Neurosci 17: 659–666.

Shannon C (1948) A Mathmatical Theory of Communication. The Bell System Technical Journal 27: 379–423.

Shannon C (1998) Communication in the Presence of Noise. Proceedings of the IEEE 86: 447–457, reprint from the Proceedings of the IRE, vol. 37 no. 1, pp. 10-21, Jan. 1949.

Sherman S, Guillery R (1998) On the Actions that one Nerve Cell can have on Another: Distinguishing "Drivers" from "Modulators". PNAS 95: 7121–7126.

Simmons P (1999) The Performance of Synapses that Convey Discrete Graded Potentials in an Insect Visual Pathway. J Neurosci 19: 10584–10594.

Single S, Haag J, Borst A (1997) Dendritic Computation of Direction Selectivity and Gain Control in Visual Interneurons. J Neurosci 17: 6023–6030.

Strausfeld N (1979) Atlas to an Insect Brain. Berlin Heidelberg New York, Springer.

Tolhurst D, Movshon J, Dean A (1983) The Statistical Reliability of Signals in Single neurons in Cat and Monkey Visual Cortex. Vision Res 23: 775–785.

Tsukamoto Y, Morigiwa K, Ueda M, Sterling P (2001) Microcircuits for Night Vision in Mouse Retina. J Neurosci 21: 9616–8623.

Uusitalo R, Juusola M, Weckström M (1995) Graded Responses and Spiking Properties of Identified First-Order Visual Interneurons of the Fly Compound Eye. J Neurophysiol 73: 1782–1792.

van Hateren J (1997) Processing of Natural Time Series of Intensities by the Visual System of the Blowfly. Vision Res 37: 3407–3416.

van Hateren J, Snippe H (2001) Information Theoretical Evaluation of Parametric Models of Gain Control in Blowfly Photoreceptor Cells. Vision Res 41: 1851–1865.

van Rossum M, Smith R (1998) Noise Removal at the Rod Synapse of Mammalian Retina. Vis Neurosci 15: 809–821.

Vähäsöyrinki M, Niven J, Hardie M RC Weckström, Juusola M (2006) Robustness of Neural Coding in *Drosophila* Photoreceptors in the Absence of Slow Delayed Rectifier K^+ Channels. J Neurosci 26: 2652–2660.

Victor J, Purpura K (1997) Metric-Space Analysis of Spike Trains: Theory, Algorithms and Application. Coumput Neural Syst 8: 127–164.

Vogels R, Spileers W, Orban G (1989) The Response Variability of Striate Cortical Neurons in the Behaving Monkey. Exp Brain Res 77: 432–436.

Warzecha AK, Egelhaaf M (1999) Variability in Spike Trains During Constant and Dynamic Stimulation. Science 283: 1927–1930.

Warzecha AK, Egelhaaf M (2001) Neuronal Encoding of Visual Motion in Real-Time. In: Zanker J, Zeil J, editors, Motion Vision - Computational, Neural, and Ecological Constraints, pp. 239–277, Berlin, Heidelberg, New York: Springer.

Warzecha AK, Kretzberg J, Egelhaaf M (2000) Reliability of a Fly Motion-Sensitive Neuron Depends on Stimulus Parameters. J Neurosci 20: 8886–8896.

White J, Rubinstein J, Kay A (2000) Channel Noise in Neurons. Trends Neurosci 23: 131–137.

Zador A (1998) Impact of Synaptic Unreliability on the Information Transmitted by Spiking Neurons. J Neurophysiol 79: 1219–1229.

3 Two Measures, Two Interpretations - Shannon Information Capacity and Response Discrimination as Measures of Photoreceptor Coding Performance

The content of this chapter has been submitted for publication: Jan Grewe, Matti Weckström, Martin Egelhaaf, and Anne-Kathrin Warzecha: *Two Measures, Two Interpretations - Shannon Information and Stimulus Discrimination as Measures of Photoreceptor Coding Performance*

3.1 Summary

Response variability is one fundamental issue in neural coding because it affects all information processing. Measures derived from information theory (Shannon, 1948) or signal detection theory(Green and Swets, 1974) have been applied to quantify the coding performance of individual neurons or neuronal populations. But how are these measures related and what do they reveal about the systems analyzed? We address these questions using time-dependent responses of blowfly photoreceptors, since their response characteristics allow the easy calculation of information capacities(de Ruyter van Steveninck and Laughlin, 1996; Juusola et al., 1996; van Hateren and Snippe, 2001). We studied the performance of single photoreceptors in encoding white noise light intensity fluctuations at different contrasts by comparing the information capacity estimated from the signal-to-noise ratio (SNR) of responses with the discriminability of the response time course. Surprisingly, a safe discrimination is possible even if the SNR is well below unity and thus, the information capacity of the photoreceptor response is low. Applying one or the other measure may therefore lead to very different interpretations concerning the system's coding performance. We stress that neither measure alone tells the whole story and that the arbitrariness in their selection can only be resolved if information coding is seen in its functional context.

3.2 Results and Discussion

Some of the most fundamental questions in neuroscience address the stimulus features encoded by a sensory system, the amount of information that can be transmitted given the neuronal response variability, the timescale on which relevant information is encoded, or the nature of the neural code. Many accounts applied information theory to quantify the amount of information conveyed by neuronal responses (Borst and Theunissen, 1999; Haag and Borst, 1997; Koch et al., 2004; Passaglia and Troy, 2004). Others characterised the reliability of synaptic transmission (de Ruyter van Steveninck and Laughlin, 1996; Simmons and de Ruyter van Steveninck, 2005). Discriminability measures have been applied, for instance, to estimate the relevant timescale of neuronal coding (Kretzberg et al., 2001; Machens et al., 2001) or to quantify the response reliability (Grewe et al., 2003; Chichilnisky and Rieke, 2005).

Here we compared estimates of system performance obtained from information theory and discrimination methods based on the same set of responses. This study was done on an intensively investigated sensory system, the photoreceptors in the blowfly (*Calliphora vicina*) retina (de Ruyter van Steveninck and Laughlin, 1996; Juusola and de Polavieja, 2003; van Hateren and Snippe, 2001). Single photoreceptors were stimulated with Gaussian distributed random light intensity fluctuations of different contrasts ('c', defined as the standard deviation over the mean luminance; figure 3.1a, b) superimposed on a background luminance. The applied contrasts ranged from no modulation at all (constant luminance) to the average contrast of natural scenes ($c_{natural}$=0.31; Laughlin et al., 1987). With increasing contrast the response amplitude increases, but the standard deviation representing response variability stays about the same (figure 3.1c). Accordingly, the noise power spectral densities (referred to as N(f), dashed lines figure 3.2a) remain at the same level independent of the respective stimulus contrast indicating the additive nature of the noise. Both the mean response as well as the membrane voltage noise are normally distributed and can be fitted well with a Gaussian function (figure 3.1d). Together with the almost linear light intensity coding in blowfly photoreceptors (Juusola et al., 1995) these conditions allowed the calculation of the information capacity (Shannon, 1998), R, from the ratio of average response and noise power spectral densities [S(f) and N(f), respectively]:

$$R = \int_0^\infty df log_2 \left[1 + \frac{S(f)}{N(f)}\right] \tag{3.1}$$

Since S(f) (solid lines in figure 3.2a) increases with increasing contrast while the different N(f) stay nearly the same, the SNR (figure 3.2b) increases with increasing stimulus contrast (Howard et al., 1987). For all tested contrasts but the largest (0.31) the SNR is well below unity for the entire frequency range, indicating that the noise component dominates the individual photoreceptor responses. Parallel to the SNR the amount of transmitted information and the bandwidth in which information is transmitted increases with contrast (figure 3.2c). The total information capacity (equation 3.1) increases with increasing contrast, initially very slowly and steeply only beyond the contrast of 0.035 (figure 3.4). One may conclude that stimuli with a contrast below 0.035 are hardly transmitted at all, because signals appear to be buried in noise.

In the second analysis of photoreceptor performance we formulated a discrimination task in which we tried to discriminate the cell responses to a certain white noise stimulus

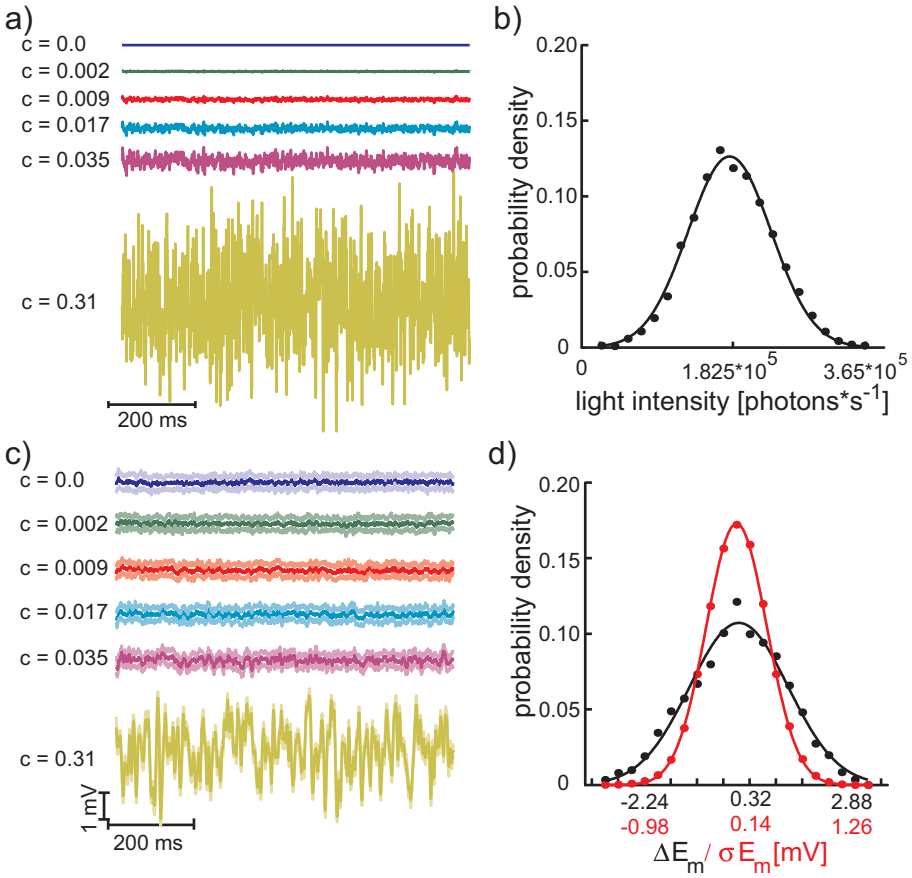

Figure 3.1: Stimulus and response properties. **(a)** Stimulus traces of different contrast. The contrast is defined as the ratio of standard deviation of the light intensity modulation and the mean light intensity ($3.04 \cdot 10^4$ effective photons per second and receptor). The light intensity values were drawn from normal distribution and the sequences were lowpass filtered with a 2nd order Butterworth filter with 256 Hz cutoff. **(b)** Probability density of the 0.31 contrast stimulus with a Gaussian fit. **(c)** Typical responses taken from a single cell with 25 trials at each contrast. Shown are the average response $\pm$ the standard deviation (lighter colours). **(d)** Probability density functions of cell response (black dots) and the response noise (red dots) fitted with Gaussian functions.

from those to different white noise stimuli. We therefore presented two sets of stimuli, one being 25 exact repetitions of the same white noise sequence (*reference stimuli*) and the other a set of 25 presentations of statistically equivalent but different sequences (*test stimuli*) with the same contrast and cutoff frequency (figure 3.3a). This procedure was repeated at each contrast level. We took the response traces used above for the SNR analysis as *reference responses* to ensure that the two neuronal performance measures are assessed on the basis of the same data. For each *reference response* two distances were determined: (i) the average distance to the other *reference responses* $\langle D_r \rangle$ and (ii) the average distance to the *test responses* $\langle D_t \rangle$ (figure 3.3b). The individual distances

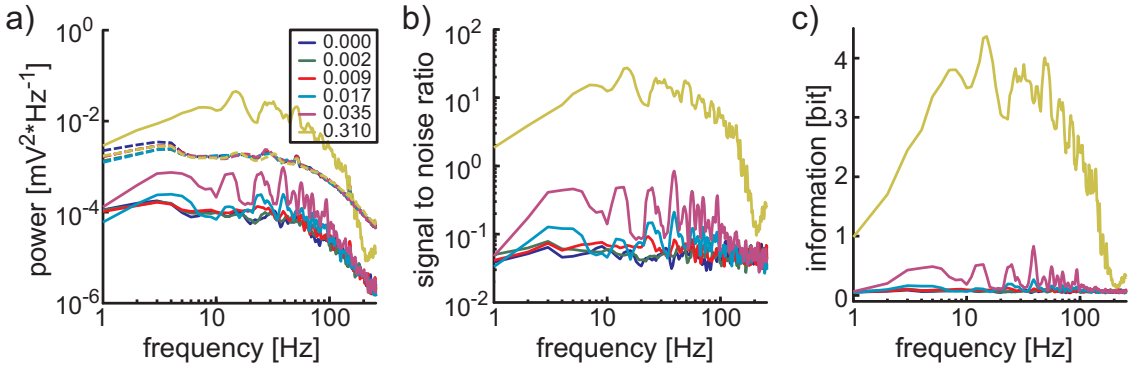

Figure 3.2: Response characteristics in the frequency domain. **(a)** S(f), the power spectral density of the stimulus induced response component (solid lines), and N(f), the power spectral density of the noise (dashed lines), normalised to the response or noise mean square amplitude. **(b)** Signal to noise ratios at the six different contrasts used [same colour code as in a]. **(c)** Shannon information as a function of frequency at the different contrasts [same colour code as in a]. Information estimated from the signal to noise ratio as: $log_2[1 + S(f)/N(f)]$. All spectra were smoothed using a 4 point running average.

were calculated as a root-mean-square distance according to

$$D_{x,y} = \sqrt{\frac{1}{N}\sum_{i=1}^{N}(x_i - y_i)^2}, \tag{3.2}$$

with x_i and y_i being the two response values (either two different *reference responses* or a *reference* and a *test response*) at time i and N the length of the data segment, i.e. the number of data points included in the analysis.

For each reference response it was assessed whether $\langle D_t \rangle$ was larger than $\langle D_r \rangle$. This was expected if the fluctuations in light intensity affected the responses in a distinct way. The percentage of correct discriminations thus indicated the fraction of reference responses for which was larger than . The discrimination performance was estimated at all contrasts except the largest (figure 3.3c).

As expected, the discriminability increases with increasing contrast. Unlike the (Shannon) information capacity (figure 3.4), the discrimination performance has its strongest increment already at contrasts exceeding only 0.009. A discrimination performance of 75% correct decisions can be achieved at a contrast of only about 0.0138 (estimated from the logistic fit, equation 3.3). Thus, this measure of neuronal performance allowed us to draw the somewhat paradoxical conclusion that the temporal structure of the responses can be discriminated safely already at contrasts where the SNR is much smaller than unity and there is hardly any information in the responses in terms of the SNR measure. In fact, the information capacity at the contrast of 0.017 is, on average, only 4.66 bit/s above the zero contrast information capacity (21.91±1.79 bit/s and 17.25±2.46 bit/s for 0.017 and zero contrast respectively). At zero contrast any information capacity larger that zero is attributable to the bias in the SNR obtained from limited data sets (van Hateren and Snippe, 2001). We therefore treated the information capacity estimate at zero contrast as a baseline. The gain of information capacity of a few bits/s in the low

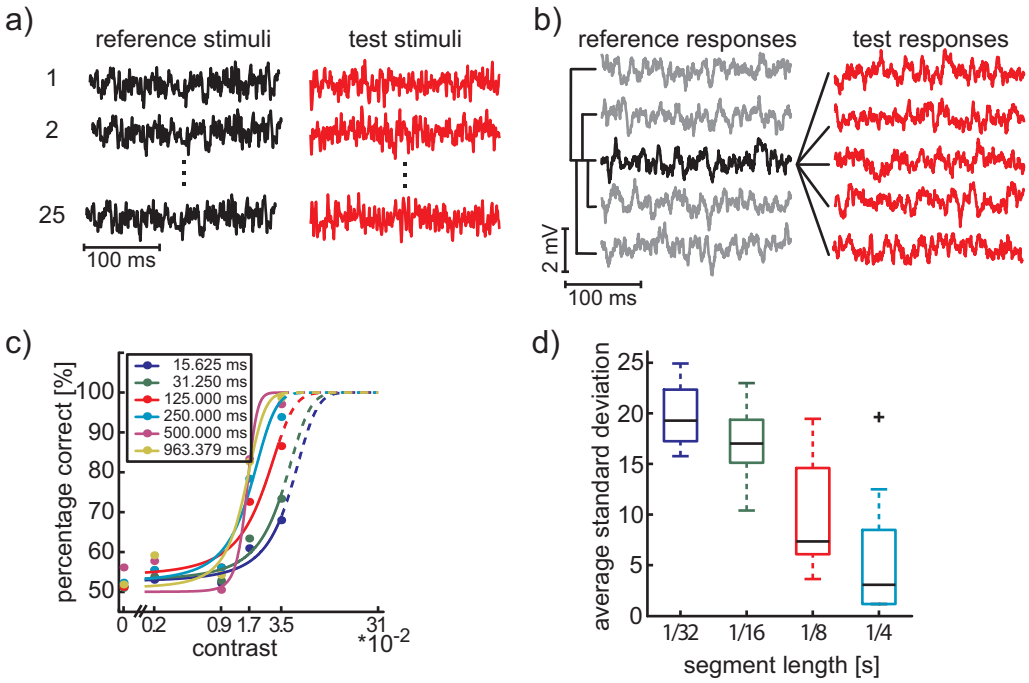

Figure 3.3: Discrimination task. **(a)** Stimulus illustration for the discrimination task at one contrast level. Left hand column: the *reference stimulus* which is repeated 25 times; right hand column: *test stimuli* at the same contrast level. Individual stimuli with the same statistics as the *reference stimulus*. **(b)** The way, the two distances $\langle D_r \rangle$ and $\langle D_t \rangle$ were estimated for each *reference response* (e.g. the highlighted one in the left box). *Test responses* in red. **(c)** Discriminability of reference and *test responses* as a function of contrast (mean ± s.e.) fitted with a logistic function (equation 3.3) ranging from 50 to 100% calculated using data segments of different lengths. **(d)** Uncertainty of distance estimation for the different segment lengths. For each of the 12 cells analysed, the standard deviation of discrimination performance gained in the single data segments is estimated and subsequently averaged across the cells. The two largest segment lengths give only one respectively two segments, thus no S.D. was calculated.

frequency range at contrasts below the natural contrast, however, appear to be negligible compared with what obtained at natural contrast (R = 449.46±57.79 bit/s for c = 0.31). The information capacities found here are in the range reported before and may be even larger for higher contrasts and larger average light levels (de Ruyter van Steveninck and Laughlin, 1996). It should be noted that contrasts exceeding 0.035 lead to saturated discrimination performance whereas information capacity appears to increase significantly only above that contrast level. This indicates a point above which the discrimination measure gives no additional clues about the system's capabilities to discriminate the time course of the responses.

The animal has only a limited time available to distinguish meaningful stimuli buried in noise, and the dependence of the duration of the evaluated data segments has to be considered. Both measures of coding performance depend differently on the length of data segment: the information capacity decreases slightly with decreasing segment length since the lowest resolvable frequency depends on segment length. Additionally, the use of less data degrades the reliability of the SNR estimation (which is certainly true

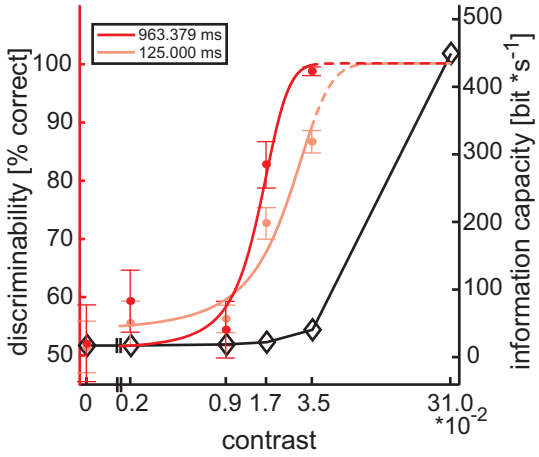

Figure 3.4: Comparison of discrimination performance and Shannon information. Dots mark the average discrimination performances at the different contrast (n = 12) ± s.e.. Data fitted with a logistic function (equation 3.3). Black diamonds mark the average information capacity. Information capacities at the lower contrasts are estimated from the same cells as the discrimination performance. At the 0.31 contrast 14 additional cells were analysed. Standard errors are smaller than marker size.

in real life discrimination tasks as well). The discrimination measure also suffers from a reduced segment length as shown in figure 3.3c, but shows insignificant differences in discrimination performance once the segment length is sufficient to reliably estimate the distance. With short segments, the reduced discrimination performance is accompanied by increased uncertainty of discrimination performance (figure 3.3d). This less reliable discrimination estimate is partly responsible for parts of the reduction in discrimination performance, due to the asymmetry of the discrimination measure, i.e. discriminability may well drop below 50% but cannot exceed 100%.

Although both measures, the SNR and the discriminability, are artificial measures of system performance, the distance estimation (equation 3.2) could well be neuronally implemented. All essential parts of the distance measure, i.e. the subtraction and the multiplicative correlation of two inputs signals are implemented for example in circuits involved in motion detection (e.g. Egelhaaf and Borst, 1993). Additionally, with a data segment of 125 ms, approximating a behaviourally relevant time for a fly to evaluate optic flow (Kern et al., 2005), i.e. the interval between subsequent saccadic turns characterizing fly orientation behaviour, two signals can be discriminated faithfully at contrasts (75% correct discrimination performance at c = 0.023). In this range the Shannon information capacity indicates hardly any increase. Here we found considerable differences between two measures of coding performance on the very first stage of visual information processing, i.e. the photoreceptor level. Related differences have been found in the electrosensory organ of the weakly electric fish (Gabbiani et al., 1996). There, signal detection and information theoretical approaches gave seemingly contradicting results after a sensory signal underwent dendritic filtering. The choice of the appropriate measure, out of the variety of applied measures (e.g. Dayan and Abbott, 2001) depends very much on the scientific question to be answered. If, for instance, the question were how many different stimulus

levels could be coded given the observed neuronal noise, the information capacity may be well suited. On the other hand, if we assume any decoding mechanism that takes temporal characteristics into account, information capacity would not be the measure of choice since it considers only the frequency content of the responses assuming their independence and not their phase relations. Instead, the discrimination measure appears appropriate to quantify the system's performance in representing the time-course of a stimulus.

3.3 Methods

Electrophysiology. Experiments were carried out on female blowflies (Calliphora vicina). The retina were accessed through a small hole cut into the fly's eye on the equatorial line close to the lateral rim. The hole was sealed with silicon grease to prevent drying-up. Sharp electrodes (Clark GC-150) were pulled on a Brown-Flaming P-97 Puller (Sutter Instruments) to have resistances of 80 to 90 $M\Omega$ when filled with 2M KCl. Recordings were done in bridge mode using a SEC-10L amplifier (npi electronics, Tamm, Germany). We accept recordings with a saturating light response of at least 50 mV and input resistance of at least 25 $M\Omega$. Responses were sampled at 4096 Hz (DAQBoard 2000, IOtech, Cleveland, OH) and stored on hard disk for offline analysis.

Light stimulation. Data shown here were collected as part of a study on motion vision therefore photoreceptors were stimulated using two LEDs (3mm diameter, 525nm light emission, type: WU-14-730GC, Vossloh-Schwabe Optoelectronic GmbH, Germany) each covering approximately 1.15° of visual space separated by 3° with one of them positioned in the optical axis of the recorded cell. The off-axis LED had only little impact on the responses of the recorded cell and, anyway, the same stimulus combinations (for on and off-axis LED) were used so that a cell received the same visual input in repeated presentations (control experiments with only a single LED revealed no different results). LEDs were driven by a voltage-to-current converter controlled by the analogue outputs of the data acquisition board, the LEDs were driven in the linear range of the current-light characteristic. Light intensities were calibrated by counting single photon responses at very low light intensities yielded with neutral density filters (Lee Filters, UK) in front of the LED.

Data analysis. Data analysis was done in MATLAB (The Mathworks, Natick, MA). Response and noise power spectral densities [S(f) and N(f)] for all but the largest contrast were calculated from 4000 data point segments (963.379 ms) zero padded to 4096 data points (1s) windowed with a 4096 point Hanning window. Power spectra were normalised to the mean square amplitude of the data. At largest contrast three such segments with 50% overlap were used, again a 4096 point Hanning window was applied. A similar method was used with the smaller data segments.
Distances were calculated from the same data stretches according to equation 3.2. The responses were lowpass filtered with a 500 Hz cutoff which is far beyond the photoreceptor cutoff. Discrimination was done according to the two average distances $\langle D_r \rangle$ and $\langle D_t \rangle$. If the difference between both was less than could be expected from electrical noise (origi-

nating form the recording setup) the according response was classified indistinguishable. Discrimination performance was fitted with a logistic function of the form:

$$P_c = \frac{1}{2} \cdot \frac{100}{1 + e^{\alpha(x_i - \beta)}} + 50, \tag{3.3}$$

with P_c the discrimination performance, x_i the contrast, α the slope, and β the position of the inflection point. The function is scaled to range from 50 to 100% correct.

References

Borst A, Theunissen F (1999) Information Theory and Neural Coding. Nat Neurosci 2: 947–957.

Chichilnisky E, Rieke F (2005) Detection Sensitivity and Temporal Resolution of Visual Signals near Absolute Threshold in the Salamander Retina. J Neurosci 25: 318–330.

Dayan P, Abbott L (2001) Theoretical Neuroscience: Computational and Mathematical Modeling of Neural Systems. MIT Press.

de Ruyter van Steveninck R, Laughlin S (1996) The Rate of Information Transfer at Graded-Potential Synapses. Nature 379: 642–645.

Egelhaaf M, Borst A (1993) Motion Computation and Visual Orientation in Flies. Comp Biochem Physiol 104A: 659–673.

Gabbiani F, Metzner W, Wessel R, Koch C (1996) From Stimulus Encoding to Feature Extraction in Weakly Electric fish. Nature 384: 564–567.

Green D, Swets J (1974) Signal Detection Theory and Psychophysics. Robert Krieger Publ. Comp., Huntington, New York.

Grewe J, Kretzberg J, Warzecha A, Egelhaaf M (2003) Impact of Photon Noise on the Reliability of a Motion-Sensitive Neuron in the Fly's Visual System. J Neurosci 23: 10776–10783.

Haag J, Borst A (1997) Encoding of Visual Motion Information and Reliability in Spiking and Graded Potential Neurons. J Neurosci pp. 4809–4819.

Howard J, Blakeslee B, Laughlin S (1987) The Intracellular Pupil Mechanism and Photoreceptor Signal: Noise Ratios in the Fly *Lucilia cuprina*. Proc R Soc Lond B Biol Sci 231: 415–435.

Juusola M, de Polavieja G (2003) The Rate of Information Transfer of Naturalistic Stimulation by Graded Potentials. J Gen Physiol 122: 191–206.

Juusola M, French A, Uusitalo R, Weckström M (1996) Information Processing by Graded-Potential Transmission through Tonically Active Synapses. Trends Neurosci 19: 292–297.

Juusola M, Uusitalo R, Weckström M (1995) Transfer of Graded Potentials at the Photoreceptor-Interneuron Synapse. J Gen Physiol 105: 117–148.

Kern R, van Hateren J, Michaelis C, Lindemann J, Egelhaaf M (2005) Function of a Fly Motion-Sensitive Neuron Matches Eye Movements During Free Flight. PLoS Biol 3: e171.

Koch K, McLean J, Berry M, Sterling P, Balasubramanian V, et al. (2004) Efficiency of Information Transmission by Retinal Ganglion Cells. Curr Biol 14: 1523–1530.

Kretzberg J, Warzecha A, Egelhaaf M (2001) Neural Coding with Graded Membrane Potential Changes and Spikes. J Comput Neurosci 11: 153–164.

Laughlin S, Howard J, Blakeslee B (1987) Synaptic Limitations to Contrast Coding in the Retina of the Blowfly *Calliphora*. Proc R Soc Lond B Biol Sci 231: 437–467.

Machens C, Stemmler M, Prinz P, Krahe R, Ronacher B, et al. (2001) Representation of Acoustic Communication Signals by Insect Auditory Receptor Neurons. J Neurosci 21: 3215–3227.

Passaglia C, Troy J (2004) Information Transmission Rates of Cat Retinal Ganglion Cells. J Neurophysiol 91: 1217–1229.

Shannon C (1948) A Mathmatical Theory of Communication. The Bell System Technical Journal 27: 379–423.

Shannon C (1998) Communication in the Presence of Noise. Proceedings of the IEEE 86: 447–457, reprint from the Proceedings of the IRE, vol. 37 no. 1, pp. 10-21, Jan. 1949.

Simmons P, de Ruyter van Steveninck R (2005) Reliability of Signal Transfer at a Tonically Transmitting, Graded Potential Synapse of the Locust Ocellar Pathway. J Neurosci 25: 7529–7537.

van Hateren J, Snippe H (2001) Information Theoretical Evaluation of Parametric Models of Gain Control in Blowfly Photoreceptor Cells. Vision Res 41: 1851–1865.

4 Intrinsic Photoreceptor Noise Reduced by Synaptic Filtering

The results presented in this chapter will be submitted for publication as: Jan Grewe, Martin Egelhaaf, and Anne-Kathirn Warzecha. *Intrinsic Photoreceptor Noise Reduced by Synaptic Filtering.*

4.1 Summary

Neuronal signals are always corrupted by noise from different sources, be it channel or synaptic noise or, in the case of the visual system, photon noise. Studies on the reliability of neuronal signalling try to unravel the noise sources and how the system deals with it. One important site of neuronal information processing is the synapse. From studies on the first synapse in the fly visual system it has been concluded on the basis of information theoretical considerations that its band-pass behaviour optimises neuronal coding by enhancing the responses to changes in the visual input, thereby reducing redundancy in the signals. Here we assess the reliability of photoreceptor responses to random brightness fluctuations in a discrimination task and investigate the impact of synaptic filtering on the discriminability of the response time-courses. We find that the filter characteristics of the first synapse can increase response discriminability if the random brightness fluctuations that are to be distinguished are superimposed on a large low frequency modulation of the background illumination. The advantage of filtering results from an increased noise induced by the slowly varying background illumination. We compare these findings with the effects of filtering on the discrimination performance of photoreceptor models that can reproduce the time course of photoreceptor responses accurately. These simulations include photon noise as the only noise source leading to response variability in the range observed experimentally. Filtering does not affect disciminability of the model responses. Comparing cellular and model noise leads to the conclusion that the increased low frequency noise is attributable to a light or activity dependent intrinsic noise source not included in the simulations. Thus, the synaptic transfer characteristic does not only reduce redundancy but also removes noise emerging within the photoreceptor itself.

4.2 Introduction

Neuronal responses are corrupted by noise from different sources. These can be intrinsic to the nervous system like ion channel (e.g. White et al., 2000) or synaptic noise (e.g. Franks et al., 2003), or, in the case of the visual system, by extrinsic noise contained in the visual input, i.e. photon noise, the random emission of photons from a light source. As a result of these noise sources neuronal responses to repeated stimulation with exactly the same stimulus may differ considerably despite a common stimulus dependent temporal structure. Since the nervous system controls an animal's behaviour, neuronal response variability limits the precision with which it can respond to environmental changes. Thus, it is likely that an animal's evolutionary fitness depends, to some extent, on the reliability of its nervous system. Consequently, different mechanisms have evolved that increase, or at least preserve, response reliability at successive levels of the nervous system.
Nervous systems invest into the reliability in different ways. For instance, convergence of about 20 rods onto one rod-bipolar cell in the mouse retina (Tsukamoto et al., 2001) or the coupling of photoreceptor axons in the fly retina (e.g. Meinertzhagen and O'Neil, 1991), sacrifices spatial resolution for enhanced response reliability. Furthermore temporal integration has been shown to increase the response reliability of spiking neurons that are driven by random input (Softky and Koch, 1993), but trades temporal resolution for response accuracy. Moreover, the transfer characteristics of synapses have been shown in several systems to enhance response reliability (e.g. Juusola et al., 1995; van Rossum and Smith, 1998; Field and Rieke, 2002). The synapses connecting vertebrate rods with rod-bipolar cells exhibit a non-linear transfer characteristic which increases the rod-bipolar reliability under dim light conditions by rejecting small rod responses which are likely to result from rod noise (Field and Rieke, 2002). Here, we addressed the potential effects of synaptic filtering on the reliability of blowfly photoreceptor responses. In the fly, the synapse linking photoreceptors to 1st order neurons, the large monopolar cells (LMCs), can be well described as a linear filter processing the photoreceptor responses (Laughlin, 1994; Juusola and French, 1997). In the light adapted state the synapse exhibits a band-pass like transfer behaviour (Juusola and French, 1997). Assuming a limited capacity of the neuronal information channel, this filtering has been concluded to be the optimal procedure to optimise coding performance when viewing natural scenes (e.g. Laughlin, 1994; Juusola et al., 1996). The power spectra of natural scenes follow a 1/f rule, meaning that the spectral power declines with frequency (f; e.g. van Hateren, 1997). This is due to the fact that neighbouring points in space and time are likely to have a similar light intensity which leads to a dominance of low frequency light intensity changes. Because of this redundancy the low frequencies are less informative than the higher frequencies. Band-pass filtering by the first synapse in the visual system attenuates the lower frequencies while it emphasises the informative higher frequencies. Reducing the redundancy in the input was concluded to lead to an efficient neuronal code (Barlow, 1961; Simoncelli and Olshausen, 2001).

By a combined experimental and modelling approach we assessed the role of synaptic filtering from a different point of view: We characterised photoreceptor response reliability using a discrimination measure (Grewe et al., 2003). This approach to led to conclusions quite different from those obtained with information theoretical approaches (Grewe et al., 2007, submitted). In the present account we compared the discriminability of experimen-

tally recorded responses with the discrimination performance after simulated synaptic filtering. We further compared the consequences of filtering on the discriminability of experimentally determined responses and of those of phenomenological photoreceptor models that have been shown to reproduce photoreceptor responses to naturalistic stimulation (van Hateren and Snippe, 2001). We extended their model by including photon noise as the only noise source. Comparison of the results gained from experimental and model data allowed us to assess the influence of nonlinearities and synaptic filtering on the system's performance.

4.3 Methods

Electrophysiology

Experiments were carried out on 1 to 7 day old female blowflies (*Calliphora vicina*) taken from the laboratory stocks. Flies were briefly immobilised with CO_2 and fixed ventral side up to a piece of glass. Legs and antennae were removed and the head bent down and fixed to the thorax with beeswax. A small hole was cut into the cornea (close to the lateral rim, on the level of the eye equator). The hole was then sealed with a drop of silicon grease to prevent the retina from drying up. Recordings were done with sharp electrodes (GC 150F-10, Clark Elektromedical, Edenbridge, UK) pulled on a Brown/Flaming P-97 Puller (Sutter Instruments, San Rafael, CA) and filled with 2M KCl. The electrodes had tip resistances of 60 to $80M\Omega$. The electrode holder's silver wire was chlorided before every recording. A SEC 10-L amplifier (npi - electronics, Germany) operated in bridge or discontinuous current clamp (DCC) mode. In DCC mode the switching frequency was about 10kHz. Only those recordings were accepted for further analysis which satisfied three criteria: (i) the resting potential in darkness had to be below -50mV, (ii) the input resistance (R_{in}), measured by injection of a 0.5 nA hyperpolarising current in DCC mode, had to be at least $25M\Omega$ (usually R_{in} was larger $30M\Omega$), and (iii) the cell response to a brief saturating light flash had to be larger than 50 mV.

Data Acquisition

The cell responses were sampled at 4096 Hz (DaqBoard2000, IOTech Inc., OH) and stored on hard disk for off-line analysis which was done in Matlab (The Mathworks, Natick, MA). The program for data acquisition was written in Delphi 7 (Borland Software Corporation). The two analogue outputs, used to control the stimulus were also paced with 4096 Hz. Additionally to the membrane potential the actual analogue output voltages were recorded as a control.

Visual stimulation

Photoreceptors were stimulated using LEDs (3mm diameter, 525nm light emission, type: WU-14-730GC, Vossloh-Schwabe Optoelectronic GmbH, Germany, covering approximately 1.15° of visual space). Since the data were collected as part of a study on motion vision two LEDs were used separated by 3°. One of them was positioned in the optical axis of the recorded cell. The off-axis LED had only little impact on the responses of the

recorded cell (control experiments with only a single LED revealed no different results). LEDs were driven by a custom built voltage-to-current converter controlled by the analogue outputs of the data acquisition board. The LEDs were driven in the linear range of the current-light characteristic. Light intensities in units of effective photons per second were calibrated by counting single photon responses at very low light intensities yielded with neutral density filters (Lee Filters, UK) in front of the LED.

Here we addressed the reliability with which the time course of a stimulus is represented by the photoreceptors. For this purpose we formulated a discrimination task in which we asked for the minimal amplitude of a brightness modulation (contrast) that made the photoreceptor responses to a certain stimulus safely recognisable among the responses to stimuli that share the same statistics but were different in detail. The contrast is defined by:

$$c = \frac{\sigma}{\overline{x}}, \tag{4.1}$$

with σ the standard deviation of the band limited (filtered with a 2nd order lowpass filter with a 256 Hz cutoff) white noise modulation and $\overline{x}$ the mean brightness. We performed the experiments at a mean brightness of about 30,000 effective photons per second. Random brightness modulations were superimposed on a background brightness including sections of constant and of 5Hz sine-wave modulated brightness (figure 4.1a).

Five different contrasts were used (c = 0, 0.0022, 0.0087, 0.0174, and 0.0348, figure 4.1b). At each contrast-level a set of 50 stimuli were presented. Half of these were exact repetitions called *reference stimuli* while the other half, called *test stimuli*, share the same statistics but were based on different random sequences and, thus, were different in detail (figure 4.1c). All 250 stimuli were presented in a pseudo-random order.

Data Analysis

We wanted to know the minimum contrast level that shaped the responses sufficiently to allow a safe discrimination of *reference* and *test responses*. Since the *reference responses* were evoked with exactly the same stimulation one can expect them to be more similar to each other than to the *test responses*, which were evoked by a different stimulation at each presentation. The similarity of the responses was estimated with a root-mean-square metric in terms of the distance D.

$$D_{x,y} = \sqrt{\frac{1}{N}\sum_{i=1}^{N}(x_i - y_i)^2}, \tag{4.2}$$

with x_i and y_i the two responses and N the number of data points. Two identical responses would have a distance D = 0. The discriminability of each reference response from the test responses is estimated by comparing the average distance within the reference responses, $\langle D_r \rangle$, with the average distance between each reference response and all test responses $\langle D_t \rangle$ (figure 4.2a). The percentage of reference responses for which $\langle D_r \rangle$ indeed is smaller than $\langle D_t \rangle$ is plotted as a function of the superimposed modulation's contrast. The resulting physiometric curve (figure 4.2b) is then fitted by a logistic function ranging from 50% to 100% correct:

$$P_c = \frac{1}{2} \cdot \frac{100}{1 + e^{\alpha(c_i - \beta)}} + 50, \tag{4.3}$$

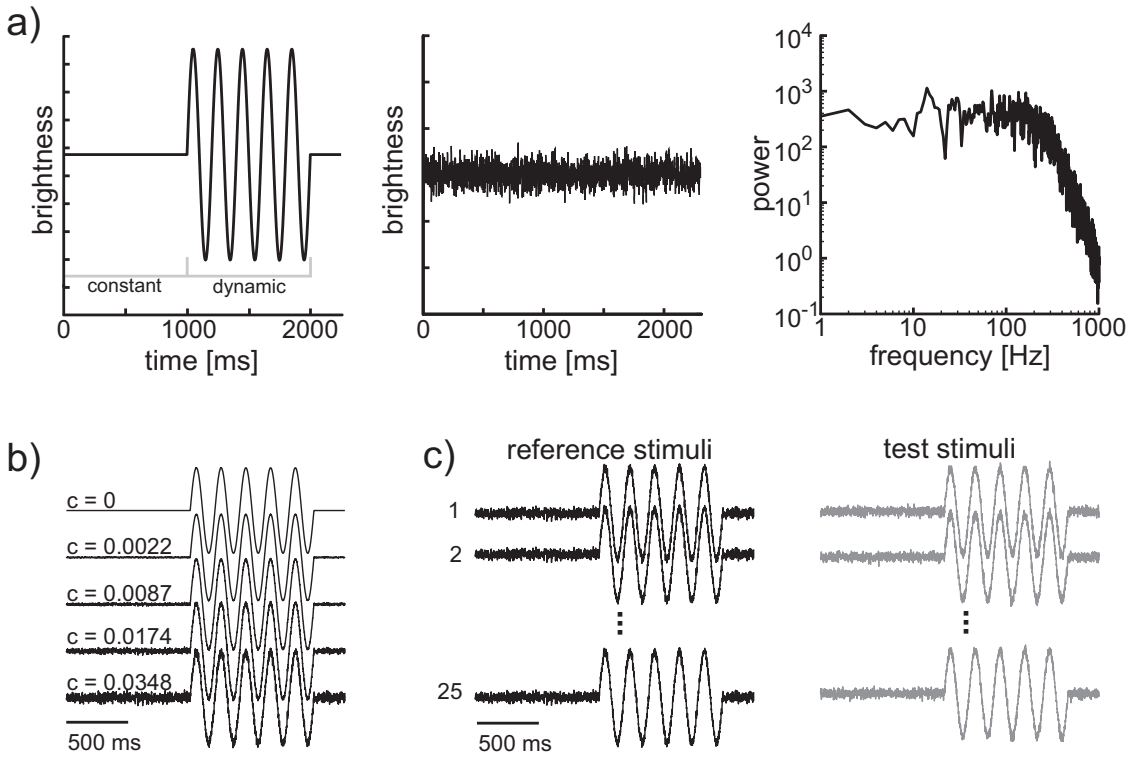

Figure 4.1: Visual stimulus. **(a)** All stimuli for the discrimination task consist of a basic structure of a constant (first second) and a dynamic (2nd second; 5Hz sine wave) background light. During this dynamic section the background luminance increases/decreases by 65% of the mean luminance. On the background a zero symmetric white noise brightness modulations (middle) is superimposed. The noise was filtered with a 2nd order Butterworth lowpass filter with a cut-off at 256 Hz (right). **(b)** The white noise sequences are scaled to give different contrasts. **(c)** At each contrast level a set of 50 stimuli is presented. 25 of which are exact repetitions (*reference stimuli*, left panel) while the other 25 share the same statistics but are different in detail (*test stimuli*, right panel). *Reference* and *test stimuli* of all contrast levels were presented in pseudorandom order.

with α representing the slope, β the position of the inflection point, and c_i the contrast. A safe discrimination was assumed to be possible if 75% of the reference responses had a smaller distance *within* the *references responses* than *between reference* and *test responses*. The contrast level at which a safe discrimination is achieved can be directly read from the parameters defining the logistic function (parameter β in equation 4.3). This threshold contrast (C_{75}) was interpreted as a measure of response reliability.

Estimating the threshold contrast from the physiometric curve has an advantage compared to testing for statistically significant differences between the distances *between* and *within*: Whereas in the case of the statistical test, the smallest differences could get significant if enough trials can be recorded for each cell, thresholding the physiometric curve makes the C_{75} largely independent of the number of trials in a single experiment and, thus, reflects in principle how well the signals can be discriminated on the basis of single trials. Of course, data points are safer if the number of trials per experiment and the numbers of experiments are larger.

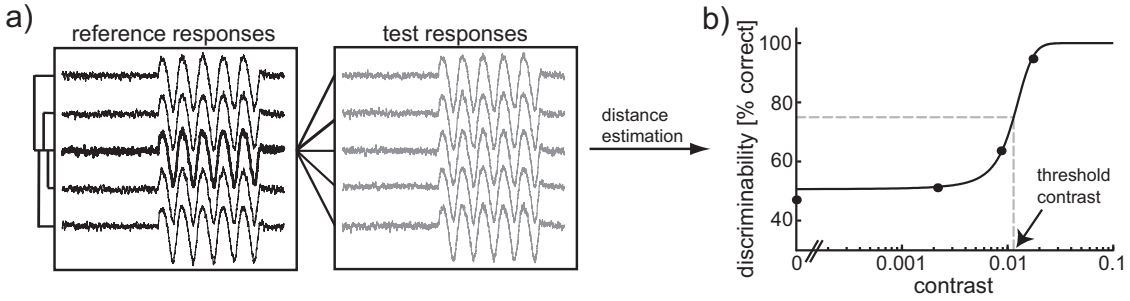

Figure 4.2: Response discrimination. (a) Each reference response (left), e.g. the bold one, is compared to all other reference responses and to all test responses (right) giving for each reference response the average distance (equation 4.2) within the reference group and between the reference response and all test responses. **(b)** The physiometric curve is defined by the percentage of reference responses for which the distance within the reference responses is smaller than the distance between the reference and the test responses as a function of the stimulus' contrast level. Data are fitted with the logistic function (equation 4.3).

Synaptic filter

The first synapse in the fly visual system changes its transfer properties with the light level (e.g. Juusola et al., 1996). At low light intensities it has lowpass characteristics and changes to a bandpass like behaviour under high light conditions. To investigate the consequences of filtering on the discriminability of the photoreceptor responses several different filters were applied to the responses. The impulse responses (figure 4.3a) of these filters were constructed according to:

$$h(t) = a_1 \cdot exp\left(\frac{-\left(ln\left(t/\tau_1\right)\right)^2}{2\sigma_1^2}\right) + a_2 \cdot exp\left(\frac{-\left(ln\left(t/\tau_2\right)\right)^2}{2\sigma_2^2}\right). \tag{4.4}$$

Using equation 4.4 five different filter kernels were constructed with the parameters shown in table 4.1. The integral under the filter was normalised to -1 indicating the sign reversal introduced by the synapse. We filtered the responses with a lowpass filter with a cutoff frequency of about 507 Hz (LP_{507}) which represents the virtually unfiltered response since the cutoff is far beyond the photoreceptor cutoff frequency (figure 4.18). The discrimination performances obtained after filtering with the LP_{507} will serve as reference. The synaptic transfer characteristic under high light were approximated by a bandpass filter (BP in table 1) with a lowpass cutoff at 75 Hz and a highpass cutoff at 20Hz We further used these low- and highpass components separately (LP_{75} and HP, respectively). Under low light conditions the synapse acts as a lowpass filter with a cutoff frequency of about 20Hz which is approximated by the LP_{20} filter.

Frequency behaviours of the filters are shown in figure 4.3b. Even though the frequency behaviour (figure 4.3b) of the HP filter does not match that of a first order highpass filter we keep on referring to it as highpass (HP). The cutoff frequencies were estimated from the power spectra as the frequency with half the maximum of the passband output which is $\frac{1}{\sqrt{2}}$ in the amplitude spectrum. The bandpass parameters were taken from (Lindemann et al., 2005) and fit the linear component of the blowfly LMC response (Juusola et al., 1995).

Table 4.1: Kernel parameter.

	cutoffs [Hz] (HP/LP)	a_1	τ_1	σ_1	a_2	τ_2	σ_2
LP_{507}	–/507	0	0	0	-1	10	0.025
BP	20/75	-1.2	10	0.197	0.35	14	0.345
LP_{75}	–/75	0	0	0	-1	10	0.15
HP	20/–	-5	0.5	0.045	0.095	2	1
LP_{20}	–/20	0	0	0	-1	11	0.45

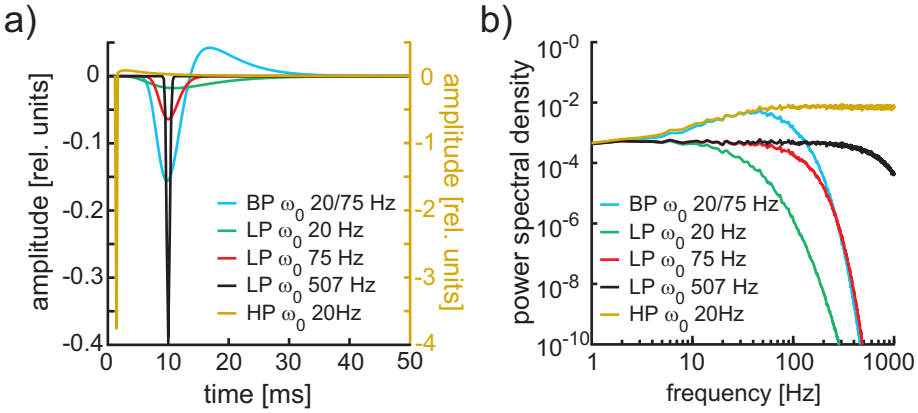

Figure 4.3: Synaptic filter kernels. (a) Different 1st order Wiener kernels as used in the data analysis. The cutoff frequencies of the bandpass, lowpass, and highpass filters (BP, LP, and HP, respectively) are estimated as the frequencies at which half of the passband power was reached. **(b)** Frequency behaviour of the different filters in form of power spectra. Spectra were calculated as the power spectra of a 100 second white noise sequence sampled at 4096 Hz convolved with the kernels shown in **(a)**. Spectra were normalised to the variance of the input signal. Note: although the HP frequency behaviour does not entirely match the frequency behaviour of a first order highpass filter we keep referring to it as highpass.

Photoreceptor Models

Experimental results were compared to phenomenological photoreceptor models. The models were either a linear temporal filter ('linear model') or a linear temporal filter followed by a static nonlinearity ('LN-model'). The only noise source that was always present in the simulations was photon noise, the random emission and absorption of individual photons. For this the stimuli given as continuous functions of time were transformed into series of individual photons. Photon emission was modelled as a Poisson process. The probability of photon absorption was estimated on the basis of the actual light intensity in the original experimental stimulus. The simulations were done with a temporal resolution of 409.6 kHz. The linear model consisted of a 1st-order Wiener kernel estimated from experimentally determined photoreceptor responses to white noise light fluctuations. It was calculated in the frequency domain (e.g. van Hateren and Snippe, 2001):

$$H(f) = \frac{\langle r(f) \cdot s(f)^* \rangle}{\langle s(f) \cdot s(f)^* \rangle}, \tag{4.5}$$

with H(f), r(f), and s(f) the Fourier spectra of the forward filter, the response, and the stimulus, respectively. * denotes the complex conjugate and the brackets denote averaging over several segments of the stimulus and responses, respectively. This forward filter was estimated from the mean response to a white-noise brightness sequence (averaged across 135 trials). Frequency components of H(f) beyond 1024 Hz were set to zero, since these frequency components are a consequence of residual noise in the average response that could not be eliminated by averaging. After eliminating the high-frequency noise, the impulse response was scaled to the same area as the impulse responses of the complete filter. Noise reduction did not significantly change the reconstruction (not shown).
The output of a linear model can reproduce the real photoreceptor responses as long as the stimulus contrast is relatively low. Larger contrasts lead to non-linear behaviours of the photoreceptor response. We accounted for this by using a static non-linearity fitted to the experimentally observed input-output characteristic (figure 4.11 centre). The static nonlinearity was a least square fit to a saturation nonlinearity of the form:

$$y = \alpha \cdot [\beta - log(x - \gamma) - \delta] \,, \tag{4.6}$$

with y the cell response and x the linear model response. α, β, γ, and δ are free parameters defining the shape. The intensity-response functions measured from step responses suggest a sigmoid shape of the input output characteristic (e.g. Matic and Laughlin, 1981). Since our data do not support this characteristic we kept the logarithmic shape.

4.4 Results

Frequently reliability of photoreceptor responses is assessed by information theoretical approaches. Here we alternatively assessed it by the response discriminability which we could show to lead to different conclusions about the photoreceptor coding performance (Grewe et al., 2007, submitted). As a first step of analysis we wanted to find out the minimal contrast that shaped the photoreceptor responses sufficiently to grant a safe discrimination of reference and test responses (see methods). For this, the discriminability was estimated for responses evoked by different contrast stimuli (figures 4.1 and 4.2). In a second step effects of synaptic filtering on response discriminability were estimated by applying different linear filters (figure 4.3) to the photoreceptor responses modelling postsynaptic responses. Finally these results were compared with predictions from phenomenological photoreceptor models.

Experimental Data

The photoreceptor responses follow the time-course of the stimulus brightness used in the discrimination task (figure 4.4). The membrane potential deflections are strongly asymmetric when the background brightness is sinusoidally modulated (dynamic section, comp. figure 4.1), i.e. hyperpolarising deflections deviate by up to 7.5mV from the response amplitude at constant background light, while depolarising deflections reach only 4.1mV at maximum. This asymmetry indicates a nonlinear relationship between light intensity and cell response. It is most likely a consequence of the activation of slow

delayed rectifiers (K^+ channels) which prevent the cell from saturating (Vähäsöyrinki et al., 2006). The average standard deviations of the individual responses from the corresponding average response during the constant (1st second of response) and dynamic (2nd second) response sections (compare figure 4.1a) are almost the same: 0.34mV and 0.35mV, respectively.

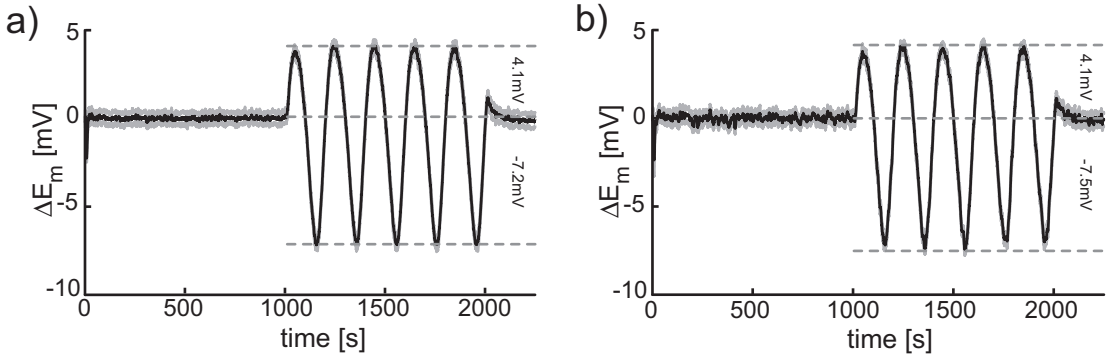

Figure 4.4: Photoreceptor response example: (a) Average responses (black line) of 25 reference responses recorded in a single photoreceptor at zero contrast. The grey lines indicate response variability in terms of the standard deviation of the stimulus independent response component. Dashed lines and numbers denote the maximal de- and hyperpolarising membrane potential deflections with respect to the resting potential. **(b)** Same as (a) but reference responses at maximum contrast used for the discrimination task (c = 0.0348).

Unfiltered Responses

We analysed this kind of data gathered from 12 photoreceptors recorded in 12 different animals with respect to their discriminability (see methods). The responses were passed through a lowpass filter with a 507 Hz cutoff frequency (LP_{507}, figure 4.3) which reduces mainly noise originating from the recording setup. The responses can still be considered virtually unfiltered since photoreceptor response power drops strongly beyond a frequency of approximately 100 Hz (e.g. Juusola et al., 1995).
Response discriminability increases with increasing contrast (figure 4.5). A safe discrimination was assumed to be possible if *reference responses* can be separated from *test responses* with a discrimination performance of at least 75% correct (dashed horizontal lines in figure 4.5). The contrast allowing response discrimination with this certainty will be referred to as the **threshold contrast** (C_{75}) which we interpret as a measure of photoreceptor response reliability (see methods).

Discrimination on basis of the entire response traces leads to a C_{75} of 0.013 (black data in figure 4.5a). This contrast is very small compared to the average contrast of natural scenes of 0.31 (e.g. Laughlin, 1981). Estimating the discriminability separately for the constant and dynamic background sections shows that the C_{75} depends strongly on the kind of background the contrast modulation is riding on. On basis of the constant background section approximately the same C_{75} is obtained as for the whole response (0.012; dark grey data in figure 4.5a). Contrast modulations superimposed on the dynamic background are more difficult to discriminate (C_{75} of 0.023, light grey line in figure 4.5a). To elucidate the reason for this difference we split up the dynamic section (with

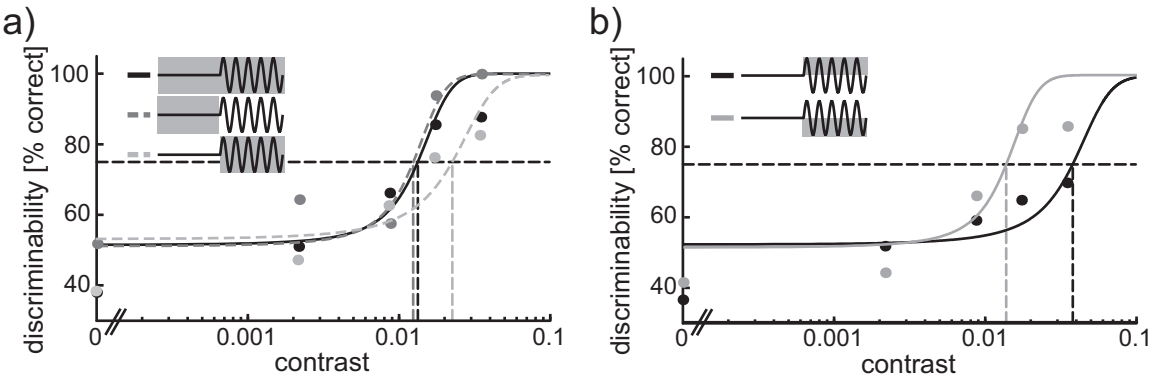

Figure 4.5: Response discriminability in different response sections. (a) Physiometric curves estimated on basis of the full response (black), the constant background section (dark grey), and the dynamic background section (light grey) as indicated by the insets. Dots represent discrimination performance averaged across 12 experiments. Lines are least-square fits of the logistic function (equation 4.3). Black dashed line is the 75% threshold. The contrast allowing a threshold performance is taken from the fitted curve. **(b)** Physiometric curves estimated in the depolarised (black) and hyperpolarised (dark grey) parts of the dynamic response section.

respect to the actual membrane potential relative to the mean potential) into depolarised and hyperpolarised parts (figure 4.5b).
It is easier to discriminate the time-course of the contrast modulations, if they are superimposed on a hyperpolarising instead of a depolarising background (C_{75} of 0.0378 and 0.0138 for depolarised and hyperpolarised response sections, respectively; figure 4.5b). Thus, there must be a quite pronounced difference in the responses depending on their polarisation, respectively the light level evoking the responses.

As was already mentioned above, the cellular response depends non-linearly on the light level (figure 4.4) as can be seen in the input output relation (figure 4.6a). This non-linearity leads to stronger membrane potential deflections in response to a decreasing than to an increasing light intensity. Since the membrane potential noise, characterised by the standard deviation of the stimulus-independent response component (difference between each single trial and the response averaged across trials), is largely independent of the light level (figure 4.6b) the signal-to-noise ratio in the hyperpolarised response section is larger than in the depolarised (shown for the extreme light intensities in figure 4.6c). This difference is reflected in an increased C_{75} obtained for the depolarising response section (figure 4.5b).

Filtered Data

Synapses, in general, and the synapse connecting fly photoreceptors to first-order interneurons, in particular, are an important site of signal processing. To investigate the impact of synaptic filtering on response discriminability the photoreceptor responses were passed through different linear filters (figure 4.3).

The discrimination performances of virtually unfiltered responses (LP_{507}-filtered) served as a benchmark. We further used the experimentally established (light adapted) bandpass-like synaptic filter (BP) and this bandpass's lowpass (LP_{75}) and highpass (HP) components separately. Additionally the LP_{20}-filter was used which represents the dark adapted

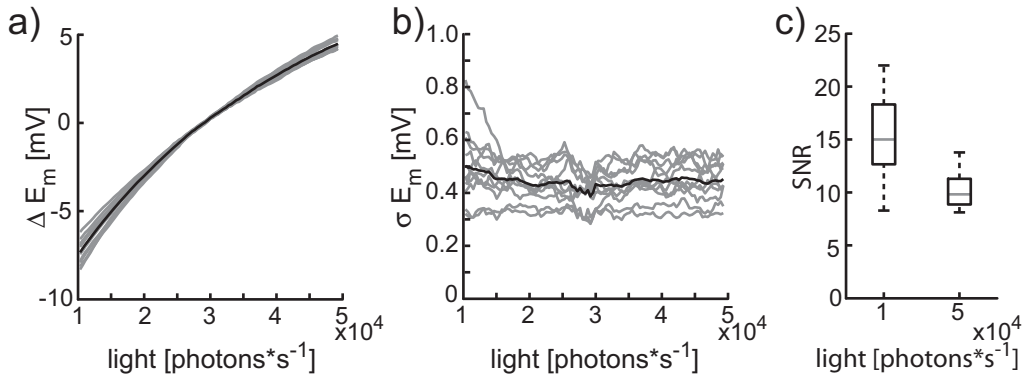

Figure 4.6: Response characteristics. **(a)** Input - output characteristic of the 12 photoreceptors analysed (grey lines) together with the average across the cells. The curve is estimated in 100 light intensity bins from the lowest to largest light intensity in the dynamic response section. Light stimulus and cellular responses were aligned by compensating the response delay estimated by cross-correlation of stimulus and response. **(b)** Noise - light dependence in the single cells recorded (grey lines) and the average (black line). The noise is the average standard deviation of the stimulus independent response component estimated in 100 light intensity bins. **(c)** Signal to noise ratio at the extreme light intensities calculated as the ration of the response (a) and the noise (b) for each cell individually. Grey lines indicate the median and the box bounds the upper and lower quartiles. Whiskers denote the extent of the data.

synaptic transfer properties.

The different filters do not strongly affect response discriminability as long as the random contrast modulation is superimposed on a constant background (figure 4.7a). C_{75} is similar for all filters except for LP_{20} where the performance is slightly inferior. The low cutoff frequency of this filter rejects most of the high-frequency component of the stimulus spectrum. Therefore, the decreased discrimination performance might be a quite obvious consequence. More obviously, filtering affects response discriminability if the contrast modulation is riding on the dynamically varying background (figure 4.7b). All lowpass filters give C_{75}s that are much larger than those resulting from BP or HP-filtering.

To understand the different filtering effects and the divergence in the two response sections (constant versus dynamic background), we assessed the spectral characteristics of the membrane potential fluctuations. We separated the responses to the contrast modulation from the response component resulting from the background by subtracting the average response when no contrast modulation was superimposed from the individual responses to the largest contrast. The remaining response component, induced only by the contrast modulation, was then divided into stimulus-induced-response-component (*signal*) and stimulus-independent-response-component (*noise*) and analysed in the frequency domain (figure 4.8). Constant and dynamic background sections were analysed separately and the power spectral densities and signal-to-noise ratios (SNR) were estimated (figure 4.8a and b, respectively). The *signal* component of constant and dynamic section have similar power spectra, whereas the *noise* power spectra of both response sections deviate from each other in the low frequency range ($\leq$ 10 Hz; dashed lines in figure 4.8a). An increase in low frequency noise in the dynamic response section leads to

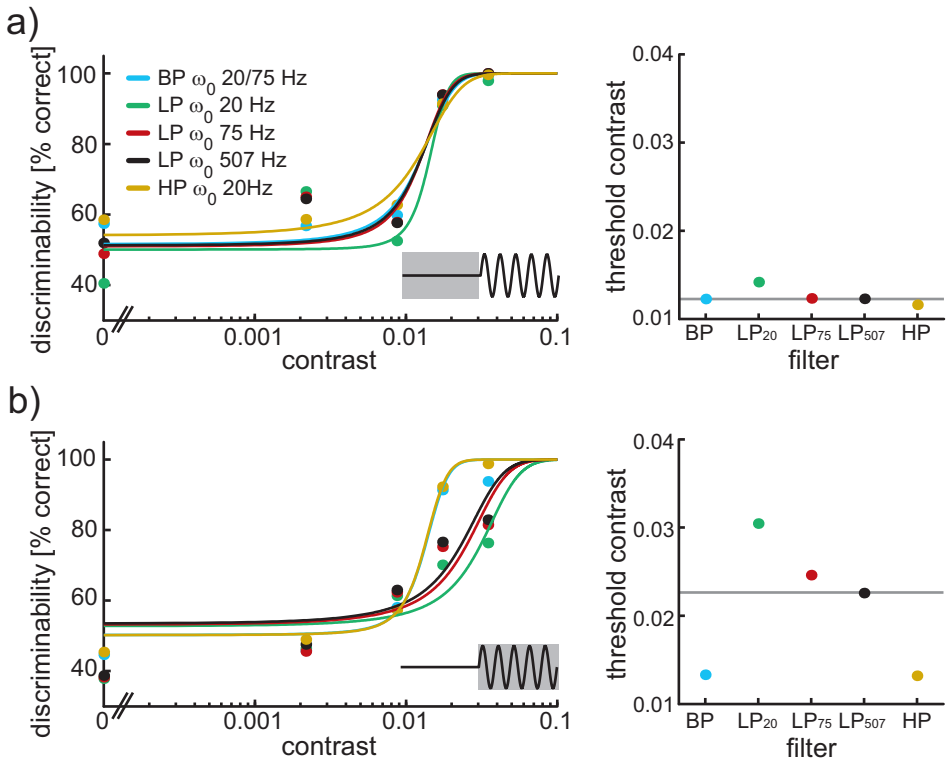

Figure 4.7: Effect of synaptic filtering on response discriminability. **(a)** Physiometric curves (left) estimated in the constant background section and the corresponding contrast thresholds (C_{75}, right). Grey solid line indicates the discrimination performance of the unfiltered responses (LP_{507}). Different colours denote different filters (compare figure 4.3). **(b)** Same but estimated in the dynamic background section.

a decreased SNR in the respective frequency band (figure 4.8b). This explains the superiority of band- and highpass filters for the discriminability in the dynamic section (figure 4.7b). Bandpass and highpass filters emphasise the more reliable middle frequencies and attenuate the less reliable low frequencies. The lowpass filters LP_{75} and LP_{20} transmit the low frequency range while cutting off parts of reliable higher frequencies, thus giving ever-decreasing discrimination performances.

Further segmenting the responses into their de- and hyperpolarised sections (figure 4.9a and b, respectively) revealed some pronounced differences: (i) irrespective of the applied filter the C_{75} is larger in the depolarised than in the hyperpolarised response section and (ii) the depolarised response section shows the same dependence of C_{75} on the applied filter as shown for the complete dynamic section (i.e. better performance of BP and HP filter and worse performance of the LP_{20}; compare figure 4.7b) whereas in the hyperpolarised response section all filters, except for the LP_{20}, lead to similar discrimination performances (figure 4.9a and b). Spectral analysis of these data was not possible since data segments available for a separate analysis of de- and hyperpolarised response sections were too short to resolve the low frequency range. Experimental approaches also do not easily resolve this issue, since prolonged high or low light stimulation would change the

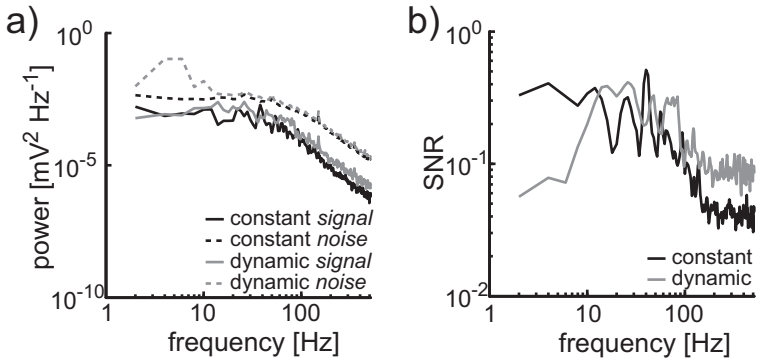

Figure 4.8: Response characteristics in the frequency domain. (a) Power spectral densities of the stimulus-induced-response-component (*signal*) and stimulus-independent-response-component (*noise*) of the constant and dynamic response section separately (black and grey lines, respectively). Power spectra were calculated from the 1 second (4096 sample points) long data stretches in three 2048 sample point segments with 50% overlap. The segments were windowed with a 2048 point Hanning window. **(b)** Signal-to-noise ratio calculated as the ratio of *signal* and *noise* power spectral densities.

adaptational state of the photoreceptor. One possible explanation of the observed differences between the two response sections could be the non-linearity in the photoreceptor input - output characteristic (figure 4.6a). This non-linearity damps contrast modulations at high light levels, but transforms the same modulation more linearly at lower light levels. It might, therefore, be advantageous to emphasise higher frequencies, which are characteristic of large contrast deflections, at high light levels and thereby counteracting the non-linearity.

In summary, the discriminability of photoreceptor responses evoked by different random brightness modulations and represented by the threshold contrast depends on the kind of background the random brightness modulations are superimposed on. The slowly varying background brightness decreases the discriminability of the unfiltered responses. Filtering the data by linear filters can be advantageous. A bandpass filter mimicking the transfer properties of the synapse between photoreceptors and LMCs in the light adapted state is almost always the better choice than transmitting the unfiltered photoreceptor response to subsequent processing stages. The different effects of the applied filters could in part be explained by a smaller signal-to-noise ratio in the low frequency range.

Responses of Model Photoreceptors

In the following we will compare the above described experimental results to results obtained from two phenomenological models that have been employed to simulate the responses of fly photoreceptors. We will compare the responses discriminabilities of of a linear and a linear-nonlinear model (LN-model) with those experimentally observed. The only noise source in both models was photon noise introduced by modelling light input as a time sequence of single photon absorptions. The occurrence of a photon was generated by a Poisson process with an event probability set by the stimulus light intensity at any instance of time.

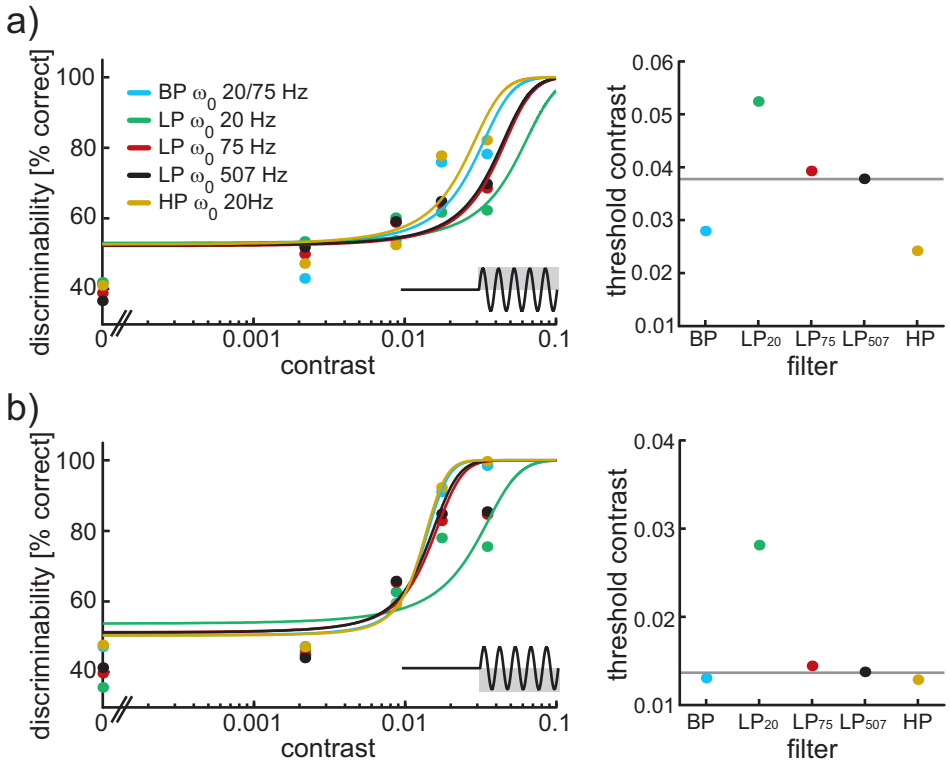

Figure 4.9: Effect of filtering on response discriminability in the dynamic section. (a) Physiometric curves (left) estimated from the depolarised response section and the according C_{75} values (right). Same colour code as in figure 4.7. Grey sold line represents the discriminability of the unfiltered response. **(b)** Same as (a) but estimated from the hyperpolarised response section.

The linear model consisted of the 1st-order Wiener kernel estimated from white noise responses following equation 4.5 (figure 4.10 centre). The model responses to white-noise brightness modulations are very close to the cellular responses (figure 4.10, left column) even though the cell exhibits a distinct non-linear behaviour (compare figure 4.6a). Responses to the stimulus used for discriminability analysis, on the other hand, are not so well fitted by the linear model (figure 4.10 right column).

To account for the non-linearity of the cellular response the LN-model consisted of the same 1st-order kernel as the linear model, but the filter output (figure 4.11 top) was passed through a static non-linearity fitted to the experimentally observed input-output characteristic (figure 4.11 centre). Measured photoreceptor responses to the discrimination stimulus are much better captured by this model (figure 4.11, bottom right). Photoreceptor white-noise responses, on the other hand, are no longer so well fitted (figure 4.11, bottom left). The static non-linearity does not capture the hysteresis effect visible in the input output characteristics (figure 4.12) when evaluated for rising and falling flanks of the sine-wave separately. This, most likely, reflects different time constants in the biophysical machinery, e.g. there are at least two different voltage gated potassium channels with different kinetics (e.g. Vähäsöyrinki et al., 2006). A dynamic non-lineartiy would have been needed to capture this behaviour. For the sake of simplicity, we decided not to account for this.

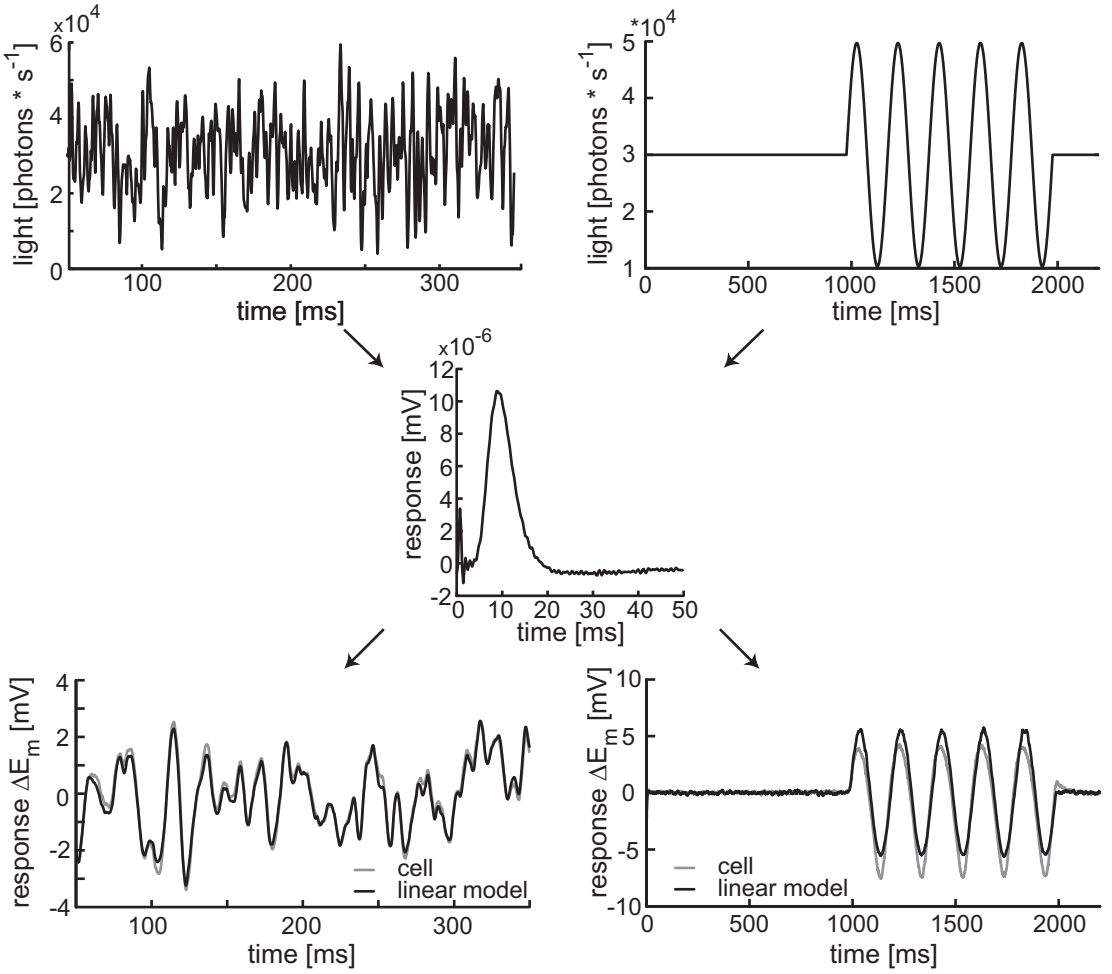

Figure 4.10: Linear model. (top) Section of a white noise stimulus (left) and the stimulus used for the discrimination task (right). The white noise stimulus was a band limited white noise brightness lumination with a cutoff at 256 Hz and a contrast of 0.31. The full sequence for the forward filter estimation had a duration of two seconds segmented into three one second sections with 50% overlap. Segments were windowed with a one second Hanning window to reduce frequency leakage. **(centre)** Forward filter estimated from the average white noise response and the stimulus according to equation 5. **(bottom)** The corresponding cellular (grey) and linear model (black) responses to the white noise (top left) and discrimination stimulus (top right).

As a consequence of photon noise both models show response variability (figure 4.13a and b). The membrane potential noise is slightly larger in the simulations than in the real data. This might be due to the calibration method by counting single photon responses under very dim light and linearly extrapolating. Anyway, less noise would not lead to qualitytively different results. Similar to the cellular responses the noise level in constant and dynamic response sections are about the same ($\sigma = 0.49$ and 0.47 in the constant and dynamic section for the linear model and $\sigma = 0.52$ and 0.52 in the respective sections of the LN-model).

Linear and LN-model have different input output characteristics (figure 4.14a, d) and their response reliability depends differently on light level. The linear model shows in-

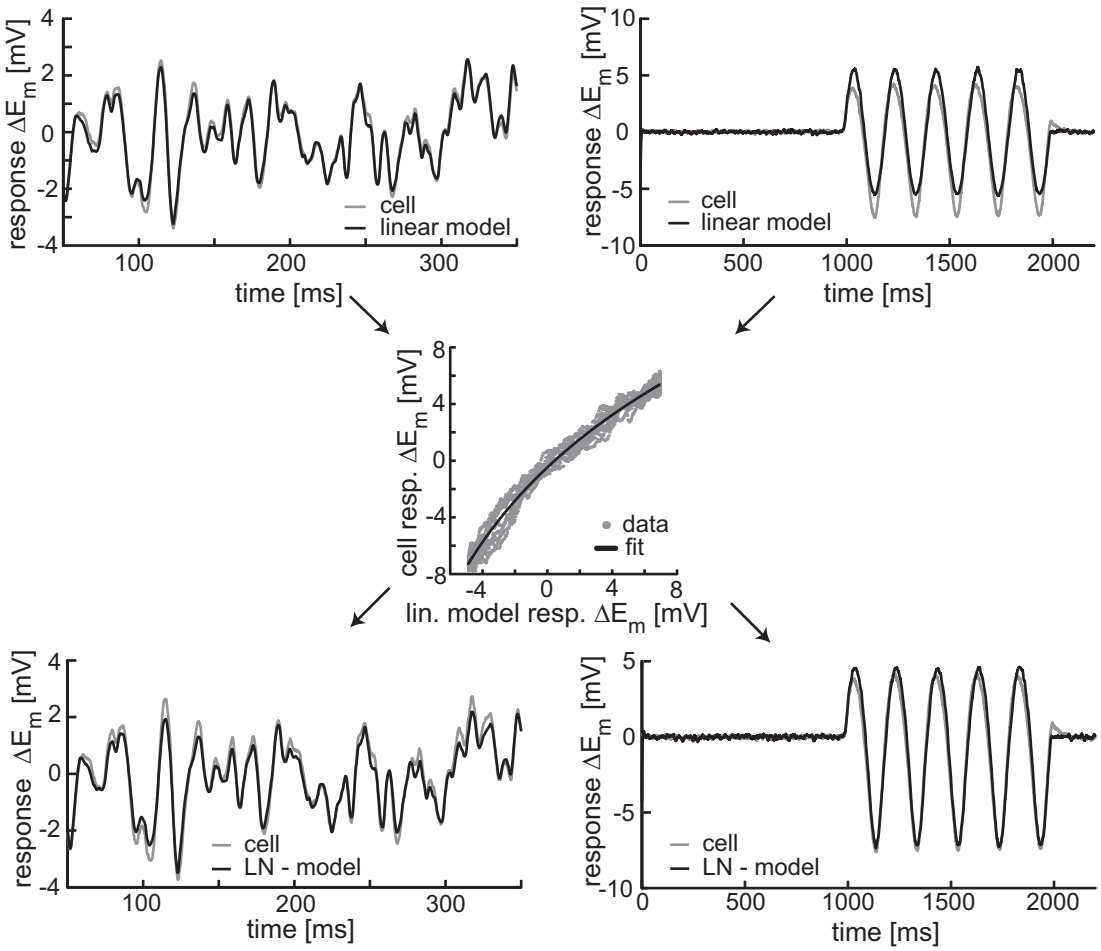

Figure 4.11: Linear-nonlinear model. (top) left: Cellular and linear model response to white noise stimulation. Top, right: Cellular and linear model responses to the discrimination stimulus (lowest contrast; c = 0). **(centre)** Static non-linearity used to map linear model responses to the cellular response amplitude. Non-linearity fitted to the experimental data by equation 4.6 with the parameters: $\alpha = 8.4032$, $\beta = 1.4687$, $\gamma = -11.6079$, and $\delta = 3.6558$. **(bottom)** Cellular and Linear-Nonlinear model responses to the white noise stimulus (left) and the discrimination stimulus (right).

creasing membrane potential noise with increasing light level (figure 4.14b). This dependence is not linear; the slight curvature reflects the fact that the variance of absorbed photons per second increases linearly with the mean light level, but the standard deviation only with the square root of the mean number of photons. The static non-linearity in the LN-model, however, leads to an almost linearly decreasing membrane potential noise with increasing light intensity (figure 4.14e). At low light levels the membrane potential noise is larger in the LN-model than in the linear one leading to a smaller SNR. The situation is inverted at high light levels. There, the LN-model has a slightly better SNR than the linear model (figure 4.14f, e). Since the model responses capture many properties of the experimental data, they will be used to further analyse the effects of linear filtering on response discriminability.

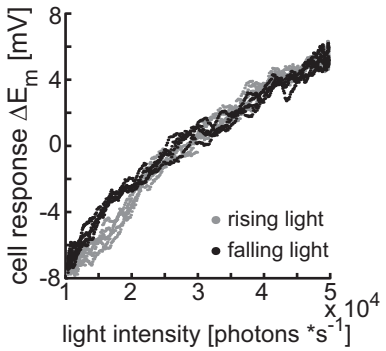

Figure 4.12: Hystersis. Cell response amplitude as a function of light intensity when analysed in rising (grey) and falling flank (black) of the dynamic section. Light stimulus and cellular response were aligned by correcting for the response delay estimated from the cross-correlation of stimulus and average response.

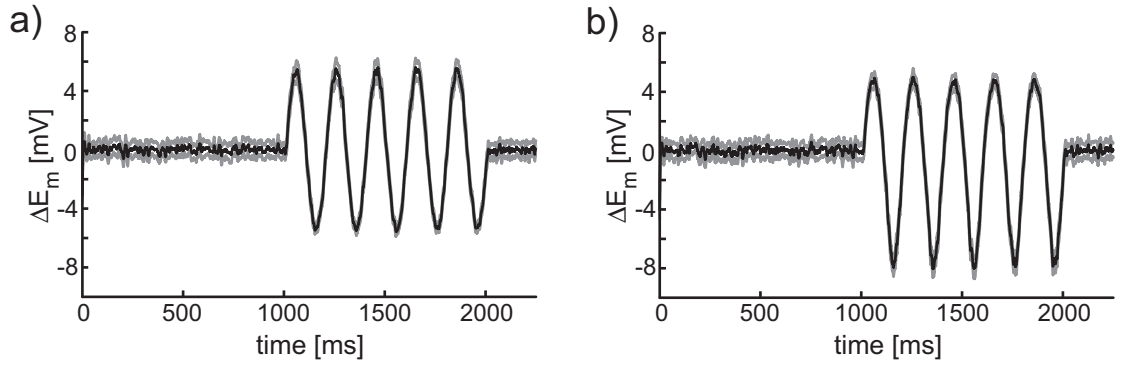

Figure 4.13: Model responses to the discrimination stimulus. **(a)** Average response of the linear model (black line, 25 trials) and the response variability indicated by the average response ± the standard deviation of the stimulus independent response component (grey lines). **(b)** Same as (a) but from the LN-model.

Discriminability of Model Responses

Response discriminability of the unfiltered model responses is worse (larger C_{75} values) in the constant section than that of the cellular responses (compare black dots in figure 4.15 top row). This was expected, since the standard deviation of the membrane potential noise is larger in the simulations (figure 4.13). In the dynamic response section (figure 4.15 bottom row) the discriminability of unfiltered model responses is on the same level as in the constant section, which is in contrast to the experimental results. Splitting up the dynamic section into de- and hyperpolarised parts leads to discriminabilities that qualitatively fit the experimental data: the C_{75} values of unfiltered responses are much lower for the hyperpolarised response section than for the depolarised section (figure 4.16 top and bottom row for de- and hyperpolarised response section, respectively). For the experimental data we identified a smaller SNR at high light levels as the main reason for the overall reduced discriminability within the dynamic section. Although the SNR obtained from both models depends in basically the same way on the light level (figure 4.14), the response discriminability in the whole dynamic section is not reduced. This

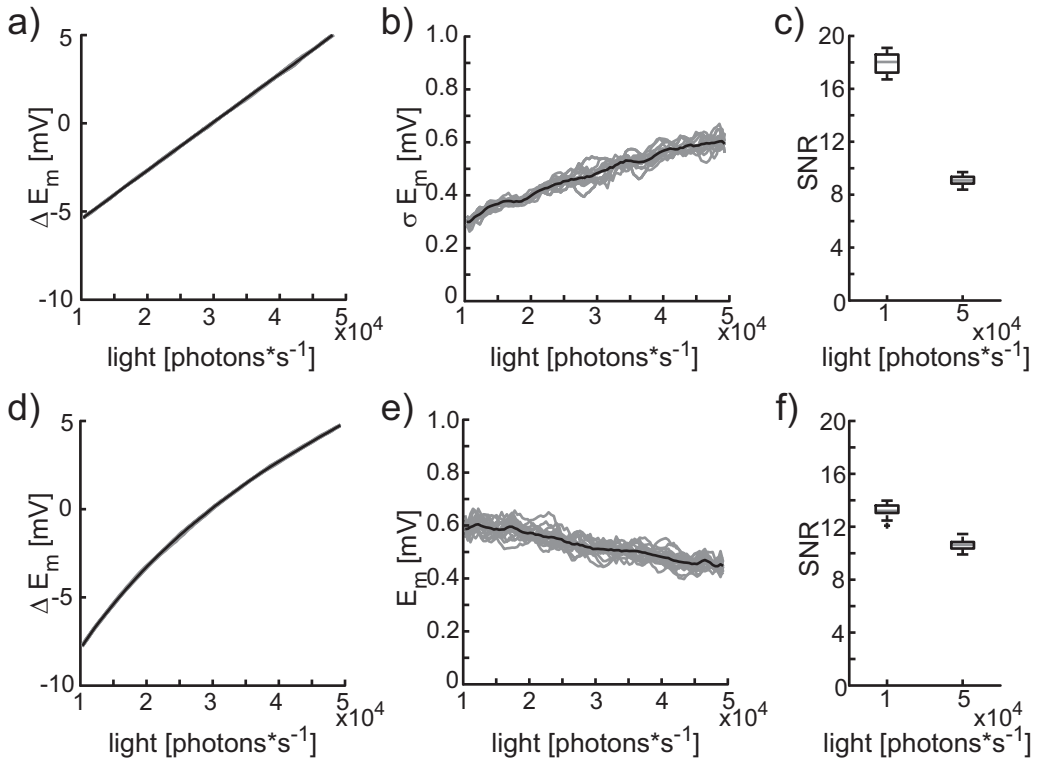

Figure 4.14: Response characteristics of linear and linear-nonlinear model. (a), (d) Input - output characteristics of linear and LN-model, respectively. Response amplitude calculated as the average response in 100 light intensity bins. **(b), (e)** Noise light dependence of linear and LN model. Noise is estimated as the standard deviation of the stimulus independent response component averaged in the same 100 light intensity bins as in (a). Grey lines indicate the 20 model cells; black line is the average across the model cells. **(c), (f)** Signal to noise ratio estimated for the highest and lowest light intensity bin for linear model (c) and LN model (f). Grey lines indicate the median SNR, the boxes include the upper and lower quartiles, and the whiskers represent the rest of the data.

finding indicates that the SNR estimated from the average response and the standard deviation of the membrane potential noise does not fully describe the relevant features.

Analysing the response characteristics in the frequency domain, i.e. power spectral densities of *signal* and *noise* response component, of the experimental data reveals a prominent increase in noise power in the low frequency range that is not present in the constant section (figure 4.8). The models do not show such increased low frequency noise. Thus, unfiltered responses in the dynamic and constant response section give about the same discrimination performance (figure 4.17). Because of the drop in the cellular SNR in the low frequency range it is advantageous to transmit the photoreceptor response after bandpass filtering to subsequent processing stages. Since the SNR of the corresponding model responses is not reduced, it does not appear to be advantageous to selectively attenuate or emphasise certain frequency bands. Accordingly, discriminability of the model responses is largely unaffected by the applied filters (figures 4.15 and 4.16). Only the LP_{20} lowpass filter always leads to C_{75} values larger than those obtained with the other filters: here the cutoff frequency is at such a low frequency that valuable information

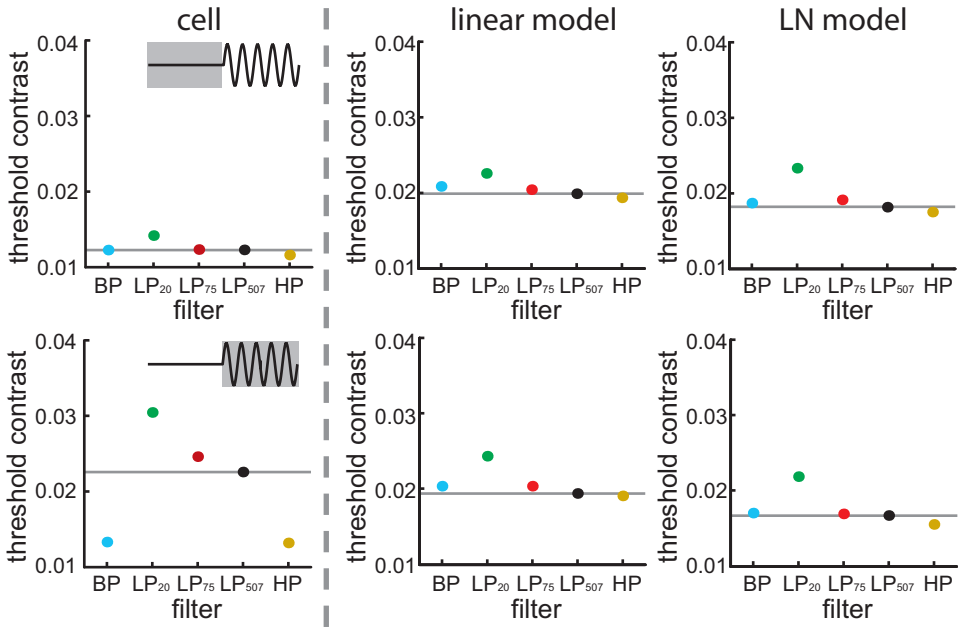

Figure 4.15: Comparison of cellular and model response discriminability in constant and dynamic section. (top) C_{75} values in dependence of the applied filter estimated in the constant section for, from left to right, the cellular responses, the linear, and the LN-model. Grey line indicates the discrimination performance of the unfiltered response. **(bottom)** Discrimination performance in the dynamic response section.

is attenuated by the filter.

In summary, the two photoreceptor models used here, the linear and the LN-model, can mimic average cellular responses quite well. The linear model is superior for white noise contrast modulations but inferior for stimuli with other statistical properties like the stimuli used in our discrimination experiments. The LN-model consisting of the same linear part plus a static non-linearity could well fit the experimental results to the discrimination stimulus; when approximating the white noise responses, however, its performance is somewhat worse. Both models fail to mimic some other aspects of the cellular responses: (i) while the membrane potential noise of the cellular responses is almost independent of light intensity, membrane potential noise of the linear model and the LN-model depend on the light intensity in an inverse way. These light dependencies are not altered even if additional noise is added to the model responses (not shown). (ii) The models do not capture the quite prominent increase in noise power of the cellular responses in the dynamic response section. This confirms indirectly that bandpass or highpass filtering is advantageous due to the decreased SNR in the low frequency range.

4.5 Discussion

In this study we analysed consequences of simulated synaptic filtering for the discriminability of fly photoreceptor responses. The applied discrimination measure has been shown previously to lead to quite different conclusions about photoreceptor coding per-

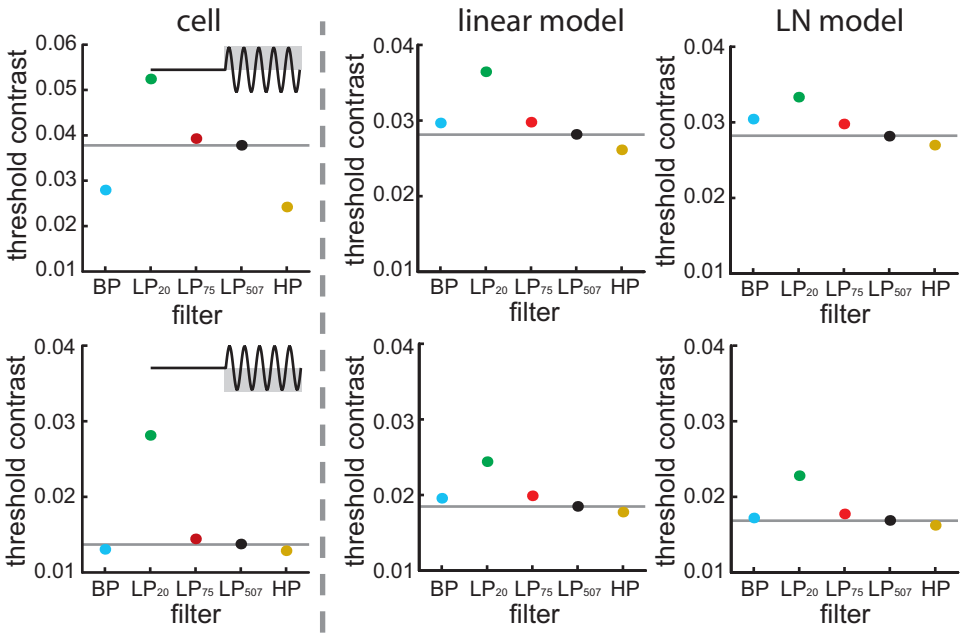

Figure 4.16: Comparison of cellular and model Response Discriminability within the Dynamic Section. (top) C_{75} values in dependence of the applied filter estimated in the depolarised response section for, from left to right, the cellular responses, the linear, and the LN-model. Grey line indicates the discrimination performance of the unfiltered response. **(bottom)** Same as on top but in the hyperpolarised response section.

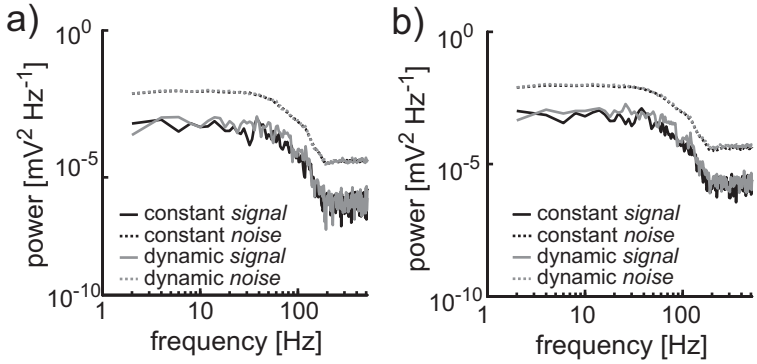

Figure 4.17: Model response characteristics in the frequency domain. (a) *signal* and *noise* power spectral densities estimated in the constant and dynamic sections for the linear model. Power spectra were calculated from the 1 second (4096 sample points) long data stretches in three 2048 sample point segments with 50% overlap. The segments were windowed with a 2048 point Hanning window. **(b)** Same as (a) but for the LN-model.

formance than conclusions based on an information theoretical evaluation of the responses (Grewe et al., 2007, submitted). Here, we found that a bandpass filter resembling the real synapse's transfer properties can increase response discriminability. Thus, bandpassing the photoreceptor response appears to be a good way to transmit visual information to subsequent processing stages. This observation is in good agreement with earlier conclusions based on information theoretical considerations (e.g. Laughlin, 1994; Juusola et al.,

1996). In our analysis we could trace the bandpass advantage back to an increased noise power in the low frequency range which occurs as soon as the stimulus contains large low frequency light intensity modulations. The question arises where this noise power originates. Is it caused by sources intrinsic to the photoreceptor itself or by photon noise as an extrinsic source?

An Intrinsic Noise Source To resolve this issue we compared the real photoreceptor response characteristics with the characteristics of the corresponding model responses. Two types of models have been used. The linear model consisted of the 1st order Wiener kernel estimated from white noise responses and the LN-model of the same kernel and a static nonlinearity. Both models are capable of reproducing the average photoreceptor responses quite well. In the model simulations the only noise source included was the extrinsic photon noise. As a consequence, the responses of both models show considerable membrane potential noise suggesting that photon noise is a major noise source in photoreceptor cells. The noise power spectra of the model responses, however, do not show the increased low frequency noise as we found in the cellular responses. Thus, we conclude that this increased noise source is attributable to intrinsic sources.

Intrinsic Noise Depends on Contrast The intrinsic noise depends on the actual stimulus: The increased noise power becomes visible only when the background brightness was modulated at a low frequency ('dynamic background'). Consequently, the SNR drops in the respective frequency band. By contrast, when the background brightness was kept constant ('constant background') the noise power spectrum is almost flat and the SNR does not decrease in the low frequency range as long as the contrast is low. At high contrasts (c = 0.31), however, the SNR is reduced in the low frequency range even when the background brightness was constant (figure 4.18; or also e.g. Juusola et al., 1995; Juusola and Hardie, 2001) and thus resembles the frequency dependence of the SNR obtained during the dynamical section. This decrease in the SNR in the low-frequency range is likely to be due to two reasons: (i) an increased noise and (ii) a reduced signal power attributed to adaptational changes induced by the large low frequency brightness changes (Juusola and Hardie, 2001). The contrasts leading to a safe discrimination of the responses in our experiments are relatively small (c = 0.012 to 0.023) and do not induce the two effects. Thus, it is a large brightness modulation that induces increased noise power. Since adaptational changes are attributed to voltage gated potassium channels (e.g. Niven et al., 2003; Vähäsöyrinki et al., 2006) it appears plausible that potassium channel activation is responsible for the intrinsic noise component. When increasing the constant background light the activation of potassium channels leads to a reduced input resistance and thereby a reduced photoreceptor gain which attenuates signal and noise in parallel (Laughlin and Weckström, 1993).

Intrinsic Noise is Light or Voltage Dependent The present results suggest that the measured photoreceptor noise is rather independent of the actual light level (figure 4.6). The photoreceptor models, on the other hand, show strong dependences on the light level (figure 4.14). Increasing light intensity goes along with increased photon noise and in the case of the linear model directly entails increased membrane potential noise. The nonlinearity incorporated in the LN-model, however, leads to decreasing membrane potential

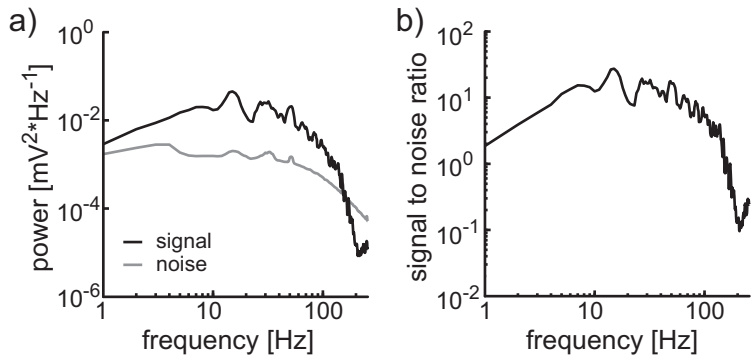

Figure 4.18: High contrast white noise response spectra. (a) *Signal* (solid) and *noise* (dashed) power spectra from high contrast white noise stimulation (c = 0.31). Shown spectra are averages across the results from 26 cells. Spectra were calculated from 2.5 second long data stretches in 1s segments (4096 sample points) with 50% overlap and windowed by a 4096 point Hanning window. **(b)** Signal-to-noise-ratio defined as the ratio of *signal* and *noise* power spectra shown in (a).

noise with increasing light level. We can assume the LN-model to be an appropriate representation of the photoreceptor, since it reproduces the average response under these conditions very well. Therefore, the intrinsic noise itself is concluded to increase with either the light level or the level of membrane depolarisation. In this way the reduced impact of photon noise is compensated by an amplification of the membrane potential noise.

Functional Implications The contrasts needed to grant a safe discriminability of time dependent stimuli based on photoreceptor responses are small compared to the average contrast encountered when viewing natural scenes. Additionally, large low frequency stimulus components induce increased intrinsic noise that makes bandpass filtering as has been described for the synapse linking photoreceptors to first-oder interneurons (e.g. James, 1992) advantageous. Can we relate these findings to the coding requirements an animal encounters in everyday life? When freely behaving, an animal's visual system is exposed to light intensity fluctuations of a statistic very different to the laboratory-used white noise. Analysing natural visual input in the frequency domain reveals that the relative contribution of frequencies to the overall signal decreases with frequency ('f') with approximately 1/f (e.g. van Hateren, 1997). This means that slow (low frequency) light intensity changes have more power, i.e. contribute more strongly to the overall modulations, than the higher frequencies (rapid light intensity changes). A fly moving around in its environment may pass through local areas with alternately high or low light intensity, e.g. depending on the leafage in the woods or when moving from a sunny spot into the shade. These light intensity changes are slower and much larger than those resulting from changes in the textures within an area of a certain overall illumination, e.g. within a sunlit scene or in the shade. In other words, the light intensity changes resulting form local textures contain much higher frequencies than those originating from large intensity changes. In this line, we may interpret the large sine-wave modulations in our experimental design as mimicking the global illumination changes in the outside world. The superimposed small contrast white noise may then be interpreted as representing

the finer light intensity variations originating from the texture of objects. To extract information about its own movement and the environmental layout the animal should rely much more on the object characteristics than on the global changes in illumination. Hence, bandpassing the photoreceptor signals can be expected to help separating object texture from overall illumination changes and, in addition, reduces the impact of low frequency noise. This interpretation results in the same conclusion as previous information theoretical analyses which stress that low-frequency components in the input largely reflect redundancies in the visual input and, therefore, may be removed from the signals without compromising the performance of the system (Laughlin, 1994; Juusola et al., 1996). We observe that the noise originating in the photoreceptor in the low-frequency range makes synaptic bandpass filtering advantageous.

References

Barlow H (1961) The Coding of Sensory Messages. In: Thorpe W, Zangwill O, editors, Current Problems in Animal Behaviour., pp. 331–360, Cambridge University Press, England.

Field G, Rieke F (2002) Nonlinear Signal Transfer from Mouse Rods to Bipolar Cells and Implications for Visual Sensitivity. Neuron 34: 773–785.

Franks K, Stevens C, Sejnowski T (2003) Independent Sources of Quantal Variability at Single Glutamatergic Synapses. J Neurosci 23: 3186–3195.

Grewe J, Kretzberg J, Warzecha A, Egelhaaf M (2003) Impact of Photon Noise on the Reliability of a Motion-Sensitive Neuron in the Fly's Visual System. J Neurosci 23: 10776–10783.

Grewe J, Weckström M, Egelhaaf M, Warzecha A (2007) Two Measures Two Interpretations - Shannon Information Capacity and Response Discrimination as Measures of Photoreceptor Coding Performance., submitted.

James A (1992) Nonlinear Operator Network Models of Processing in the Fly Lamina. In: Pinter R, Nabet B, editors, Nonlinear Vision: Determination of Neural Receptive Fields, Function, and Networks, chap. 2, CRC Press.

Juusola M, French A (1997) Visual Acuity for Moving Objects in First- and Second-order Neurons of the Fly Compound Eye. J Neurophysiol 77: 1487–1495.

Juusola M, French A, Uusitalo R, Weckström M (1996) Information Processing by Graded-Potential Transmission through Tonically Active Synapses. Trends Neurosci 19: 292–297.

Juusola M, Hardie R (2001) Light Adaptation in *Drosophila* Photoreceptors: I. Response Dynamics and Signaling Efficiency at 25 Degrees C. J Gen Physiol 117: 3–25.

Juusola M, Uusitalo R, Weckström M (1995) Transfer of Graded Potentials at the Photoreceptor-Interneuron Synapse. J Gen Physiol 105: 117–148.

Laughlin S (1981) A Simple Coding Procedure Enhances a Neuron's Information Capacity. Z Naturforschung 36: 910–912.

Laughlin S (1994) Matching Coding, Circuits, Cells, and Moleculees to Signals: General Principals of Retinal Design in the Fly's Eye. Progress in Retinal and Eye Research 13: 165–196.

Laughlin S, Weckström M (1993) Fast and Slow Photoreceptors - a Comparative Study of the Functional Diversity of Coding and Conductances in Diptera. J Comp Physiol [A] 172: 593–609.

Lindemann J, Kern R, van Hateren J, Ritter H, Egelhaaf M (2005) On the Computations Analyzing Natural Optic Flow: Quantitative Model Analysis of the Blowfly Motion Vision Pathway. J Neurosci 25: 6435–6448.

Matic T, Laughlin S (1981) Changes in the Intensity-Response Function of an Insect's Photoreceptors Due to Light Adaptation. J Comp Physiol [A] 145: 169–177.

Meinertzhagen I, O'Neil S (1991) Synaptic Organization of Columnar Elements in the Lamina of the Wild Type in *Drosophila melanogaster*. J Comp Neurol 305: 232–263.

Niven J, Vähäsöyrinki M, Kauranen M, Hardie R, Juusola M, et al. (2003) The Contribution of Shaker K^+ Channels to the Information Capacity of *Drosophila* Photoreceptors. Nature 421: 630–634.

Simoncelli E, Olshausen B (2001) Natural Image Statistics and Neural Representation. Annu Rev Neurosci 24: 1193–1216.

Softky W, Koch C (1993) The Highly Irregular Firing of Cortical Cells is Inconsistent with Temporal Integration of Random EPSPs. J Neurosci 13: 334–350.

Tsukamoto Y, Morigiwa K, Ueda M, Sterling P (2001) Microcircuits for Night Vision in Mouse Retina. J Neurosci 21: 9616–8623.

van Hateren J (1997) Processing of Natural Time Series of Intensities by the Visual System of the Blowfly. Vision Res 37: 3407–3416.

van Hateren J, Snippe H (2001) Information Theoretical Evaluation of Parametric Models of Gain Control in Blowfly Photoreceptor Cells. Vision Res 41: 1851–1865.

van Rossum M, Smith R (1998) Noise Removal at the Rod Synapse of Mammalian Retina. Vis Neurosci 15: 809–821.

Vähäsöyrinki M, Niven J, Hardie M RC Weckström, Juusola M (2006) Robustness of Neural Coding in *Drosophila* Photoreceptors in the Absence of Slow Delayed Rectifier K^+ Channels. J Neurosci 26: 2652–2660.

White J, Rubinstein J, Kay A (2000) Channel Noise in Neurons. Trends Neurosci 23: 131–137.

5 Impact of photon noise on the reliability of a motion sensitive neuron in the fly's visual system

The content of this chapter has already been published as: Jan Grewe, Jutta Kretzberg, Anne-Kathrin Warzecha, and Martin Egelhaaf: *Impact of photon noise on the reliability of a motion sensitive neuron in the fly's visual system.*, Journal of Neuroscience 23(34): pages 10776 - 10783, 2003

5.1 Summary

Variable behavioural responses to identical visual stimuli can, in part, be traced back to variable neuronal signals, which provide unreliable information about the outside world. This unreliability in encoding of visual information is due to several noise sources such as photon noise, synaptic noise or the stochastic nature of ion channels. Neurons of the fly's visual motion pathway have been claimed to represent perfect encoders with photon noise as the main noise source limiting their performance. Other studies on the fly's visual system suggest, however, that internal noise emerging within the nervous system also affects the reliability of motion vision. To resolve these contradictory interpretations we carried out an electrophysiological investigation, inspired by the "equivalent noise" paradigm applied in psychophysics, on the fly's motion-sensitive H1 neuron. Noise-like brightness fluctuations of different strength were superimposed on the motion stimuli. Since the noise level found to affect the temporal properties of the spike responses is much larger than the estimate of photon noise under the experimental conditions, our results indicate that motion vision is more likely to be limited by internal sources of variability than by photon noise.

5.2 Introduction

Animals including humans respond to sensory stimuli with limited reliability. In the brain, this behavioural or perceptual variability is reflected in variable neuronal responses providing unreliable information about the outside world. For instance, neurons in the visual cortex of cats and monkeys respond to stimuli with a spike count variance in the range of the mean activity (e.g. Tolhurst et al., 1983; Vogels et al., 1989; Britten et al., 1993; Barberini et al., 2000). Although neuronal variability of insect visual interneurons (Warzecha and Egelhaaf, 1999; Warzecha et al., 2000; Warzecha and Egelhaaf, 2001; de Ruyter van Steveninck et al., 2001; Borst and Haag, 2002) and of vertebrate retinal ganglion cells is somewhat smaller (Levine et al., 1988; Berry et al., 1997; Kara et al., 2000), it still limits the reliability of behavioural reactions. Various noise sources within the nervous system constrain the reliability of neuronal responses, such as the phototransduction process (e.g. Rodieck, 1998), the stochastic nature of ion channels, as well as synaptic transmission (e.g. Johnston and S., 1995). In addition, the incoming visual signal is inherently noisy because of the quantum nature of light (e.g. Rodieck, 1998). Especially at extremely low light levels, the absorption of single photons triggers prominent membrane potential changes in the photoreceptor (e.g Hardie, 1979; Rodieck, 1998). In flies, single-photon effects could then be detected in spike patterns of the motion-sensitive H1-neuron that is several synapses away from the photoreceptors (Lillywhite and Dvorak, 1981) and in behavioural responses (Reichardt, 1965). In humans single-photon absorptions were found to affect perception (Bouman et al., 1985). Thus, at the sensitivity threshold, the reliability of motion vision is limited by photon noise. Although individual photons contribute much less to the overall photoreceptor response at higher light levels, it was concluded that, even in daylight, photon noise is the major source of variability in the fly motion-sensitive H1-neuron (de Ruyter van Steveninck and Bialek, 1995; Lewen et al., 2001; Borst and Haag, 2001). The H1-neuron is a well-established system for analysing the reliability of neural coding (reviews e.g. Egelhaaf and Warzecha, 1999; Warzecha and Egelhaaf, 2001; de Ruyter van Steveninck et al., 2001; Haag and Borst, 2002; Egelhaaf et al., 2002). All internal sources of variability were claimed to be of minor relevance implying that neuronal information processing is virtually perfect (de Ruyter van Steveninck and Bialek, 1995; Lewen et al., 2001; Borst and Haag, 2001). However, at least for the light-adapted eye, noise sources inherent in synaptic transmission between photoreceptors and second-order neurons were shown to significantly affect the reliability with which visual information is signalled to higher-order processing stages (Laughlin et al., 1987; de Ruyter van Steveninck and Laughlin, 1996). Is H1's response reliability limited by photon noise or also shaped by noise sources inherent in the nervous system? In an experimental design adapted from psychophysics, external noise was introduced into the system. Random brightness modulations, which corrupt the input signal similar to photon noise, were superimposed on random dots, moving in the preferred direction of H1. We examined how much noise could be added before the motion response was affected noticeably and how this noise level relates to photon noise under the experimental conditions.

5.3 Materials and Methods:

Electrophysiology

Experiments were carried out on 21 two-to-eight-days old female blowflies (*Lucilia* spec.) at temperatures between 22° and 26°C. The animals were obtained from laboratory stocks. Dissection was done as described previously (Warzecha et al., 1993). After dissection the flies were adjusted in the experimental setup with respect to the symmetry of the deep pseudopupil (Francescini, 1975). The spike activity of the H1-cell, a directionally-selective motion-sensitive neuron (e.g. Hausen, 1976) was recorded extracellulary at its output region in the left half of the fly's visual system. This H1-cell has its input region in the right visual field and conveys visual motion information to the contralateral visual system. To reduce background noise resulting from the activity of neurons that receive input from the left visual field, the left eye was covered with black varnish. Insulated tungsten electrodes were used for recording. As reference electrode a glass capillary filled with Ringer's solution (Hausen, 1982) was used. The recorded signals were amplified (factor 3000) and bandpass filtered (corner frequencies: 300 Hz and 3 kHz). Recorded action potentials were transformed into pulses of fixed height and duration, fed into a PC and stored onto hard disk for further analysis. Data acquisition was done at a sampling frequency of 1200 Hz using the analogue input of a VSG 2/3 card (Cambridge Research Systems, Cambridge UK). Data were analysed using Matlab (Version 6.5, Release 13, The Mathworks Inc.) and some routines written in C.

Visual Stimulation

Visual stimuli were presented to the fly at 300 Hz with a Joyce Scope DM5 monochrome (P-31 phosphor, decay to 10% in approximately 40μs) computer monitor (Joyce Electronics Ltd., UK). The brightness range of the monitor was resolved with 8 bits. The monitor was controlled using the VSG2/3 graphics card (Cambridge Research Systems, UK). The card was programmed using Borland Delphi 3.0 and VSG Software Library Version 6.0. As seen by the fly, the monitor screen (464x375 pixel resolution) had a horizontal and vertical extent of 127 and 120 respectively. The screen centre was positioned at 0° elevation and 20° azimuth. At this point, one pixel had a vertical and horizontal extent of approximately 0.5°. While the frame rate was 300 Hz, the update rate of the presented motion stimulus was 150 Hz. Cross-correlation of 200 response traces of H1 revealed no time locking to either of these frequencies.

Random dot stimuli

Random dot kinematograms were used as visual stimuli. They consisted of ten bright dots with a vertical and horizontal extent of approx. 1.5° as seen by the fly. In the first frame of the stimulus sequence the dots were randomly positioned in front of a dark background. In subsequent frames these dots were moved in the H1-cell's preferred direction, i.e. from back to front, by steps of 3 pixels (corresponding to 1.5) per frame. The position of the dots was updated at a rate of 150 Hz which results in a velocity of approx. 450 °/s in the screen centre. The same dot pattern was used in every stimulus presentation. The stimulation sequence consisted of 3 seconds motion and 7 seconds interstimulus interval

during which the monitor showed the starting image of the motion sequence. At mean brightness all dots had a radiance of $2.7 \cdot 10^{-1} W \cdot m^{-2} \cdot sr^{-1}$ and the background of $3.0 \cdot 10^{-5} W \cdot m^{-2} \cdot sr^{-1}$ (corresponding to $130 cd/m^2$ and $0.001 cd/m^2$ respectively). In the following, we indicate light intensities and intensity changes in relative units. Since the brightness range of our stimulus was resolved with 8 bits (i.e. 256 intensity levels), an intensity level of 127 corresponds to the mean brightness of the dots and 0 to the background brightness. The gamma correction of the video screen was approved to result in an virtually linear relationship between intensity level and real brightness.

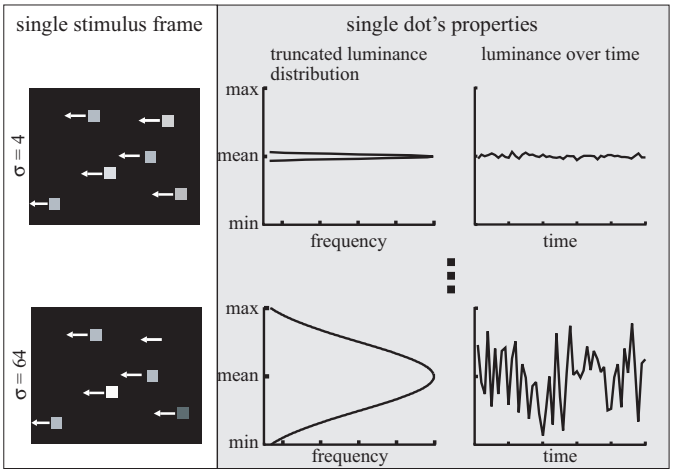

Figure 5.1: Visual Stimuli. Illustration of the visual stimuli for the smallest ($\sigma = 4$, upper part) and the largest ($\sigma = 64$, lower part) noise level. On the left side the same frame of the motion sequence is shown. For the first frame a number of dots is randomly placed on the screen, in subsequent frames the dots are shifted in the preferred direction of the H1-cell (indicated by the arrows). As can be seen, each dot has its own brightness. The right part shows the properties of a sample dot. The noise sequence applied to this dot during presentation was made up of randomly drawn brightness values drawn from a Gaussian distribution centred at the mean brightness ('127' on the 8 bit scale) and a standard deviation of $\sigma = 4, 8, 16, 32$ or 64, defining the noise level (shown for $\sigma = 4$ and 64). This distribution was truncated at mean $\pm 2\sigma$. While the brightness variations over time are quite small in the upper part, modulations covering the full brightness range are possible at the largest noise level ($\sigma = 64$).

To introduce external noise into the fly's visual system, random brightness modulations were superimposed on the dots, i.e. each dot's brightness was varied between subsequent frames. As is illustrated in figure 5.1 the brightness values were randomly taken from Gaussian distributions with the same mean but different standard deviations. The distributions were truncated at mean level $\pm 2\sigma$. We define the noise level as the standard deviation of the original Gaussian. Five noise levels were used in the experiments ($\sigma =$ 4, 8, 16, 32 and 64 brightness levels on the 8 bit scale). Thus, at maximum noise level, brightness modulations covered the available brightness range entirely (compare figure 5.1 lower part). In a first set of experiments, the time-dependent noise sequences added to all ten dots were statistically independent. In a second set of experiments the noise added on fractions of the dots was correlated. We used 6 correlation levels (0, 20, 40, 60, 80 and 100%) at two different noise levels($\sigma = 16$ and $\sigma = 64$). In both sets of experiments the noise was added in two different ways: The same brightness noise sequence was

superimposed on the dots in each stimulus presentation ('reference stimulus'). Different brightness noise sequences, yet with the same statistical properties, were employed in each presentation ('test stimulus').

Experimental protocol

Prior to data acquisition, the fly was adapted to the stimulus and laboratory conditions. For this purpose the stimulus with a randomly chosen noise level was presented 40 times in a row which lasted 7 minutes. After this adaptation period the experiments were done block-wise for each noise level (σ = 4, 8,16, 32, and 64) or each correlation level (0, 20,40, 60, 80 or 100%). The interstimulus interval during which the monitor showed the starting image of the motion sequence with all dots at mean brightness was used for data storage and providing Ringer's solution to the fly if necessary. Both reference and test stimuli were presented 30 times in random order within each noise level/correlation block. The blocks were also shuffled in experiments performed on different H1-cells in different animals. For further analysis, 25 out of the 30 responses to each stimulus type were used. We selected those 25 spike trains that deviate least with respect to their mean activity from the mean response averaged over all reference and test responses.

Data analysis and comparison of spike trains

The aim of the experiments was to find the level of external noise which leads to a major change in the cell's responses to the test stimuli as compared to the responses to the reference stimulus. Since reference and test stimuli have the same statistical properties we expected them to lead to the same spike rate but possibly to different spike patterns. We applied two approaches to detect differences in the temporal properties of the spike trains. The first approach compares spike trains by calculating the minimal costs of transforming one spike train into another (Victor and Purpura, 1997). The transformation is done by either deleting, inserting or temporally shifting of single spikes. Each of these procedures is linked to defined costs. Deleting or inserting of single spikes has the cost of '1'. The cost for a temporal shift ('q' per second) is variable and determines the temporal resolution of the measure. For example, a 'q' value of 200 equals a temporal resolution of 10 ms: for this time-scale spikes in two response traces are considered as "nearly coincident" if a given spike in one of the spike trains is shifted by less than 10ms with respect to the corresponding spike in the other spike train. As long as this condition is met, it is "cheaper" to temporally adjust the spikes in the two spike trains by shifting than by deleting and inserting one of them. In our analysis we used a set of 9 different values for q (q = 2, 4, 8, 16, 32, 64, 128, 256 and 512) which correspond to temporal resolutions of 1000, 500, 250, 125, 62.5, 31.25, 15.625, 7.8125 and 3.90625 ms. Moreover, we calculated the similarity between test and reference responses on the basis of the mean spike rate over the entire stimulation interval (see figures 5.4b, 5.5b, e rightmost data points). The second approach calculates the distance between two spike trains by determining spike-count differences between the smoothed spike trains (Kretzberg et al., 2001)

$$D(X^\tau, Y^\tau) = \sqrt{\frac{1}{N} \cdot \sum_{j=1}^{N} (X_j - Y_j)^2}, \tag{5.1}$$

with N = number of time steps, τ = filter width (milliseconds), and X^τ, Y^τ = the smoothed spike trains that are to be compared. A rectangular filter of variable width was used for smoothing. We calculated the distances using six different filter widths (500, 200, 100, 50, 20 and 10 msec).

Classification of responses

To determine the similarity of the spike trains we took each single reference response (e.g. the highlighted spike train in figure 5.2a) and computed the mean similarity (see above) to the other reference responses and to the test responses. We can assume the reference responses to be more similar to each other than compared to the test responses if the external noise affects the responses. Thus, a reference response is subsequently classified correctly as a reference response when its similarity within the reference responses is higher than between reference and test responses. This procedure is done for all 25 reference responses. The percentage of correct classifications represents a measure of the discriminability of reference and test responses. If the test responses do not differ more from the reference responses than the reference responses do from each other, the percentage of correct assignments is 50%. In this case, the added noise does not detectably affect the temporal structure of the spike trains and their variability is dominated by noise sources intrinsic to the nervous system and/or by photon noise. If both types of responses can be discriminated perfectly, the percentage of correct classification is 100%. In this case, the responses are heavily affected by the external noise that was added to the stimuli. We assume a major influence of the external noise on the responses when the discrimination performance exceeds 75%, a threshold-value often used in psychophysics.

Domain of uncertainty

To assess whether deviations of the discrimination performance from chance level (figure 5.2 compare b,c) are attributable to the external noise, we calculated the percentage of correct decisions for ten different sets of shuffled responses; i.e. we replaced half of the reference responses (selected by chance) with the same number of randomly chosen test responses. For each shuffle, the classification performance was calculated as described above. A 50% performance is expected, since the shuffle consists of responses of either type mixed in equal shares. A deviation from chance level can thus be understood as a measure of variability caused by any kind of noise. The shaded area in figure 5.2 b and c show the "domain of uncertainty" which is defined by the mean (dotted line) and twice the standard deviation of the classification performances obtained by comparing the ten different sets of shuffled responses. Classification performances that fall into the domain of uncertainty are likely to be a result of the noise in the system (including photon noise) and not of the added external noise.

Estimation of photon noise

Following the approach of de Ruyter van Steveninck (1986), the number of photons impinging per second on a single photoreceptor can be estimated according to

$$N = \epsilon_{sp} \cdot \int_0^\infty L_{ph}(\lambda) \cdot S_{pr}(\lambda) d\lambda \tag{5.2}$$

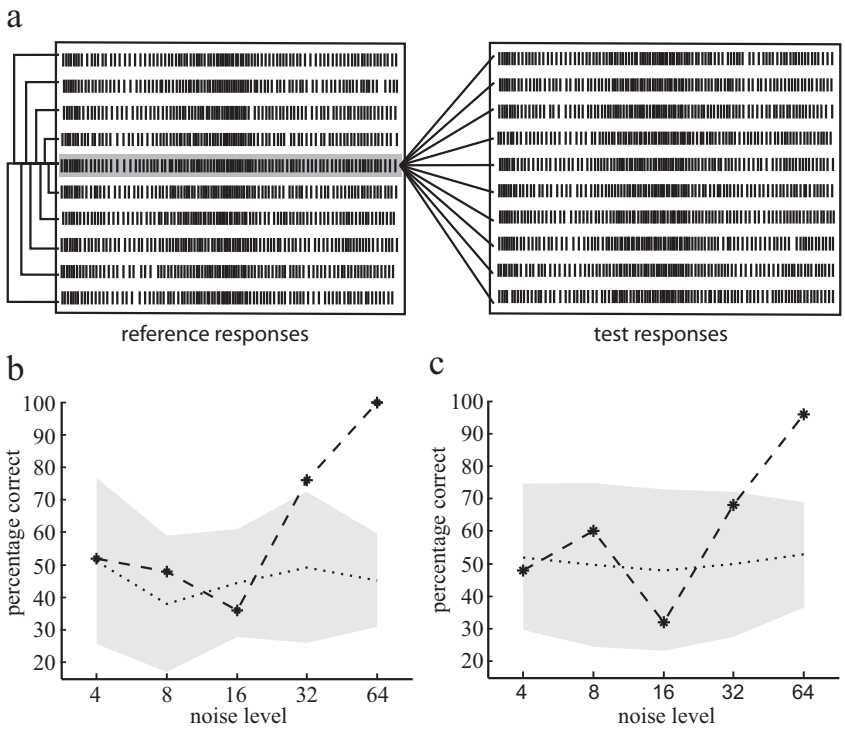

Figure 5.2: Illustration of the data analysis for a single cell example. (a) The raster plots show 750ms sections of ten responses to reference (left) and test (right) stimulus at maximum noise level ($\sigma = 64$). A common spike pattern can be seen in all responses despite differences in timing of individual spikes. Although all reference responses were elicited by the same stimulus, they do not seem to be more similar to each other than compared to the test responses that were evoked by stimuli, which were statistically equivalent but differed in the noise sequence added on the stimuli. The way of analysing more subtle changes in the temporal structure of the responses is sketched by the lines drawn between the highlighted reference response and all other reference and test responses. (i) Each reference response is compared to all other reference responses (solid lines) with two different measures of similarity (see Methods) and the average similarity within the reference responses is calculated. (ii) The mean similarity of each reference response to all test responses is determined (dashed lines), and the average similarity between reference and test responses is calculated. **(b)** If the external noise affects the responses the reference responses should be more similar to each other than compared to the test responses. With this assumption we tried to classify the individual reference responses on the basis of the similarity values estimated with the measure developed by Victor and Purpura, (1997) (see Methods for details). The percentage of correct classifications is plotted as a function of added noise level for this single cell example. The shaded area represents the domain of uncertainty (see Methods for details). Discrimination performances falling into this range are likely to be a consequence of chance. A significant effect of the added noise on the responses can be assumed if the actual percentage-correct value is outside the domain of uncertainty. **(c)** same as b but the responses were compared using the measure developed by Kretzberg et al., 2001.

with λ the wavelength, ϵ_{sp} $(m^2 \cdot sr)$ the spatial efficiency factor, $L_{ph}(\lambda)$ $(photons \cdot m^{-2} \cdot sr^{-1} \cdot s^{-1} \cdot nm^{-1})$ the spectral density of the photon flux, and $S_{pr}(\lambda)$ the relative spectral sensitivity of fly photoreceptors (type R1-6). The spatial efficiency factor is given by the

product of lens surface and photoreceptor solid angle, which results in

$$\epsilon_{sp} = 3.5 \cdot 10^{-13} m^2 \cdot sr \tag{5.3}$$

assuming a circular lens (van Hateren, 1984) with a point spread function approximation as a circular symmetric Gaussian (Götz, 1965). The lens diameter and the acceptance angle are assumed as D = $30\mu m$ and $\Delta\rho = 1.2°$, respectively (Smakman et al., 1984). The integral in formula 5.2 is the spectral overlap L_{so} which can be calculated for the mean radiance of the dots of $2.7 \cdot 10^{-1} W \cdot m^{-2} \cdot sr^{-1}$ to (de Ruyter van Steveninck, 1986)

$$L_{so} = 4.47 \cdot 10^{17} photons \cdot m^{-2} \cdot sr^{-1} \cdot sec^{-1} \tag{5.4}$$

Inserting (5.3) and (5.4) in (5.2) we get:

$$N = L_{so} \cdot \epsilon_{sp} = 1.56 \cdot 10^{5} photons \cdot sec^{-1} \tag{5.5}$$

Thus, approximately 1034 photons impinge on a photoreceptor while a dot is in its receptive field (1/150 s). Because the number of photon arrivals is a statistical event following the Poisson distribution, the variance of which is equal to the mean, the standard deviation and thus the signal-to-noise-ration (SNR) amounts to approximately 32. In order to mimic a SNR matching photon noise in our stimulation paradigm, brightness noise with a standard deviation of $\sigma = 4$ [with mean brightness of 127 on the 8 bit scale $(0 \ldots 255)$] would have to be added to the moving dots (i.e. $128/4 = 32$). Persistence of the P-31 phosphor increases the time a dot stimulates a photoreceptor and thus, slightly increases the number of photons impinging on the receptors. Consequently, photon noise is slightly overestimated by the above approximation.

5.4 Results

To find out whether the reliability of H1 responses to motion stimuli is limited by photon noise or noise sources intrinsic to the nervous system the consequences of external brightness noise superimposed on a random dot cinematogram were analysed. The brightness of the ten dots moving coherently in the preferred direction of the H1-cell was modulated in two ways. The time-dependent brightness noise was either exactly the same in each stimulus presentation ('reference stimulus') or it was different, but had the same statistical properties in each presentation ('test stimulus'). We examined for a wide range of time-scales to what extent the temporal structure of spike responses was affected by the added noise. In case of photon noise being the dominant noise source limiting motion vision, the added noise, as soon as it is larger than photon noise itself, should affect the responses. Thus, the reference responses should be more similar to each other than compared to the test responses. This is because the reference stimulus is, apart from photon noise, the same for each trial, the variability in the reference responses reflects the consequences of noise sources in the nervous system and/or of photon noise. In contrast, the variability of the test responses is also affected by the external noise introduced by using a different stimulus for every presentation - unless the external noise level is negligible in the presence of the other noise sources that cannot be controlled by the experimenter. The larger the brightness noise level needed to have a major impact on the responses the less important is photon noise for the reliability of motion vision in H1.

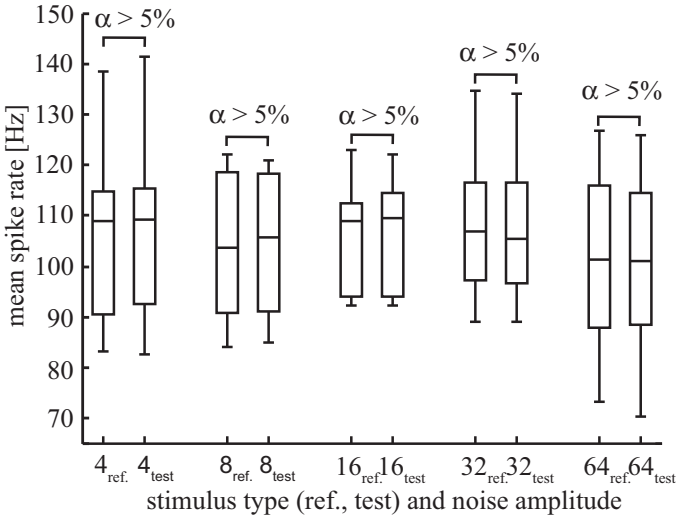

Figure 5.3: Mean firing rate of H1 in response to reference and test stimuli at the five noise levels (σ = 4, 8, 16, 32 and 64) used in the experiments. The box and whisker diagrams represent the distribution of mean firing rates, averaged over all presentations of each stimulus type. All diagrams are based on the same 11 H1-neurons recorded in 11 different flies. The boxes' horizontal lines represent the lower, median and upper quartile of the data. The whiskers extending vertically from the boxes show the extent of the rest of the data. The distributions were tested for significant differences using a Wilcoxon test for paired samples. An α-value, shown above each pair of distributions, larger than 5% denotes a non significant difference.

Impact of uncorrelated noise

Since the statistical properties of reference and test stimuli were identical, we expected them to elicit the same average responses. Comparing the mean response amplitudes for all noise levels using a Wilcoxon test for paired samples confirmed this expectation (figure 5.3). Thus, if there were differences in the responses to reference and test stimuli, they exist only on a finer time-scale, i.e. in the temporal spike-pattern. The raster plots shown in figure 5.2a reveal some variability in the spike-trains even if the responses were elicited by repeated presentation of the same stimulus (figure 5.2a; reference responses at maximum noise level). In case of different noise sequences superimposed on the moving dots at each presentation (figure 5.2a; test responses at maximum noise level), the responses appear not to be more variable than the reference responses. Under both stimulus conditions, a common time structure is visible despite differences in the timing of individual spikes. Based on the raster plots it is hard to tell whether the individual spike trains obtained under the reference condition are more similar to each other than to spike trains obtained with the test stimulus. Therefore, we scrutinised the responses by quantitative measures.

Two different measures were applied to quantify the similarity of individual spike trains (see methods). As is shown for the single cell example in figure 5.2b and figure 5.2c (measures developed by Victor and Purpura (1997) (figure 5.2b) and Kretzberg et al. (2001) (figure 5.2c) were used), the classification performance varies around 50% for small noise levels; it increases with increasing noise level to almost perfect discrimination. The

responses of this H1-cell to reference and test stimulus can be reliably distinguished at noise levels larger than $\sigma = 32$ if the 75% criterion is satisfied and the data value is outside the domain of uncertainty. At maximum noise level the responses can be distinguished perfectly. Since both measures of similarity lead to qualitatively the same results for all analysed cells, only results obtained with the measure of Victor and Purpura (1997) will be shown in the following.

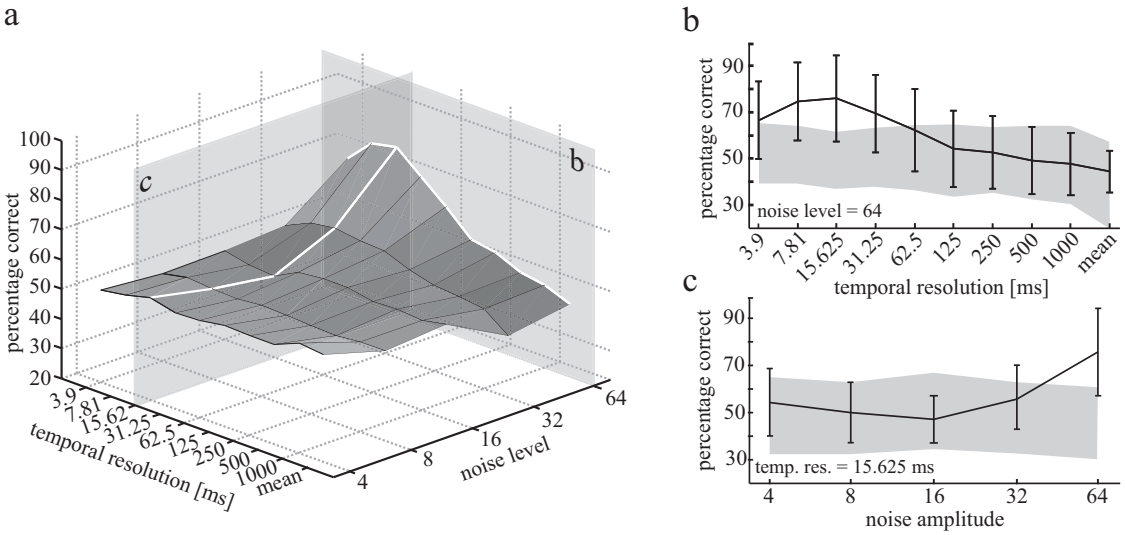

Figure 5.4: Response discriminability. (a) Averaged discriminability of reference and test responses as a function of the noise level added to the stimuli and the temporal resolution of the measure of discrimination as developed by Victor and Purpura (1997). Data are based on a set of 11 H1 neurons recorded in 11 different flies. Transects 'b' and 'c' are shown in more detail in **(b)** and **(c)**. Mean discriminability of reference and test responses at maximum noise level ($\sigma = 64$) in dependence of the temporal resolution used for data analysis. The error bars show the standard deviation of percentage correct decisions across the 11 cells. The shaded area represents the domain of uncertainty (see Methods for details). As b, but the noise amplitude was varied at the "best" temporal resolution (15.625ms).

The average discrimination performance (n = 11 H1-cells recorded in 11 different flies) is shown in figure 5.4a as a function of both, the temporal resolution and the noise level. In some flies the 75% criterion, as shown in figure 5.2b, was reached for high noise levels while other recordings revealed discrimination performances below this threshold even at the highest noise levels used in the experiments. The averaged discrimination performance peaks at large noise levels and at temporal resolutions between 5 and 20ms. Finer resolutions yield performances, even at the highest noise level, below threshold and only weakly above the domain of uncertainty (figure 5.4b). On average, also temporal resolutions coarser than 62.5ms result in no significant discriminability. Even for the temporal resolution at which the discrimination performance is best (15.625ms), the performance is significantly better than chance level only at noise levels above $\sigma = 32$ (figure 5.4c). Hence, the temporal structure of the neuronal responses is systematically affected only at noise levels exceeding this value. However, even at the highest noise level the 75% threshold is not reached on average. In none of the recordings the discrimination threshold was reached with noise levels lower than $\sigma = 32$. As it is common in psychophysical

experiments, this value may be understood as an estimate of the overall noise in the system, including internal sources of variability as well as photon noise (see e.g. Pelli, 1990). In our stimulus paradigm photon noise is estimated to equal a brightness modulation of approximately $\sigma = 4$ (see methods). As can be concluded form the experiments, this level of added noise has no major impact on the cell's mean response amplitude nor the temporal fine structure.

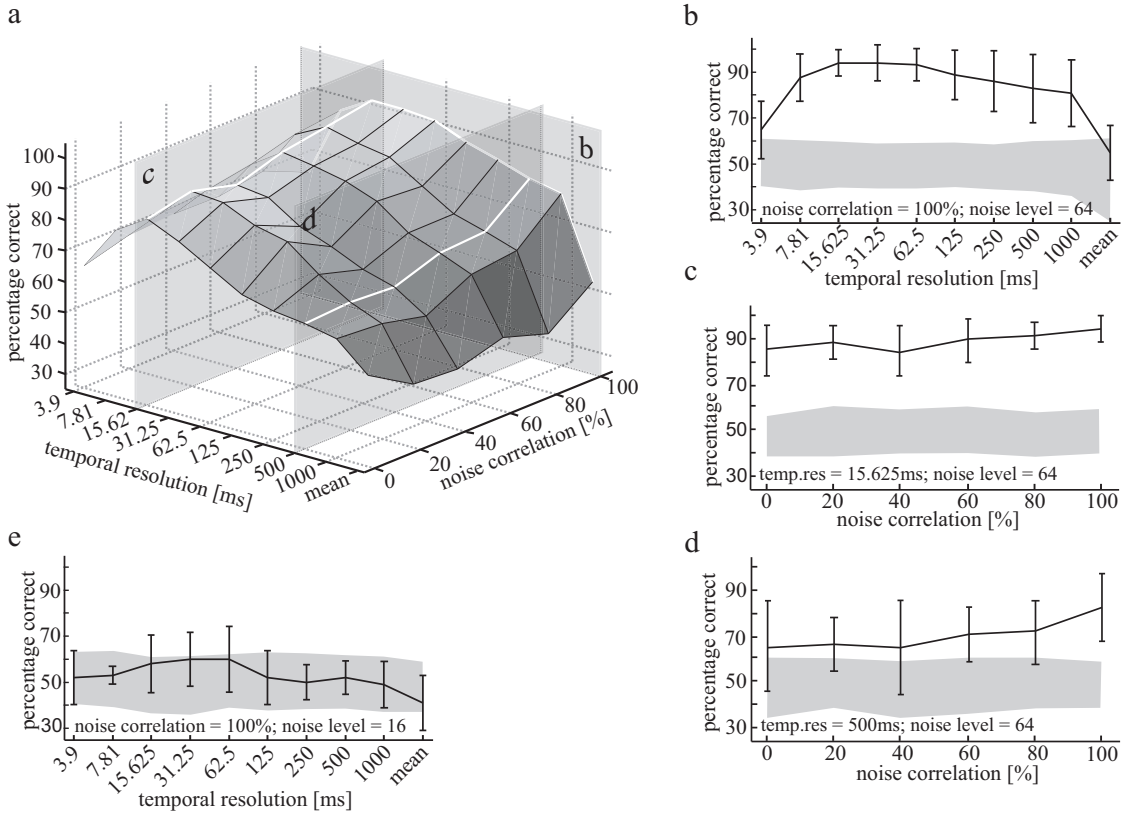

Figure 5.5: Response Discriminability with correlated noise. **(a)**Mean discrimination performance as a function of the noise-correlation and the temporal resolution of the measure of discrimination as developed by Victor and Purpura (1997). The experiments were performed at maximum noise level ($\sigma = 64$). The average performance is based on 10 H1 recordings in another set of 10 different flies than those on which the data shown in figure 5.4 are based. The transections refer to sections shown in **(b)**, **(c)** and **(d)**. Average discrimination performance at 100% noise correlation expressed in percentage correct decisions as a function of the temporal resolution used for data analysis. Error bars show the standard deviation across the 10 H1 recordings. The shaded area illustrates the domain of uncertainty (for explanation see Methods). As b but the noise correlation was varied at the "best" temporal resolution. The temporal resolution was 15.625ms. As c but at a temporal resolution used for data analysis of 500ms.**(e)** Mean discrimination performance at 100% noise correlation and a noise level of $\sigma = 16$ as a function of the temporal resolution for 4 H1 recordings of 4 different flies. The error bars represent the standard deviation of performance levels. In grey the domain of uncertainty, which represents the performance levels which are likely to be the result of internal noise and photon noise but not of the added external noise.

Impact of correlated noise

In the experiments described so far, the noise added to the different moving dots was uncorrelated. The effect of external noise on a neuron can be expected to increase if the noise carried by the neuron's different inputs is correlated to some extent (see e.g. Zohary et al., 1994). Since photon noise is uncorrelated at the different photoreceptors, the degree of correlation needed to affect the neuronal response pattern can be used as another way to assess the role of photon noise versus noise intrinsic to the nervous system for the reliability of visual motion computation. In a second set of experiments (n = 10 recorded H1-cells in another set of 10 different flies) the noise superimposed on a fraction of the dots was correlated. The number of dots with correlated noise was either 0, 2, 4, 6, 8 or 10 out of 10 dots. When the correlation at maximum noise level was increased, the H1 responses were affected not only on a relatively fine time-scale, as is the case for uncorrelated noise, but also on a coarser time-scale. When the noise was 100% correlated, i.e. the brightness fluctuations of all ten dots are identical, reference and test responses could be discriminated with temporal resolutions of up to 1000ms (figure 5.5b and transection 'b' in figure 5.5a). With the finest temporal resolution the discrimination performance is significantly different from chance level but does not reach the 75% threshold. However, even with 100% noise correlation at maximum noise level ($\sigma = 64$), no effect on the mean spike rate could be observed (only one of the 10 cells showed a significant difference in the mean spike rate; $\alpha < 5\%$, Wilcoxon rank sum test, the mean spike frequency of the corresponding reference responses was 78.6Hz with a standard deviation of 1.55Hz the test responses had a mean and standard deviation of 80.7 and 2.3Hz respectively). At the temporal resolution which led to the best discrimination performance (15.625ms) with uncorrelated external noise (compare figure 5.4), we found a weak increase in performance with increasing noise-correlation (figure 5.5c and transection 'c' in figure 5.5a). At this temporal resolution the performance was above threshold for all correlation levels. Again, the responses of some cells could not be distinguished with more than 75% performance. With a coarser temporal resolution (500ms; figure 5.5d and transection 'd' in figure 5.5a), a more obvious increase in performance could be observed. While it was below threshold and not clearly different from chance level without noise-correlation, a major impact of the external noise was obtained at 100% noise-correlation. When adding noise to the moving dots with a noise level of $\sigma = 16$ and 100% correlation, the responses to reference and test stimuli are nearly indistinguishable for all temporal resolutions (n = 4 recorded in 4 different flies; figure 5.5e). Hence, even for absolutely correlated noise, a noise level, more than four times larger than photon noise, is needed to affect the responses significantly.

Conclusion

The temporal structure of the H1 responses to motion stimuli are affected by superimposed noise only if the noise fluctuations cover most of the available brightness range of the monitor screen, and thus, is much larger than photon noise under our experimental conditions. Then the temporal structure of the responses is affected on a time-scale in the range of approximately 15 ms. If the noise added to different dots of the motion stimulus is correlated, the range of temporal resolutions at which changes in the response can be detected is extended. Nevertheless a high noise level is needed to affect the responses, even when the noise in the input signal is 100% correlated. Thus, both sets of experi-

ments, using uncorrelated as well as correlated noise superimposed on the input signal, support the conclusion of photon noise being of only minor importance for the reliability of motion vision in H1.

5.5 Discussion

Comparison with Photon noise

Is the neuronal variability a consequence of the noisy visual input, i.e. photon noise, as has recently been proposed (Borst and Haag, 2001; Lewen et al., 2001), or does it emerge within the nervous system? While these studies applied more indirect methods to tackle this question, with our approach we directly manipulated the input signal. The brightness modulations superimposed on the dots mimicked photon noise and by varying the strength of the modulations allowed us to assess the impact of photon noise on the reliability of the H1 responses. The overall system noise is approximately equivalent to a noise level of $\sigma > 32$ in our stimulus paradigm (compare figure 5.4). How much of the overall noise can be attributed to photon noise respectively noise emerging within the visual system? As estimated in the methods section, photon noise under the conditions of our experiments corresponds to a noise of approximately $\sigma = 4$ in our paradigm. Thus, neuronal unreliability, rather than photon noise appears to be the major noise source that limits the reliability of visual motion computation. This conclusion needs to be qualified in two respects: (i) The estimation of the relevant photon noise is based on the implicit assumption that noise in only those photoreceptors that are stimulated by the moving dots contribute to the response variability of H1. This assumption appears to be justified, in a first approximation, because the stationary background was much darker than the dots and the variability found in fly motion-sensitive neurons during stimulation with stationary dark patterns was much smaller than during motion stimulation (Hengstenberg, 1982; Warzecha, 1994). (ii) It was assumed that each motion dot perfectly covers the receptive field of just a single photoreceptor and does not affect neighbouring receptors. Since this may frequently not be the case, the photons emitted by a dot may be shared, as a consequence of the hexagonal lattice of ommatidia, by three adjacent photoreceptors. As a consequence, the amount of photons reaching a single receptor and, thus, the SNR of the input signal may be reduced. In the 'worst case' a single dot is centred above the corner of three neighbouring ommatidia. This would reduce the number of photons reaching a single photoreceptor by two-thirds. To meet the worsened signal-to-noise-ratio caused by light reduction an added noise with standard deviation of approximately $\sigma = 6.8$ would be needed. Even this noise level is much smaller than the noise level found to influence the H1 responses. On the other hand, in the fly retina the signals of six photoreceptors sampling the same point in space are averaged by electric coupling of their axons (e.g. Laughlin, 1994). This coupling would reduce the variance in the averaged signal by the square-root of 6, since photon noise is independent for each of them. Moreover, at noise levels of more than twice this noise level, the responses to the reference and to the test stimulus are indistinguishable even when the noise added to all moving dots is completely correlated (see figure 5.5e). Since photon noise affecting different photoreceptors is statistically independent, this finding further corroborates our conclusion that under the conditions of our experimental analysis photon noise does not limit the reliability of

neural coding. Rather, we can conclude that the variability in the timing of spikes in H1 is mainly a consequence of noise sources intrinsic to the nervous system. This conclusion is likely to extend to most light levels when the diurnal flies fly around, because our stimulus was much darker than daylight. Under behaviourally relevant light conditions the number of photon arrivals, and thus the SNR, is much higher. The conclusion that noise intrinsic to the nervous system limits the reliability of motion information processing is in accordance with experimental data on the peripheral visual system of the fly. Although in completely dark-adapted eyes single photons could be inferred to affect the signal of the H1-neuron (Lillywhite and Dvorak, 1981), even at moderate light levels that are still much lower than daylight individual photons only have a small effect on the overall photoreceptor potential and the synapse between photoreceptor and second-order neurons contribute significantly to the response variability at this processing stage (e.g. Laughlin et al., 1987; Juusola et al., 1995; de Ruyter van Steveninck and Laughlin, 1996). Thus our results are in line with earlier findings which suggest that, at least for light levels as used in our experiments and for larger ones, internal noise sources are of more importance than the noise in the visual input (Laughlin et al., 1987; de Ruyter van Steveninck and Laughlin, 1996), but are in contrast with other interpretations (Lewen et al., 2001; Borst and Haag, 2001).

Comparison with contradictory interpretations

Lewen et al. (2001) performed methodologically challenging outdoor recordings of H1 while rotating the whole fly about its vertical body axis in a naturalistic manner. Experiments were done with the same fly at different times of the day and thus at different mean light levels. From noon to half an hour after sunset, the H1-cell responded to the same motion sequence with decreasing mean spike rate. The conclusion of photon noise being the limiting factor is based on the finding that information rate increases with increasing light level and, thus, with an increasing signal-to-noise ratio of the stimulus. However, in other studies, the information rate was shown to be linked approximately linearly to the mean number of spikes, even if spike activity was increased at the same mean light level by changes in stimulus parameters such as velocity or contrast (Schneidman et al., 2001; Borst and Haag, 2001). Hence, the changes in information rate observed during the course of the day may be interpreted as consequence of increasing spike rate rather than signal-to-noise ratio of the incoming signals. This suggestion is corroborated by the finding that during the course of the day changes in spike rate are more likely linked to changes in ambient temperature than to changes in light level (Egelhaaf et al., 2001; Warzecha and Egelhaaf, 1999). On this basis we conclude that the experimental results of Lewen et al. (2001) do not necessarily disagree with our finding that the performance of the H1-neuron is mainly limited by noise sources intrinsic to the nervous system rather than by photon noise. Borst and Haag (2001) analysed the amount of information transmitted by H1 in dependence of the activity level that was altered by visual motion stimulation. The experimental results were compared to predictions which were drawn from a model H1 which receives input from eight correlation type motion detectors and transforms the resulting graded membrane potential changes into spike trains using a Hodgkin-Huxley-type spike generator. The model's input signal was additionally corrupted by brightness modulations mimicking photon noise which were adjusted to match

experimentally found response variability. Since the performance of both real and model H1 were similar and no other noise but photon noise was introduced into the system, it was concluded that photon noise is the dominant noise source of the fly's visual motion pathway. Given that the model H1-cell was driven by only eight motion detectors, their gain had to be sufficiently high to drive the cell to a realistic activity level. However, under the stimulus conditions of the experiments of (Borst and Haag, 2001) the H1-cell receives input from hundreds of motion-sensitive elements which contribute to the overall response. Hence, the individual input channels are likely to have contributed much less to the variability of the H1-neuron than was assumed in the corresponding model simulations. Thus, these results do not appear to contradict our conclusion, that the noise level found in H1 is mainly determined by sources intrinsic to the nervous system rather than by photon noise.

References

Barberini C, Horwitz G, Newsome W (2000) A Comparison of Spiking Statistics in Motion Sensing Neurons of Flies and Monkeys. In: Zanker J, Zeil J, editors, Computational, Neural and Ecological Constraints of Visual Motion Processing., pp. 307–320, Berlin, Heidelberg, New York: Springer.

Berry M, Warland D, Meister M (1997) The Structure and Precision of Retinal Spike Trains. PNAS 94: 5411–5416.

Borst A, Haag J (2001) Effects of Mean Firing on Neural Information Rate. J Comput Neurosci 10: 213–221.

Borst A, Haag J (2002) Neural Networks in the Cockpit of the Fly. J Comp Physiol [A] 188: 419–437.

Bouman M, van de Grind M, Zuidema P (1985) Quantum Fluctuations in Vision. In: Wolf E, editor, Progress in optics., pp. 79–144, Amsterdam, New York, Oxford, Tokyo: North Holland.

Britten K, Shadlen M, Newsome W, Movshon J (1993) Responses of Neurons in Macaque MT to Stochastic Motion Signals. Vis Neurosci 10: 1157–1169.

de Ruyter van Steveninck R (1986) Real-Time Performance of a Movement-Sensitive Neuron in the Blowfly Visual System. Ph.D. thesis, Groningen University, Netherlands.

de Ruyter van Steveninck R, Bialek W (1995) Reliability and Statistical Efficiency of a Blowfly Movement-Sensitive Neuron. Phil Trans R Soc Lond B 348: 321–340.

de Ruyter van Steveninck R, Borst A, Bialek W (2001) Real-Time Encoding of Motion: Answerable Questions and Questionable Answers from the Fly's Visual System. In: Zanker J, Zeil J, editors, Motion Vision, pp. 279–306, Berlin, Heidelberg, New York: Springer.

de Ruyter van Steveninck R, Laughlin S (1996) The Rate of Information Transfer at Graded-Potential Synapses. Nature 379: 642–645.

Egelhaaf M, Grewe J, Kern R, Warzecha A (2001) Outdoor Performance of a Motion-Sensitive Neuron in the Blowfly. Vision Research 41: 3627–3637.

Egelhaaf M, Kern R, Krapp H, Kretzberg J, Kurtz R, et al. (2002) Neural Encoding of Behaviourally Relevant Visual-Motion Information in the Fly. TINS 25: 96–102.

Egelhaaf M, Warzecha A (1999) Encoding of Motion in Real Time by the Fly Visual System. Curr Opin Neurobiol 9: 454–460.

Francescini N (1975) Sampling of the visual environment by the compound eye of the fly: Fundamentals and applications. In: Snyder AW MR, editor, Photoreceptor optics, pp. 98–125, Berlin, Heidelberg, New York: Springer.

Götz K (1965) Die optischen Übertragungseigenschaften der Komplexaugen von Drosophila. Kybernetik 2: 215–221.

Haag J, Borst A (2002) Dendro-Dendritic Interactions between Motion-Sensitive Large-Field Neurons in the Fly. J Neurosci 22: 3227–3233.

Hardie R (1979) Electrophysiological Analysis of the Fly Retina. I. Comparative Properties of R1-6 and R7 and R8. J CompPhysiol [A] 129: 19–33.

Hausen K (1976) Functional charaterization and anatomical identification of motion sensitive neurons in the lobula plate of the blowfly *Calliphora erythrocephala*. Z Naturforsch 31: 629–633.

Hausen K (1982) Motion Sensitive Interneurons in the Optomotor System of the Fly. I. The Horizontal Cells: Structure and Signals. Biol Cybern 45: 143–156.

Hengstenberg R (1982) Common Visual Response Properties of Giant Vertical Cells in the Lobula Plate of the Blowfly Calliphora. J Comp Physiol [A] 149: 179–193.

Johnston D, S W (1995) Foundations of Cellular Neurophysiology. Cambridge, MA: MIT.

Juusola M, Uusitalo R, Weckström M (1995) Transfer of Graded Potentials at the Photoreceptor-Interneuron Synapse. J Gen Physiol 105: 117–148.

Kara P, Reinagel P, Reid R (2000) Low Response Variability in Simultaneously Recorded Retinal, Thalamic, and Cortical Neurons. Neuron 27: 635–646.

Kretzberg J, Warzecha A, Egelhaaf M (2001) Neural Coding with Graded Membrane Potential Changes and Spikes. J Comput Neurosci 11: 153–164.

Laughlin S (1994) Matching Coding, Circuits, Cells, and Moleculees to Signals: General Principals of Retinal Design in the Fly's Eye. Progress in Retinal and Eye Research 13: 165–196.

Laughlin S, Howard J, Blakeslee B (1987) Synaptic Limitations to Contrast Coding in the Retina of the Blowfly *Calliphora*. Proc R Soc Lond B Biol Sci 231: 437–467.

Levine M, Zimmerman R, Carrion-Carire V (1988) Variability in Responses of Retinal Ganglion Cells. Journal of the Optical Society of America A 5: 593–597.

Lewen G, Bialek W, de Ruyter van Steveninck R (2001) Neural Coding of Naturalistic Motion Stimuli. Network 12: 317–329.

Lillywhite P, Dvorak D (1981) Responses to Single Photons in a Fly Optomotor Neurone. Vis Res 21: 279–290.

Pelli D (1990) The Quantum Efficiency of Vision. In: Blakemore C, editor, Vision: Coding and Efficiency., pp. 1–24, Cambridge: Cambridge University Press.

Reichardt W (1965) Quantum Sensitivity of Light Receptors in the Compound Eye of the Fly *Musca*. Cold Spring Harbor Symp Quant Biol 30: 505–515.

Rodieck R (1998) The First Steps in Seeing. Sunderland, MA: Sinauer.

Schneidman E, Brenner N, Tishby N, de Ruyter van Steveninck R (2001) Universality and Individuality in a Neural Code. In: Leem T, Dietterick T, Tresp V, editors, Advances in neural information processing, vol. 13, pp. 151–165, Cambridge, MA: MIT.

Smakman J, Hateren J, Stavenga D (1984) Angular Sensitivity of Blowfly Photoreceptors: Intracellular Measurements and Wave-Optical Predictions. J Comp Physiol [A] 155: 239–247.

Tolhurst D, Movshon J, Dean A (1983) The Statistical Reliability of Signals in Single neurons in Cat and Monkey Visual Cortex. Vision Res 23: 775–785.

van Hateren J (1984) Waveguide Theory Applied to Optically Measured Angular Sensitivities of Fly Photoreceptors. J Comp Physiol [A] 154: 761–771.

Victor J, Purpura K (1997) Metric-Space Analysis of Spike Trains: Theory, Algorithms and Application. Coumput Neural Syst 8: 127–164.

Vogels R, Spileers W, Orban G (1989) The Response Variability of Striate Cortical Neurons in the Behaving Monkey. Exp Brain Res 77: 432–436.

Warzecha A (1994) Reliability of Neuronal Information Processing in the Motion Pathway of the Blowflies *Calliphora erythrocephala* and *Lucilia cuprina*. Ph.D. thesis, Universität Tübingen, Germany.

Warzecha A, Egelhaaf M, Borst A (1993) Neural Circuit Tuning Fly Visual Interneurons to Motion of Small Objects. I. Dissection of the Circuit by Pharmacological and Photoinactivation Techniques. J Neurophysiol 69: 329–339.

Warzecha AK, Egelhaaf M (1999) Variability in Spike Trains During Constant and Dynamic Stimulation. Science 283: 1927–1930.

Warzecha AK, Egelhaaf M (2001) Neuronal Encoding of Visual Motion in Real-Time. In: Zanker J, Zeil J, editors, Motion Vision - Computational, Neural, and Ecological Constraints, pp. 239–277, Berlin, Heidelberg, New York: Springer.

Warzecha AK, Kretzberg J, Egelhaaf M (2000) Reliability of a Fly Motion-Sensitive Neuron Depends on Stimulus Parameters. J Neurosci 20: 8886–8896.

Zohary E, Shadlen M, WT N (1994) Correlated Neuronal Discharge Rate and its Implications for Psychophysical Performance. Nature 370: 140–143.

6 Implications of Functionally Different Synaptic Inputs for Neuronal Gain and Computational Properties of Fly Visual Interneurons

The content of this chapter has already been published as: Jan Grewe, Nélia Matos, Martin Egelhaaf, and Anne-Kathrin Warzecha: *Implications of Functionally Different Synaptic Inputs for Neuronal Gain and Computational Properties of Fly Visual Interneurons.*, Journal of Neurophysiology 96: pages 1838 - 1847, 2006

6.1 Summary

Neurons embedded in networks are thought to receive synaptic inputs that do not drive them on their own, but modulate the responsiveness to driving input. Although studies on brain slices have led to detailed knowledge of how non-driving input affects dendritic integration, its origin and functional implications remain unclear. We tackle this issue using an ensemble of fly wide-field visual interneurons. These neurons offer the opportunity to combine *in vivo* recording techniques and natural sensory stimulation as well as to interpret electrophysiological results in a behavioral context. By targeted manipulation of the animal's visual input we find a pronounced modulating impact of non-driving input, whereas functionally important cellular properties like direction tuning and the coding of pattern velocity are left almost unaffected. We propose that the integration of functionally different synaptic inputs is a mechanism that immanently equalizes the ensemble's sensitivity irrespective of the specific stimulus conditions.

6.2 Introduction

Dendritic integration is a central and often highly nonlinear stage of neuronal information processing. The many different presynaptic signals a neuron receives have been classified as drivers and modulators (Sherman and Guillery, 1998). Driving input is thought to carry the relevant information, while the modulating input shapes the neuronal computations without any driving contribution. Shunting inhibition is one example of modulating input, which may even veto the driving input (Koch et al., 1983). Cortical neurons are assumed to be continually bombarded with excitatory and inhibitory inputs induced by background network activity. The impact of background activity leads e.g. to a drop in input resistances *in vivo* as compared to those *in vitro* or in anaesthetized animals when there is only reduced network activity (Destexhe et al., 2003). Accordingly, the background activity has been proposed to be a mechanism that modulates the gain of a neuron (Chance et al., 2002; Mitchell and Silver, 2003; Prescott and De Koninck, 2003). Despite great methodological advances such as the dynamic clamp technique, applied to mimic background activity in slice preparations (Prinz et al., 2004), conclusions about the functional significance and origin of background input are still limited.
Here we address the functional significance of modulating synaptic background input linking cellular physiology with the functional aspects of encoding and representing visual stimuli. We investigate how visual shunting input affects the encoding of visual motion stimuli in fly visual interneurons. The task of these tangential cells (TCs) is to evaluate optic flow patterns, i.e. the retinal image flow evoked during self-motion of the animal (Borst and Haag, 2002; Egelhaaf et al., 2002, 2004; Hausen, 1984). Optic flow patterns are the only source of information about the environmental layout when airborne. TCs spatially integrate the excitatory and inhibitory outputs of thousands of retinotopically arranged local motion sensitive elements (Brotz et al., 1996). Accordingly, TCs have receptive fields that cover large parts of the visual field and are tuned to optic flow as is generated on the eyes during certain types of translational or rotational self-motion of the animal (Egelhaaf et al., 2002; Kern et al., 2005; Krapp et al., 2001; van Hateren et al., 2005). The activation ratio of excitatory and inhibitory inputs depends on stimulus parameters as pattern contrast and texture or the direction and velocity of visual motion. Even during motion in the preferred direction, which distinctly depolarizes the cell, the inhibitory inputs are activated, though to a much smaller extent than the excitatory input (Borst et al., 1995; Single et al., 1997). Motion orthogonal to the preferred direction is assumed to activate both types of inputs in approximately equal shares, whereas during null-direction motion the inhibitory input predominates. Fly TCs offer the opportunity to investigate under *in vivo* conditions the influence of selectively manipulated sensory input in a well established functional context. In this study we examined the functional consequences of modulating input on neuronal sensitivity, direction tuning, and the representation of the time course of pattern velocity. Coherent motion as driving input and balanced motion noise as the modulating background input were combined for visual stimulation. This decomposition of the visual input into a driving and a modulating component was done for the sake of systems analysis only, although under natural conditions TCs are exposed to optic flow containing motion vectors in a wide range of directions driving its activity to a different extent or not at all. Thus, in behavioral situations TCs receive inputs that have both driving and modulating impact.

6.3 Methods

Electrophysiology

Experiments were carried out on 1-7 day old female blowflies (*Calliphora vicina*). The animals were prepared as described in Warzecha et al. (1993). In short: the flies were briefly anaesthetized with CO_2 and fixed ventral side up on a small piece of glass. The head was bent down and waxed to the thorax to allow access to the backside of the head. The head-capsule was opened and tissue like air-sacs, fat bodies, and trachea that cover the lobula plate were removed. In some preparations we also removed the gut to eliminate peristaltic movements that can cause disturbances. After preparation, the flies were adjusted according to the symmetry of the deep pseudopupil (Francescini, 1975) to ensure that different animals received the same visual input.

Extracellular recordings The H1 neuron was recorded extracellulary with self-made tungsten electrodes. A Ringer-filled glass capillary, through which we could provide Ringer solution if necessary (for composition see Hausen, 1982a), was used as indifferent electrode. The recorded signals were amplified by a factor of 3000, bandpass filtered (corner frequencies of 300 Hz and 3 kHz), and subsequently passed through a threshold device that transforms detected spikes into uniform pulses. The H1 neuron was recorded in the left half of the brain in its output arborization. It can be easily identified by its preferred direction, i.e. back to front motion in front of the right eye.

Intracellular recordings VS neurons were recorded in or close to their main dendrite with sharp electrodes pulled on a Brown/Flaming P-97 Puller (Sutter Instruments) and filled with 2M KCl. The electrodes had resistances between 30 and 40 $M\Omega$ and the electrode holder's silver wire was chlorided before every recording. We used a SEC 10-L amplifier (npi - electronics, Germany) operated in bridge or discontinuous current clamp (DCC) mode. In DCC mode the switching frequency was about 8 kHz. The raw data traces of intra- and extracellular recordings as well as the thresholded H1 spike trains were sampled at 4 kHz (DaqBoard2000, IOTech Inc., OH) and stored on hard disk for offline analysis. The program for data acquisition was written in Delphi 7 (Borland Software Corporation).

Visual Stimulation

Visual stimuli were generated using a VSG 2/3 graphics card (Cambridge Research Systems, Cambridge, UK) and presented on a Joyce Scope DM5 monochrome (P-31 phosphor) monitor (Joyce Electronics Inc., Cambridge, UK). As seen by the fly, the monitor screen (464 x 375 pixel spatial resolution) had a horizontal and vertical extent of 127° and 120°, respectively. The screen centre was positioned at 0° elevation and 20° azimuth. At this point, one pixel had a vertical and horizontal extent of 0.5°. While the frame rate was 300 Hz, new stimulus pictures were presented with 150 Hz. We could disprove time-locking of H1 spikes to either frequency by cross-correlating 200 response traces to identical stimulation (data not shown). The stimuli consisted of two sets of dots moving on the black screen (luminance: 0.001cd/m^2). The first set of dots, the motion dots, were randomly positioned in the first frame and moved coherently in the preferred direction of

the recorded TC. These served as driving input, forming the sensory signal to be encoded by the TCs. Each dot had a vertical and horizontal extent of 3 pixels resulting in an angular size of approximately 1.5°x1.5° as seen by the fly; it was surrounded by a 6° 'forbidden zone' in which no other dot was allowed to be placed. By varying the number of dots (between 4 and 64) different movement strengths were produced. The motion dots were always presented at full brightness (300cd/m^2). The second set of dots consisted of 112 noise dots, which have the same size and forbidden zone as the motion dots. The noise dots were designed to constitute the modulating background input. Initially the noise dots were also randomly placed. In subsequent frames they performed a random walk, in which eight directions (the horizontal, vertical, and diagonal directions) were possible. For each time step the direction of each dot was chosen randomly from a predefined distribution. This distribution of directions was defined so that the directions into which the noise dots moved were balanced, i.e. the resulting motion noise did not, on average, excite or inhibit the recorded neuron. Balancing was done in control experiments for one sample VS-cell and H1-cell. The distribution of movement directions that led to the best balancing, that is, with no clear excitation or inhibition, was used for all other experiments on the same cell type. The strength of the motion noise was altered by changing the brightness of the noise dots to 30 cd/m2 (weak motion noise), 150 cd/m^2 (medium motion noise), and 300 cd/m^2 (strong motion noise). Even the lowest brightness value was sufficient to significantly affect the neuronal responses, increasing the firing rate of the H1-neuron when dots of this brightness moved in the cell's preferred direction. As mentioned above, the dots were surrounded by a "forbidden zone", in which no other dot occurred. This zone was introduced to prevent the motion dots and noise dots from interacting on a local basis, i.e. generating apparent motion. In flies, adapted to total darkness, it is possible to evoke a weak direction-selective response in H1 when the two stimuli of an apparent motion paradigm are separated up to 12° (Schuling et al., 1989). Although the flies in our experiments were not completely dark adapted, we could show in a control experiment that increasing the forbidden zone to above 12° (with a reduced number of dots) or completely separating motion and noise dots (coherent motion in the upper third of the screen and motion noise in the lower third or vice versa) does not significantly alter the effect of motion noise on H1 responses.

Measurements of TC input resistance

The input resistances of VS-cells were measured by injecting 200 ms pulses of constant hyperpolarizing current (-0.75 to -1.5 nA) into the cells. Trials with and without current were recorded in a pseudo-random order which allows to calculate the input resistances from direct comparisons of the corresponding response sections (Figure 6.2a).

Gain modulation by visual motion noise

To investigate the consequences of motion noise on the sensitivity of TCs for preferred direction motion, we tested the neuronal responses to motion stimuli of five different strengths, determined by the number of dots moving on the screen (4, 8, 16, 32, and 64 dots) combined with (or without) motion noise. As mentioned above, three different strengths of motion noise were used. Each trial consisted of three test sections: (i) coherent motion with the actual number of motion dots moving, (ii) the motion noise

alone at a given intensity, and (iii) coherent motion and motion noise combined. These were alternated with so-called reference sections in which the maximum number of motion dots moved and breaks showing a stationary image (Table 6.1). This image was the first image of the following section.

Table 6.1: Experimental protcol describing the images shown.

Duration, s	Gain modulation	Direction tuning
0.5	Blank screen	Blank screen
	Reference section	
1.0	Pure motion	Pure motion
1.0	Stationary image	Stationary image
	Test section I	
1.0	Pure motion (4-64 dots)	Pure motion (various directions)
1.0	Stationary image	Stationary image
	Reference section	
1.0	Pure motion	Pure motion
1.0	Stationary image	Stationary image
	Test section II	
1.0	Noise (weak, medium, strong)	Noise (weak, strong)
1.0	Stationary image	Stationary image
	Reference section	
1.0	Pure motion	Pure motion
1.0	Stationary image	Stationary image
	Test section III	
1.0	Motion (4-64 dots)+noise	Motion (various directions)+noise
1.0	Stationary image	Stationary image

Direction tuning in the presence of motion noise

A similar stimulus protocol was used to test the direction selectivity of TCs (Table 6.1, right). In these reference sections the maximum number of motion dots moved in the preferred direction of the cell. In the test sections the coherently moving dots (16 or 64) were moved in one of the 8 tested directions (0-315° in 45° steps). To reduce the number of conditions (in order to have a reasonable number of trials for each condition) we used only the medium and strong motion noise.

Representation of pattern velocity in the presence of motion noise

We investigated the representation of pattern velocity with extracellular recordings of the H1-cell, because this analysis requires stable recordings over a longer time than can routinely be accomplished by intracellular recording. The motion dot velocity was dynamically modulated (Figure 6.6, left column). The underlying velocity profile was built up from sinewaves of 1, 3, 5, 7, and 9 Hz at random phases. The frequencies were

matched to the frequency band in which the H1-cell codes pattern velocity with a high gain (Warzecha et al., 1998). Here we used a stimulus protocol consisting of three test sections (dynamic motion alone, motion noise alone, and the combination of both, each of 1000ms duration). The test sections were separated by stationary image sections of 5000ms duration. The interstimulus interval between consecutive trials of any experiment was 5000ms. This time was used to save the data and to provide Ringer solution if necessary.

Data analysis

Offline analysis was done with Matlab Release 14 (the Mathworks, MA). To analyze the performance of H1 to encode stimulus velocity (see above) we employed the coherence analysis (Haag and Borst, 1998; van Hateren and Snippe, 2001) using the coherence function distributed with Matlab. For this purpose the responses were aligned with the velocity profile by removing the response delay which was calculated from the cross correlation of the mean response and the velocity profile. Both stimulus and response vectors were zero padded to give 4096 sample points. Due to the rectification non-linearity inherent in the spike generation process, the H1 can only code pattern velocity in its preferred direction. Therefore, we rectified the stimulus velocity accordingly and set it to zero if the dots moved in the null-direction. The coherence between stimulus and response was calculated using a 4096 point Hanning window and an overlap of 2048 points. The coherence analysis quantifies the similarity between the stimulus and the stimulus reconstructed from the responses using the best linear filter. In the case of a noise-free linear encoder the coherence is 1 for all frequencies. Deviations from unity could be a consequence of noise and of non-linearities in the system. To separate these two effects the expected coherence (van Hateren and Snippe, 2001) was used. The expected coherence is defined as the coherence between the individual responses and the "noise free" average response. The deviation of the expected coherence from unity can be traced back to noise in the system. The difference between coherence and expected coherence is due to non-linearities. To estimate the information that is transmitted by the neuronal responses about the stimulus the coherence rate was calculated from the coherence spectrum according to van Hateren and Snippe (2001).

$$R_{coh} = -\int_0^\infty log_2(1-\gamma^2)df \tag{6.1}$$

with R_{coh} the coherence rate and γ the coherence. The expected coherence rate (R_{exp}) was calculated accordingly. Since the interpretation of the coherence rate in terms of transmitted information depends on assumptions that neuronal noise is Gaussian and additive, an assumption which is not strictly correct, we additionally calculated the information rate with the measure developed by Brenner et al. (2000).

$$I = \frac{1}{T}\int_0^\infty dt \left(\frac{r(t)}{\overline{r}}\right) log_2 \left(\frac{r(t)}{\overline{r}}\right) \tag{6.2}$$

with T the number of time bins, r(t) the time-dependent spike rate and $\overline{r}$ the average spike rate. Both measures implicitly assume that information is encoded by the spike rate of the neuron. This assumption appears justified as a first approximation, since TC

spikes were concluded to lock precisely to the stimulus in a frequency range of velocity fluctuations that are only weakly represented in TC responses (Kretzberg et al., 2001; Warzecha et al., 1998).

6.4 Results

We analyze the nonlinear dendritic integration of driving and modulating synaptic input in two types of directionally selective, motion sensitive neurons: (1) The H1 neuron (Hausen, 1976) offers the opportunity of stable long lasting extracellular recordings, which is required for a detailed analysis of coding properties (Bialek et al., 1991; Warzecha et al., 2000). The H1-cell is excited by back-to-front motion and inhibited by motion in the opposite direction within almost the entire visual field of one eye. It uses spikes to transmit information from one brain hemisphere to the other. (2) The VS-cells (Hengstenberg, 1982; Krapp et al., 1998) can be recorded intracellularly and respond to downward and upward motion within a broad vertical stripe of the visual field with graded de- and hyperpolarizations, respectively. These graded membrane potential shifts are assumed to represent the summated postsynaptic potentials of the cell and can be recorded even close to the output terminal of the cells (e.g. Egelhaaf and Warzecha, 1999). Since VS graded depolarization may be superposed by spikes, reminiscent of the variable spikes observed in cortical neurons (e.g. Azouz and Gray, 1999), VS-cells can also be employed to study the transformation of postsynaptic potentials into spikes. In this study we concentrate on two types of the ten VS-cells, i.e. VS1 and VS2/3. Since VS2 and VS3 are two cells with largely overlapping receptive fields and virtually indistinguishable functional properties (Krapp et al., 1998), they are lumped here into one category of cells 'VS2/3'. The analyzed VS-cells have their receptive fields in the frontal part of the visual field. To test the influence of modulating input on the response to a driving visual signal, two types of stimuli were employed (Figure 6.1, insets): (1) The driving visual input consists of a variable number of dots moving coherently either in the cell's preferred or null direction. (2) The modulating input consists of dots moving in a variety of directions so that excitatory and inhibitory effects cancel each other ('motion noise'). The driving input and the motion noise can be presented individually or combined. The motion noise component then acts as a modulating background input (see methods for details).

Balanced motion noise has shunting characteristics

The motion noise was balanced having no pronounced driving effect on the membrane potential on its own (Figure 6.1a right shaded response section). To achieve balance, more dots were required with a motion component in the null-direction than into the preferred direction of the respective cell. This is most likely due to the stronger driving force for the excitatory currents than for the inhibitory ones. Although the motion noise neither excites nor inhibits the neuron considerably, it increases the membrane potential fluctuations around the resting potential (Figure 6.1a, right shaded area). These fluctuations were smaller in some recordings, like the one shown in Figure 6.2. This might be due to the slight hyperpolarising effect of the motion noise in this experiment or to the different recording sites (close to the dendrites and close to the output terminals for the experiments shown in Figure 6.1 and 6.2 respectively).

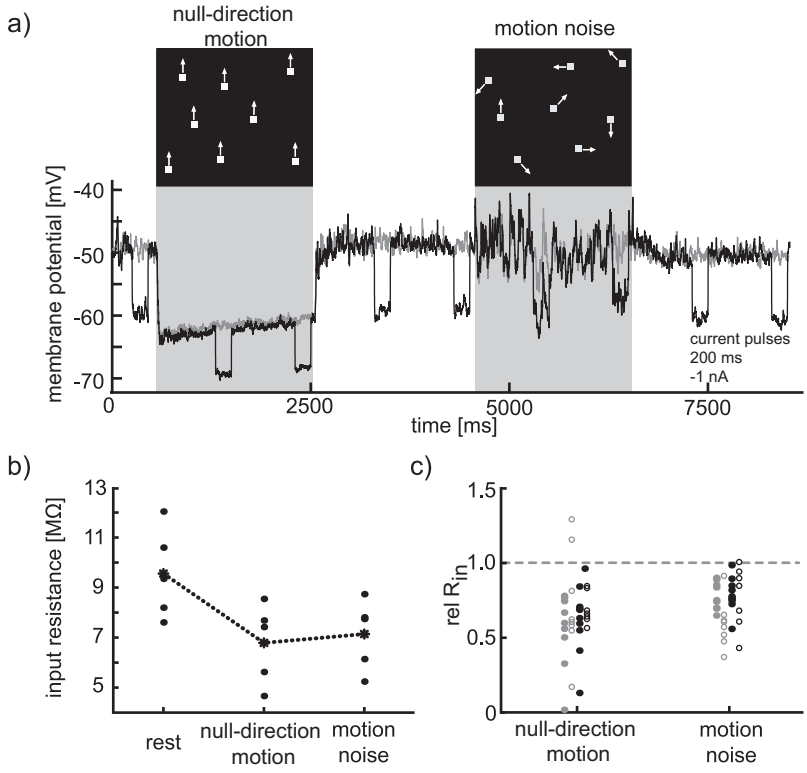

Figure 6.1: Measurement of the TC input resistance. (a), Average response of one VS-cell (5 trials) to coherent null direction motion and to motion noise (first and second shaded area). The strongest motion noise was chosen for this measurement. In half of the trials (black trace) 1nA hyperpolarising current pulses of 200ms duration were injected into the cell. The input resistance was calculated from the difference between the "current responses" and the "no-current" responses (black and grey traces, which were recorded alternately). **(b)**, Input resistance on single trial basis (black dots) and on average across the 5 trials on this condition (asterisks) of the same cell as shown in a). Input resistances were measured at rest, during null-direction motion and motion noise. **(c)**, Pooled results from 4 VS-cells recorded in 4 different animals, each dot is the input resistance estimated in a single trial. The input resistances are normalized to the respective input resistances at rest. The different symbols denote results from the different cells.

To determine whether motion noise has shunting characteristics, we measured the changes in input resistance of VS neurons relative to the resting input resistance induced by motion noise stimulation and by null-direction motion stimulation, respectively (Figure 6.1). The input resistance was estimated by injecting hyperpolarizing current pulses into the cells. The VS-cell input resistances at rest were on average $6.81 \pm 2.56\ M\Omega$ (n=4 cells) which is in the range reported before (Borst and Haag, 1996). However, the resting input resistances varied considerably. In one VS-cell (shown in Figure 6.1 a, b) an input resistance of $10.5\ M\Omega$ at rest was measured deviating much from the average. We did not find any obvious correlation between the difference in input resistance and the visually induced responses of VS-cells. Anyway, during coherent null direction motion, when the cell is hyperpolarized, the input resistance is decreased relative to the resting input resistance [$4.71 \pm 2.05\ M\Omega$; -32.23 $\pm$ 5.86% (Figure 6.1b, c)]. Motion noise does not depolarize or hyperpolarize the cell significantly but it reduces the input

resistance to 5.06 ± 1.95 MΩ [-26.05 ±6.52 % (Figure 6.1b, c)]. This reduction is in the same range, though slightly smaller, as the reduction of the input resistance during coherent null-direction motion. From these experiments we conclude that visual motion noise can be considered a shunting input comparable to the background input artificially induced in slice preparations (Chance et al., 2002; Mitchell and Silver, 2003; Prescott and De Koninck, 2003).

Non-linear integration of motion information

To analyze the effect of motion noise on the neuronal gain we determined the response amplitudes of VS- and H1-cells as a function of stimulus strength in the presence of motion noise of different levels. Stimulus strength was varied by varying the number of coherently moving dots. The strength of the motion noise was altered by increasing the brightness of the dots constituting the motion noise.

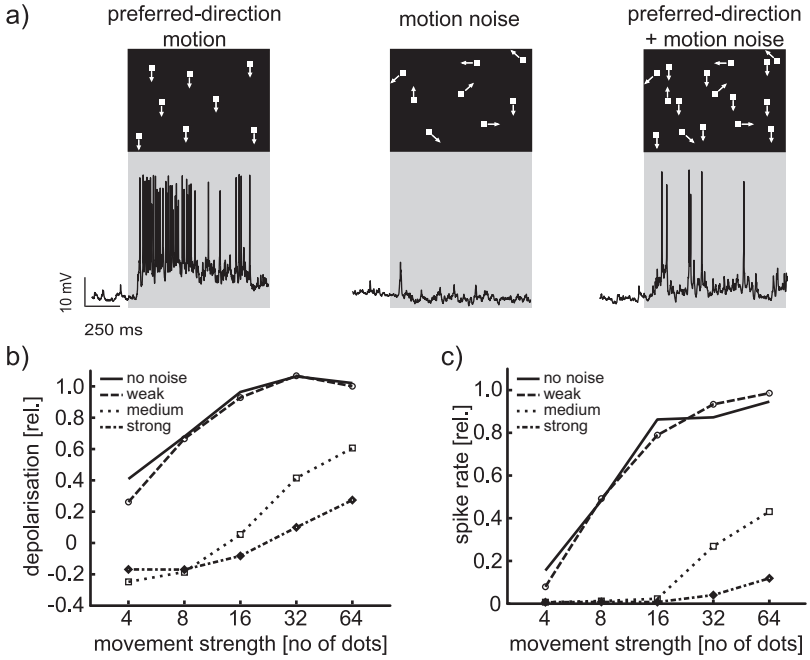

Figure 6.2: Influence of motion noise on VS sensitivity to preferred direction motion. **(a)**, Individual VS1 responses to coherent preferred direction motion, motion noise and the combination of coherent motion and motion noise recorded close to the axon terminal. These responses were evoked by the strongest motion stimulus (64 dots moving coherently) and the strongest motion noise (maximal brightness of the 112 motion noise dots). VS-cells show graded shifts of the membrane potential superimposed with spikes. **(b)**, Input-output characteristics of the graded membrane potential shift on different motion noise intensities. Motion strength was varied by increasing the number of dots moving coherently while the intensity of the motion noise was altered by varying the brightness of the dots constituting the motion noise (solid line, dashed line with open circles, dotted line with open squares, and dash-dotted line with open diamonds represent no, weak, medium and strong motion noise, respectively). Response amplitudes are normalized to the response to the strongest coherent motion (64 dots moving in preferred direction). **(c)**, Same as b but for the spike response of this cell.

Whereas both graded postsynaptic potentials and spikes can be recorded in VS-cells (Figure 6.2a), the H1-cell allows only spike responses to be recorded, though for extended periods of time (Figure 6.3). For both response modes of VS-cells the cell's sensitivity to motion stimuli is reduced by motion noise, independent of motion strength (Figures 6.2, 6.3). Stronger motion noise produces larger reductions in response amplitude. This reduction cannot be explained by a summation of the respective responses to coherent motion and motion noise (Figure 6.2a left and middle sections). Thus, the reduction in responsiveness is mainly due to the shunting effect of the motion noise. This is true despite the slight hyperpolarization of about -3.5 mV for the strongest motion noise in the example shown in Figure 6.2 a (middle column). Similar reductions were observed in other recordings in which motion noise led to slight depolarizations. The reduction in sensitivity for the driving input induced by coherent motion is similar for both the graded membrane potential shift and the spiking response of the VS recording (compare Figures 6.2a and b). However, the threshold nonlinearity of spike generation is apparent, since strong motion noise suppresses completely the spike responses to small and moderate motion strengths. Similar results were found in two other VS recordings and two recordings from other TCs (1 HSE and 1 CH cell). H1 is a spiking tangential cell which we recorded extracellularly. The responses of one sample recording are shown as PSTHs in Figure 6.3a. Figure 6.3b shows the average characteristics measured in 4 cells (similar results were found in 4 additional recordings which are not included since a slightly different stimulus protocol was applied). As for VS cells H1 spike frequency increases with increasing stimulus strength. When the motion stimulus is combined with motion noise the response amplitude is reduced in a similar way as those found in VS-cells. As for VS-cells, this reduction is present even if the motion noise induces a slight increase of the spike rate on its own. Thus, the interaction of the input mediated by coherent motion, on the one hand, and the input by motion noise, on the other hand, is far from linear. Shunting inhibition resulting from motion noise has severe consequences on the response amplitude and the cell's sensitivity for preferred direction motion.

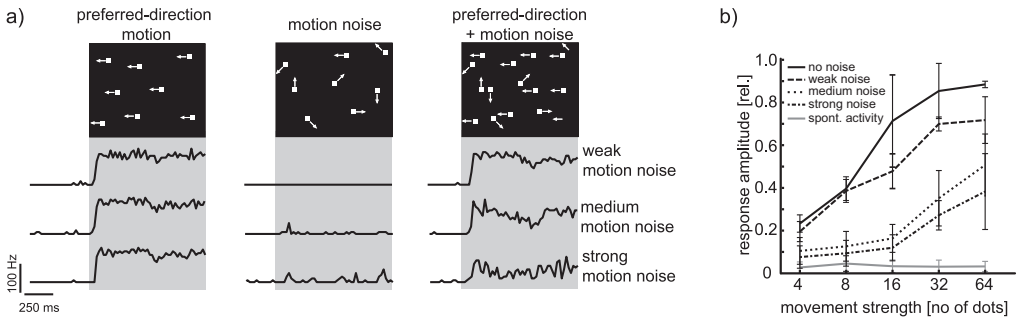

Figure 6.3: Influence of motion noise on H1 sensitivity to preferred direction motion. **(a)**, Averaged responses of a single H1-cell shown as PSTHs (peri stimulus time histograms, bin width 20 ms) to coherent preferred direction motion, motion noise, and the combination of coherent motion and motion noise (columns from left to right) for three different motion noise intensities (weak, medium, and strong motion noise in the upper, middle, and bottom row). **(b)**, Input-output characteristics averaged over four cells recorded in four different animals at different motion noise intensities (black solid, dashed, dotted, and dash-dotted lines represent no, weak, medium, strong motion noise, respectively; the grey solid line is the spontaneous activity). Errorbars are standard errors.

Robust direction tuning

In which way does motion noise affect the coding properties of blowfly motion sensitive TCs? We used the motion noise to target the robustness of direction tuning of TCs. For this analysis H1 responses were recorded extracellulary to obtain sufficiently long and stable recordings. The coherent motion pattern moved in different directions (45° steps) and was combined with motion noise. We used three conditions: (i) no motion noise (ii) medium and (iii) strong motion noise. The solid lines in Figure 6.4 show the direction tuning curves for coherent motion alone (64 or 16 motion dots in Figure 6.4a and b, respectively) averaged across 6 H1 recordings. The response amplitude was normalized to the average response amplitude determined in the first reference section at the beginning of the trial where all 64 dots moved coherently in the cell's preferred direction (see methods). H1 exhibits the typical broad direction tuning, with an abnormal "dent" in the response amplitude at the "preferred direction". This seemingly surprising finding is in line with the conclusions drawn by Buchner (1976). Given the hexagonal lattice of the fly's eye, there are three ways to detect for example horizontal movement involving nearest neighbor interactions (inset Figure 6.4, shown for left to right movement). In addition to interactions along the horizontal axis of the eye, there are also strong interactions along the oblique axes of the ommatidial lattice (Buchner, 1976; Schuling et al., 1989). If the direction sensitivity of TCs is probed with grating patterns (Hausen, 1976, 1982b) the dent in the tuning curve did not appear. In contrast to stripe patterns, which simultaneously activate all three types of movement detectors when moving horizontally, the dots used here (each dot's size approximates the acceptance angle of a single photoreceptor) stimulate only one type of detector at a time. Depending on the relative weight of the different types of nearest neighbor interactions, dot stimuli may, thus, lead to the dent in the tuning curve observed here.

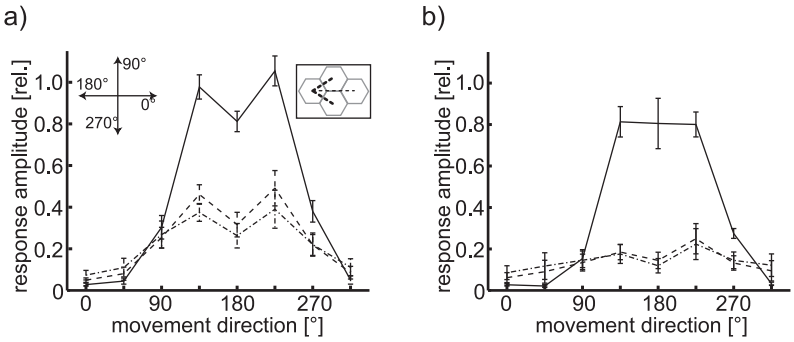

Figure 6.4: H1 Direction tuning when combined with motion noise. (a), H1 responses as a function of the coherent motion direction (64 dots) without motion noise (solid line) and combined with medium and strong motion noise (dashed and dash-dotted lines, respectively). 180° corresponds to the right H1's preferred direction. Plots are averages across 6 H1 recordings done in 6 different animals. Errorbars represent the standard error. The right inset sketches the ommatidial lattice of the fly compound eye. The dashed lines indicate the three different connections responding to horizontal motion from left to right. **(b)**, Same as a but with 16 dots moving coherently.

When the motion stimulus is combined with motion noise, the peak amplitudes of the direction tuning curve decrease considerably (dashed curves in Figure 6.4). The

tuning width does not significantly change for the combinations of coherent motion with medium and strong motion noise (Figure 6.4, dashed and dash-dotted line). Rather than sharpening, the tuning curves become slightly broader. With a very weak motion stimulus of only 16 dots moving in the different directions (Figure 6.4b) the motion noise reduces the response so much that the cell's direction tuning almost vanishes. Nevertheless, if we take into account that the very weak motion stimulus consists of only 16 dots and is combined with motion noise consisting of 112 dots moving in random directions, the direction tuning can be concluded to be quite robust against motion noise.

Robust representation of pattern velocity

From analyses with white noise velocity fluctuations it is known that the spike rate of the H1-cell represents the time course of velocity of a moving pattern up to frequencies of about 10 Hz, as long as the velocities are sufficiently small (Bialek et al., 1991; Haag and Borst, 1998; Warzecha et al., 1998). Here we tested the velocity coding of the H1-cell when the dynamic motion signal is corrupted by motion noise. The motion dots moved with a dynamic velocity profile which contained frequencies up to 10 Hz (Figure 6.5 left column). Motion noise of different strengths was added. To quantify the coding performance we calculated the coherence (Haag and Borst, 1998; van Hateren and Snippe, 2001) between the time-dependent velocity profile of the motion stimulus and the neuronal responses under three conditions, (i) without, (ii) with weak, and (iii) with strong motion noise (Figures 6.5 upper, middle and bottom plots). The time course and amplitude of the H1 responses to the first and the second condition are very similar. The spike rate reflects the pattern velocity in the preferred direction to a certain extent, while the null direction velocity cannot be resolved due to the rectifying effect of spike generation. Like the response amplitude, the overall response power and the coherence spectra under these two conditions are very similar. The coherence is close to 0.9 for almost the entire tested frequency range (grey solid lines in Figure 6.5). A noise-free linear system would give a coherence of one. The difference between one and the measured coherence may be due to both the noise and the non-linearities in the fly visual motion pathway. To obtain an estimate of the relative contribution of these two sources, the expected coherences were calculated. The expected coherence (black solid lines in Figure 6.5) is defined as the coherence between the individual responses and the mean response which can be considered the noise-free response if a sufficiently large number of trials is averaged. The deviation of the expected coherence from one is due to noise in the responses (van Hateren and Snippe, 2001). Consequently, the difference between measured and expected coherence reflects the non-linearity of the system. The data shown in Figure 6.5 are based on a single cell with 80 trials per condition. Neither the measured coherence nor the expected coherence changed much when fewer trials were evaluated (not shown). Thus, the responses to dynamically varied pattern velocity are quite reliable and the H1-cell is well able to code stimulus velocity even in the presence of the motion noise. When the strong motion noise is added the response amplitude drops in accordance with the results obtained with constant velocity motion. Nonetheless, the time course of the response is still very similar to those obtained with weak or without noise (compare the reduction in Figures 6.3 and 6.4). With the reduced response amplitude the response power drops as well but the coherence declines only slightly. Though the decrease is much smaller than

the corresponding reduction in spike frequency, the coherence remains high (between 0.6 and 0.8). This reflects that the time course of the H1 response does not much change and that the pattern velocity is still encoded very well even though motion noise reduces the spike rate to about 50%. The expected coherence is somewhat lower for strong motion noise than under the other two stimulus conditions suggesting that the noise in the responses increases when the strong motion noise is added to the stimulus.

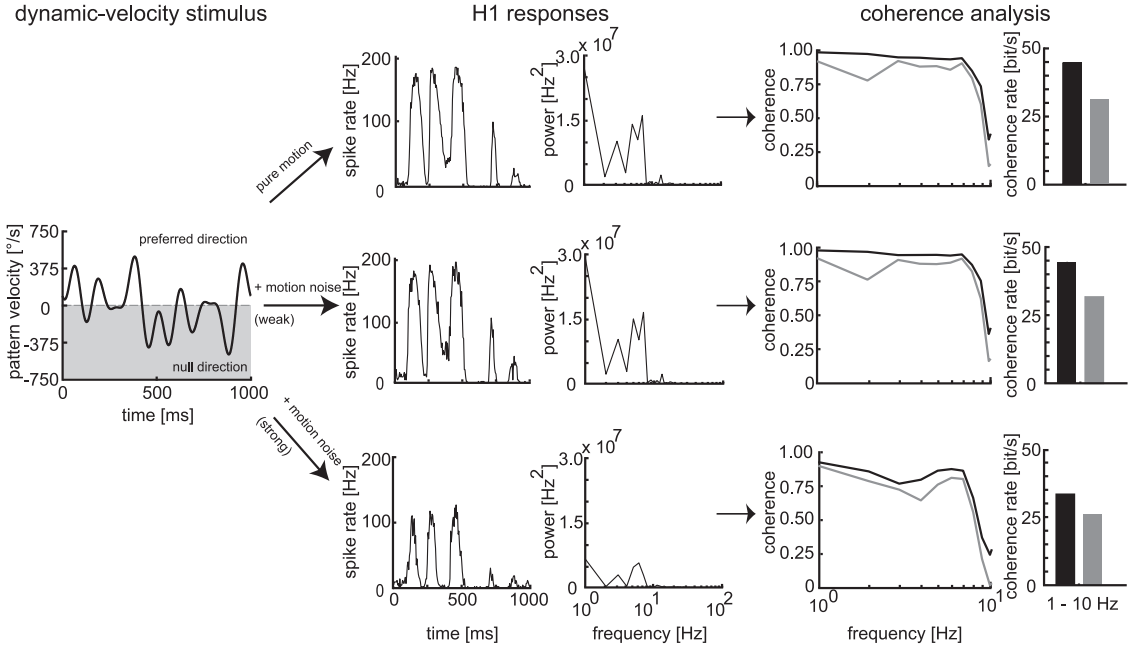

Figure 6.5: Representation of pattern velocity in the H1 responses. (Left column) Stimulus time-course. Positive and negative velocities denote movement in the preferred and null-direction, respectively. The coherent motion following this velocity profile was presented without motion noise and combined with weak and strong motion noise. **(middle column)** Averaged responses of a single H1-cell (80 stimulus presentations per condition) as PSTHs and the response power spectrums. **(Right column)** Coherence (grey solid line) and expected coherence (black solid line) spectra and expected coherence rates (black) and the coherence rates (grey) obtained under the three conditions (no, weak, and strong motion noise, top to bottom).

The information transmitted by spike responses can be estimated from the coherence spectrum under certain conditions. For additive Gaussian noise, the so-called coherence rate is related to the Shannon information (van Hateren and Snippe, 2001) and is given in bits/s. Even if these requirements are not met, the coherence rate can still be treated as an approximation of the Shannon information. Figure 6.5 (rightmost plots) shows the coherence rates and the expected coherence rates for the three conditions. For this sample recording the coherence and expected coherence rates are about the same for the conditions with and without weak motion noise (31.6 and 30.4 bits/s coherence rates and 41.3 and 43.5 bits/s expected coherence rates), but are reduced to a coherence rate of 26.3 bits/s and an expected coherence rate of 33.7 bits/s when strong motion noise is added. Again, the coherence rate in the presence of strong motion noise still amounts to 86.5% of the coherence rate obtained under the no motion noise condition, although the spike rate dropped to only 43.6% (49.5±3.25 and 21.6±2.5 spikes, for no noise and strong motion

noise, respectively). Thus, the contribution of a single spike to the coherence rate is higher when strong motion noise is added to the dynamic motion stimulus than without added noise. Figure 6.6 shows the coherence rate per spike for the two conditions (black symbols) as an average over 5 cells. We find the coherence rate per spike almost doubled (0.55±0.06 bit/spike to 1.07±0.22 bit/spike under the no-noise condition and strong motion noise condition, respectively). Similar results were obtained using a different measure (Brenner et al., 2000) which estimates the information transmitted per spike on the basis of the time dependent spike rate (0.912±0.10 bit/spike and 1.22±0.26 bit/spike for the two conditions, grey symbols in Figure 6.6). Despite the increased information per spike the total transmitted information decreases. The dashed lines in Figure 6.6 indicate the coherence rate (information) per spike that would be needed to fully counterbalance the decreased spike rate when strong noise is added to the dynamic motion stimulus. A similar change in the information per spike was found in the context of motion adaptation: the loss of spikes was largely balanced by an increased information per spike (Heitwerth et al., 2005).

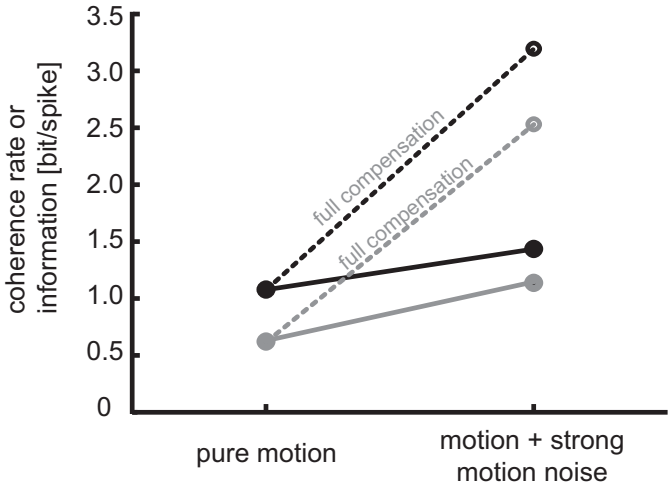

Figure 6.6: Information content of individual spikes. The information transmitted by each single spike is shown for two conditions (no motion noise and combined with strong motion noise). The information was estimated from the coherence analysis (black symbols) and according to Brenner et al. (2000) (grey symbols). Open symbols represent the information content that would be needed to fully compensate the loss of spikes.

To conclude, H1 is well able to encode the time course of pattern velocity, even if a dynamically moving pattern is combined with strong motion noise that reduces the response amplitude quite drastically. The loss of spikes is partly compensated by the increased information carried by individual spikes.

6.5 Discussion

We addressed how different types of synaptic inputs interact on dendritic trees under *in vivo* conditions. By manipulating the natural sensory input of fly tangential cells (TCs), we find that visually induced responses and the input resistance of the cells are strongly

affected by motion noise that was designed to be balanced and not to drive the cell on its own. Although the response amplitudes to coherent visual motion are strongly reduced in the presence of motion noise, functionally important properties like the direction tuning and the ability to encode time-varying motion are robust against motion noise. From these results we hypothesize that the integration of functionally different synaptic inputs is a mechanism that immanently equalizes the ensemble's sensitivity irrespective of the specific stimulus conditions (see below).

Integration of functionally different synaptic inputs

Inputs to neurons in the primate lateral geniculate nucleus were classified as drivers or modulators depending on their origin (Sherman and Guillery, 1998). For rat cortical neurons a classification was suggested based on the context in which the inputs are activated rather than on their origin (Chance et al., 2002). Those excitatory and inhibitory inputs which are active at different times drive the neuron, while those active simultaneously cancel each other and constitute the modulating input. Simultaneous activation of excitatory and inhibitory inputs affects the membrane potential or the firing rate only little, but increases the membrane conductance and therefore represents a shunting input. In our stimulus design the impact of a dot of the motion noise moving in one direction is counteracted by another dot moving in the opposite direction. Thus, the motion noise as a whole constitutes a modulating input and does not drive the cell on its own. In contrast, those inputs which are activated by coherent motion drive the neuron by either depolarizing or hyperpolarizing it, depending on the direction of motion. Motion noise was found reduce the cell's sensitivity to simultaneously presented coherent motion by reducing the cell's input resistance and can therefore be considered as a shunting input to the cell. Even though this classification of the synaptic inputs into drivers and modulators is artificial in the case of TCs, especially since both components are embedded in the same visual input, it is useful for the system analysis presented here. In the real *in vivo* situation the actual role of an input signal depends on the context in which it is active, as was put forward for cortical neurons (Chance et al., 2002). The specific consequences of a shunting input on dendritic computation of driving inputs is still controversially discussed. On the level of the postsynaptic potential, a decreased input resistance acts divisively on driving inputs (e.g. Holt and Koch, 1997). The slope of the input output characteristic is reduced as the membrane conductance increases. Things appear differently when the postsynaptic potential is converted into spikes. Several *in vitro* and modeling studies concluded that a tonic shunt then shifts the input-output characteristic along the input axis (Berman et al., 1992; Connors et al., 1988; Holt and Koch, 1997). This is often described as a subtractive effect since it resembles the effect of a hyperpolarizing input although the underlying postsynaptic potential is in fact divisively modulated (e.g. Holt and Koch, 1997). Recent analyses mimicking the natural synaptic input by the dynamic clamp technique concluded that shunting can modulate a neuron's gain resulting in slope changes of the input-output characteristic (Chance et al., 2002; Fellous et al., 2003; Mitchell and Silver, 2003). Prerequisite is an increased membrane potential noise induced as a by-product of the shunting input as is characteristic of synaptic signals. Consequently, driving stimuli, which on their own would not suffice to induce spiking, are enabled to cross spike threshold, an effect reminiscent of stochastic resonance (e.g. Wiesenfeld and Moss, 1995).

In our experiments done under *in vivo* conditions, the shunting effect and the increased membrane potential fluctuations induced by the modulating input (Figure 6.1) lead, at least in principle, to conditions for a divisive change of the spike response. However, the changes observed in the input-output characteristics (Figures 6.2 and 6.3) do not allow us to infer a shift or a slope change as exclusive mechanism. On the other hand, subtractive and divisive mechanisms affect tuning curves of spiking neurons very differently: in case of a subtractive shift, non-optimal directions fail to induce spiking and the tuning curve is sharpened, the so called iceberg effect (e.g. Anderson et al., 2000). As a consequence of a divisive mechanism the overall spike rate is scaled but the width of the tuning curve stays the same. Thus, the observed reduction in directional gain with an almost unaffected tuning width (Figure 6.4) suggests a divisive in favor of a subtractive effect on the H1 spike responses. As mentioned above, this might be the consequence of the increased membrane potential fluctuations at higher motion noise levels which allow occasional action potential generation even at suboptimal directions, i.e. when the average postsynaptic potential is below spike threshold. This is in line with conclusions drawn by Anderson et al. (2000) who showed that membrane potential noise is the key for contrast invariant tuning curves in cat complex and simple cells.

Alternative explanations of gain control

Similar changes of the input-output characteristics as described above are also found in simple cells of the macaque visual cortex. For instance, the contrast dependence of the response to an optimally oriented drifting grating is shifted when simultaneously presented with an orthogonal grating which has no own driving impact. Likewise, superimposed visual noise reduces the response to the drifting grating (Carandini et al., 1997; Carandini and Heeger, 1994). These gain changes were interpreted by shunting input to the considered neuron mediated by another cortical neuron pooling many local retinotopic inputs (Carandini et al., 1997; Carandini and Heeger, 1994). This scheme is reminiscent of a model originally proposed to account for gain control of fly TCs which also relies on a shunting pool cell (Reichardt et al., 1983). Since in later studies this gain control could be explained in a more parsimonious way by realizing, in line with our present findings, that the driving input does not only drive the cell, but also leads to pronounced shunting (Borst et al., 1995), a similar influence of the direct peripheral input of cortical cells on the cell's input resistance may also play a role in controlling the gain of these neurons.

Robustness of temporal encoding properties

Both effects of motion noise, the reduced gain and the increased membrane potential noise could impair the coding performance of TCs. Surprisingly, the stimulus time course can be recovered from the neuronal responses almost as well in the presence of motion noise as in its absence, although the corresponding spike rate decreased to 50%. This result seems to contradict findings that visual flicker impairs the ability of monkey area MT/MST neurons to discriminate between motion in different directions (Churan and Ilg, 2002). This discrepancy may be a consequence of the method used to discriminate between neuronal responses. Churan and Ilg (2002) employed a measure derived from signal detection theory to discriminate between two alternative directions of motion on the basis of the mean response to constant velocity stimuli combined with flicker. In

contrast, we tested how well the time course of the dynamic stimulus can be recovered from the neuronal response.

Functional implications

The fly's visual system offers the opportunity to link neuronal performance to the animal's behaviour (reviews: Egelhaaf et al., 2002; Egelhaaf and Borst, 1993; Hausen, 1984). TCs are involved in the evaluation of optic flow and have been shown to encode information about the three-dimensional layout of the environment (Kern et al., 2005) as well as certain self-motions like body roll (Karmeier et al., 2005; Krapp et al., 1998, 2001). Some TCs project directly to motoneurons that control compensatory head movements (Gilbert et al., 1995; Gronenberg et al., 1995; Milde et al., 1995; Strausfeld et al., 1987). During aerobatic flight maneuvers the fly induces optic flow, which is characterized by peculiar patterns of motion vectors depending on the type of self-motion and the environmental layout. While some maneuvers induce motion vectors optimally driving a certain TC, they are ineffective for other TCs (Karmeier et al., 2006). Irrespective of the efficiency of driving a specific combination of TCs at a given time, the input resistance and thus the gain of all TCs is decreased regardless of the actual stimulus situation. Hence, under natural conditions the gains of all TCs can be expected to be about the same level at any time. This level may be low when the animal is flying rapidly and thus confronted mainly with rapid retinal motion, somewhat higher when the animal is walking and thus experiencing mainly slower retinal motion and at its highest level when the animal is just sitting and thus experiencing virtually no motion at all. Hence, all TCs are proposed to operate with a similar gain and thus a similar sensitivity to motion, irrespective of the overall strength of the optic flow and thereby the behavioral context. Thus, the continuous bombardment with motion stimuli, though not necessarily driving all TCs, can equalize the network's gain, leaving it well able to code for different parameters as we could show for the direction tuning of constant motion or a dynamically varying stimulus.

References

Anderson J, Lampl I, Gillespie D, Ferster D (2000) The Contribution of Noise to Contrast Invariance of Orientation Tuning in Cat Visual Cortex. Science 290: 1968–1972.

Azouz R, Gray C (1999) Cellular mechanisms contributing to response variability of cortical neurons In Vivo. J Neurosci 19: 2209–2223.

Berman N, Douglas R, Martin K (1992) GABA-Mediated Inhibition in the Neural Networks of Visual Cortex. Prog Brain Res 90: 443–476.

Bialek W, Rieke F, de Ruyter van Steveninck R, Warland D (1991) Reading a Neural Code. Science 252: 1854–1857.

Borst A, Egelhaaf M, Haag J (1995) Mechanisms of Dendritic Integration Underlying Gain Control in Fly Motion-Sensitive Interneurons. J Comput Neurosci 2: 5–18.

Borst A, Haag J (1996) The Intrinsic Electrophysiological Characteristics of Fly Lobula Plate Tangential Cells: I. Passive Membrane Properties. J Comput Neurosci 3: 313–336.

Borst A, Haag J (2002) Neural Networks in the Cockpit of the Fly. J Comp Physiol [A] 188: 419–437.

Brenner N, Strong S, Koberle R, Bialek W, de Ruyter van Steveninck R (2000) Synergy in a Neural Code. Neural Comput 12: 1531–1552.

Brotz T, Gundelfinger E, Borst A (1996) Cholinergic and GABAergic Receptors on Fly Tangential Cells and their Role in Visual Motion Detection. J Neurophysiol 76: 1786–1799.

Buchner E (1976) Elementary Movement Detectors in an Insect Visual System. Biol Cybern 24: 85–101.

Carandini M, Heeger D (1994) Summation and Division by Neurons in Primate Visual Cortex. Science 264: 1333–1336.

Carandini M, Heeger D, Movshon J (1997) Linearity and Normalization in Simple Cells of the Macaque Primary Visual Cortex. J Neurosci 17: 8621–8644.

Chance F, Abbott L, Reyes A (2002) Gain Modulation from Background Synaptic Input. Neuron 35: 773–782.

Churan J, Ilg U (2002) Flicker in the Visual Background Impairs the Ability to Process a Moving Visual Stimulus. Eur J Neurosci 16: 1151–1162.

Connors B, Malenka R, Silva L (1988) Two Inhibitory Postsynaptic Potentials, and GABAA and GABAB Receptor-Mediated Responses in Neocortex of Rat and Cat. J Physiol 406: 443–468.

Destexhe A, Rudolph M, Pare D (2003) The High-Conductance State Of Neocortical Neurons *in vivo*. Nat Rev Neurosci 4: 739–751.

Egelhaaf M, Borst A (1993) Motion Computation and Visual Orientation in Flies. Comp Biochem Physiol 104A: 659–673.

Egelhaaf M, Grewe J, Karmeier K, Kern R, Kurtz R, et al. (2004) Novel Approaches to Visual Processing in Insects: Case Studies on Neuronal Computations in the Blowfly. In: TA C, editor, Methods in Insect Sensory Neuroscience., pp. 185–212, CRC Press.

Egelhaaf M, Kern R, Krapp H, Kretzberg J, Kurtz R, et al. (2002) Neural Encoding of Behaviourally Relevant Visual-Motion Information in the Fly. TINS 25: 96–102.

Egelhaaf M, Warzecha A (1999) Encoding of Motion in Real Time by the Fly Visual System. Curr Opin Neurobiol 9: 454–460.

Fellous J, Rudolph M, Destexhe A, Sejnowski T (2003) Synaptic Background Noise Controls the Input/Output Characteristics of Single Cells in an *in vitro* Model of *in vivo* Activity. Neuroscience 122: 811–829.

Francescini N (1975) Sampling of the visual environment by the compound eye of the fly: Fundamentals and applications. In: Snyder AW MR, editor, Photoreceptor optics, pp. 98–125, Berlin, Heidelberg, New York: Springer.

Gilbert C, Gronenberg W, Strausfeld N (1995) Oculomotor Control in Calliphorid Flies: Head Movements During Activation and Inhibitions of Neck Motor Neurons Corroborate Neuroanatomical Predictions. J Comp Neurol 361: 285–297.

Gronenberg W, Milde J, Strausfeld N (1995) Oculomotor Control in Calliphorid Flies: Organization of Descending Neurons to Neck Motor Neurons Responding to Visual Stimuli. J Comp Neurol 361: 267–284.

Haag J, Borst A (1998) Active Membrane Properties and Signal Encoding in Graded Potential Neurons. J Neurosci 18: 7972–7986.

Hausen K (1976) Functional charaterization and anatomical identification of motion sensitive neurons in the lobula plate of the blowfly *Calliphora erythrocephala*. Z Naturforsch 31: 629–633.

Hausen K (1982a) Motion Sensitive Interneurons in the Optomotor System of the Fly. I. The Horizontal Cells: Structure and Signals. Biol Cybern 45: 143–156.

Hausen K (1982b) Motion Sensitive Interneurons in the Optomotor System of the Fly. II. The Horizontal Cells: Receptive Field Organization and Response Characteristics. Biol Cybern 46: 67–79.

Hausen K (1984) The Lobula-Complex of the Fly: Structure, Function and Significance in Visual Behaviour. In: Ali M, editor, Photoreception and vision in invertebrates, pp. 523–555, Plenum Press.

Heitwerth J, Kern R, van Hateren J, Egelhaaf M (2005) Motion Adaptation Leads to Parsimonious Encoding of Natural Optic Flow by Blowfly Motion Vision System. J Neurophysiol 94: 1761–1769.

Hengstenberg R (1982) Common Visual Response Properties of Giant Vertical Cells in the Lobula Plate of the Blowfly Calliphora. J Comp Physiol [A] 149: 179–193.

Holt G, Koch C (1997) Shunting Inhibition does not have a Divisive Effect on Firing Rates. Neural Comput 9: 1001–10013.

Karmeier K, Krapp H, Egelhaaf M (2005) Population Coding of Self-Motion: Applying Bayesian Analysis to a Population of Visual Interneurons in the Fly. J Neurophysiol 94: 2182–2194.

Karmeier K, van Hateren J, Kern R, Egelhaaf M (2006) Encoding of Naturalistic Optic Flow by a Population of Blowfly Motion Sensitive Neurons. J Neurophysiol 96: 1602–1614.

Kern R, van Hateren J, Michaelis C, Lindemann J, Egelhaaf M (2005) Function of a Fly Motion-Sensitive Neuron Matches Eye Movements During Free Flight. PLoS Biol 3: e171.

Koch C, Poggio T, Torre V (1983) Nonlinear Interactions in a Dendritic Tree: Localization, Timing, and Role in Information Processing. PNAS 80: 2799–2802.

Krapp H, Hengstenberg B, Hengstenberg R (1998) Dendritic Structure and Receptive-Field Organization of Optic Flow Processing Interneurons in the Fly. J Neurophysiol 79: 1902–1917.

Krapp H, Hengstenberg R, Egelhaaf M (2001) Binocular Contributions to Optic Flow Processing in the Fly Visual System. J Neurophysiol 85: 724–734.

Kretzberg J, Egelhaaf M, Warzecha A (2001) Membrane Potential Fluctuations Determine the Precision of Spike Timing and Synchronous Activity: a Model Study. J Comput Neurosci 10: 79–97.

Milde J, Gronenberg W, Strausfeld N (1995) Oculomotor Control in Calliphorid Flies: Organization of Descending Neurons to Neck Motor Neurons Responding to Visual Stimuli. J Comp Neurol 361: 267–284.

Mitchell S, Silver R (2003) Shunting Inhibition Modulates Neuronal Gain During Synaptic Excitation. Neuron 38: 433–445.

Prescott S, De Koninck Y (2003) Gain Control of Firing Rate by Shunting Inhibition: Roles of Synaptic Noise and Dendritic Saturation. PNAS 100: 2076–2081.

Prinz A, Abbott L, Marder E (2004) The Dynamic Clamp Comes of Age. Trends Neurosci 27: 218–224.

Reichardt W, Poggio T, Hausen K (1983) Figure-Ground Discrimination by Relative Movement in the Visual System of the Fly. Part II: Towards the Neural Circuitry. Biol Cybern 46: 1–30.

Schuling F, Mastebroek H, Bult R, Lenting B (1989) Properties of Elementary Movement Detectors in the Fly *Calliphora erythrocephala*. J Comp Physiol [A] 165: 179–192.

Sherman S, Guillery R (1998) On the Actions that one Nerve Cell can have on Another: Distinguishing "Drivers" from "Modulators". PNAS 95: 7121–7126.

Single S, Haag J, Borst A (1997) Dendritic Computation of Direction Selectivity and Gain Control in Visual Interneurons. J Neurosci 17: 6023–6030.

Strausfeld N, Seyan H, Milde J (1987) The Neck Motor System of the Fly *Calliphora erythrocephala* I. Muscles and Motor Neurons. J Comp Physiol [A] 160: 205–224.

van Hateren J, Kern R, Schwerdtfeger G, Egelhaaf M (2005) Function and Coding in the Blowfly H1 Neuron During Naturalistic Optic Flow. J Neurosci 25: 4343–4352.

van Hateren J, Snippe H (2001) Information Theoretical Evaluation of Parametric Models of Gain Control in Blowfly Photoreceptor Cells. Vision Res 41: 1851–1865.

Warzecha A, Egelhaaf M, Borst A (1993) Neural Circuit Tuning Fly Visual Interneurons to Motion of Small Objects. I. Dissection of the Circuit by Pharmacological and Photoinactivation Techniques. J Neurophysiol 69: 329–339.

Warzecha A, Kretzberg J, Egelhaaf M (1998) Temporal Precision of the Encoding of Motion Information by Visual Interneurons. Curr Biol 8: 359–368.

Warzecha AK, Kretzberg J, Egelhaaf M (2000) Reliability of a Fly Motion-Sensitive Neuron Depends on Stimulus Parameters. J Neurosci 20: 8886–8896.

Wiesenfeld K, Moss F (1995) Stochastic Resonance and the Benefits of Noise: From Ice Ages to Crayfish and Squids. Nature 373: 33–36.

Danksagung

Natürlich entstand diese Arbeit nicht im Alleingang, weshalb ich mich an dieser Stelle bei allen Helfern bedanken möchte:

An erster Stelle danke ich Anne-Kathrin Warzecha und Martin Egelhaaf für ihre, trotz verschiedener anderweitiger Verpflichtungen, intensive Betreuung und dafür, mir dieses Projekt zugetraut zu haben.
Mein Dank geht auch nach Finnland zu Matti Weckström, der mich in die Geheimnisse der Photorezeptor Ableitungen einweihte und auch aus der Ferne immer für Fragen zur Verfügung stand, kiitos.
Weiterhin danke ich Jens Peter Lindemann dafür, dass er den Neurobio-Cluster am Laufen hält und in der Cafeteria immer ein offenes Ohr für noch so dumme Fragen hatte.
Ich danke der gesamten Arbeitgruppe für die gute Atmosphäre und die nachmittäglichen Kaffeeraum-Diskussionen. Einschließen möchte ich noch die Ehemaligen Katja Karmeier und Norbert Boeddeker, die immer mit Rat und Tat zur Verfügung standen.
Zu guter Letzt möchte ich meiner Familie danken, die in der letzten Zeit nicht ganz viel von mir hatte. Vielen Dank für eure Geduld!